行政院及所屬各機關出國報告
（出國類別： 實習 ）

參與第39屆 AOC 年會課程及參訪廠商之出國報告

服務機關：中山科學研究院
出國人職稱：聘用技正
姓　　名： 謝金和
出國地區： 美國
出國期間： 91.10.29 至 91.11.05
報告日期： 91.12.12

I8/
/C09201740

H207

國外公差報告

報　告　資　料　頁

1. 報告編號：CSIPW-91E-K0009	2. 出國類別：共他 資習	3. 完成日期：91.12.12	4. 總頁數：20

5. 報告名稱：參與第 39 屆 AOC 年會課程及參訪廠商之出國報告

6. 核准文號	人令文號	(九一)詮鑑字第００七三二０號
	部令文號	

7. 經　　　費	新台幣：壹拾壹萬柒仟壹百參拾捌元
8. 出(返)國日期	91.10.29 至 91.11.05
9. 公　差　地　點	美國納須維爾市及洛杉磯市
10. 公　差　機　構	中山科學研究院電子系統研究所
11. 附　　　記	

C09201740

行政院及所屬各機關出國報告提要

出國報告名稱：參與第 39 屆 AOC 年會課程及參訪廠商之出國報告

頁數 __19__　含附件：∨是□否

出國計畫主辦機關/聯絡人/電話

中山科學研究院/楊培基/(03)4712201 轉 355624

出國人員姓名/服務機關/單位/職稱/電話

謝金和/中山科學研究院/電子系統所空用電子組/聘用技正/ (03)4712201 轉 355855

出國類別：□ 1 考察□2 進修□3 研究∨4 實習□5 其他

出國期間：　　　　　　　出國地區：

91.10.29 至 91.11.05　　美國納須維爾市及洛杉磯市

報告日期：91.12.12

分類號/目
關鍵詞：
    (1) Electric Signal Measurement(ESM)
    (2) Electric Counter Counter Measurement(ECCM)
    (3) CROSS-EYE angle jamming
    (4) FMCW
    (5) LPI

內容摘要：（二百至三百字）

    依據中山科學研究院執行軍民通用經濟部科專[先進機載航電技術四年發展計畫]之奉核需求，於十月三十一日至十一月一日赴美國田納西州納須維爾市參加第三十九屆AOC年會所開的ELINT and Modern Signals及Cross-Eye/Angle Jamming兩天的課程，蒐集FMCW雷達系統設計的核心暨關鍵技術最新之發展趨勢及資訊，俾作為先進機載航電高度計精進設計之參考依據。此行並於十一月三日至四日前往美國洛杉磯Goleta Engineering公司就FMCW雷達之系統分析設計及模擬等相關技術進行研討，並進一步爭取合作與技術引進，以利明年之科專計畫得以順利進行。

    本文電子檔已上傳至出國報告資訊網
    （http://report.gsn.gov.tw）

中山科學研究所出國公差人員心得報告目錄

壹、出國目的及緣由

一、 依據中山科學研究院執行軍民通用經濟部科專[先進機載航電技術四年發展計畫]之奉核需求,呈請核准派員於十月三十一日至十一月一日赴美國田納西州納須維爾市參加第三十九屆 AOC 年會所開的 ELINT and Modern Signals 及 Cross-Eye/Angle Jamming 兩天的課程,並利用上課期間蒐集 FMCW 雷達系統設計的核心暨關鍵技術最新之發展趨勢及資訊,俾作為先進機載航電高度計精進設計之參考依據。此行並於十一月三日至四日前往美國洛杉磯 Goleta Engineering 公司就 FMCW 雷達之系統分析設計及模擬等相關技術進行研討,進一步爭取合作與技術引進,以利明年之科專計畫得以順利進行。

貳、公差心得

此次公差心得分兩個主題,一為課程部份,另一為參訪廠商之討論部份:

一、課程部份

第一堂課程[ELINT and Modern Signals]:講授的內容題提到當前雷達設計方式朝向低功率、連續波(FMCW 雷達)之 LPI 雷達趨勢,使 ESM 更加困難(但並非不可能),ESM 系統則必須能對此等雷達及傳統 High power、Pulse 型式的雷達都能適用。以 1 W 之 FMCW 雷達為例,偵測 100 m^2 的目標,其偵測距離可達 28 公里,但被典型的 ESM 系統偵測到有效距離為 2.5 公里,即使是高性能的 ESM 系統,也只能在 25 公里範圍內才可能偵測到。相較於 10kW、Pulse 型

式的傳統雷達，其偵測 100 ㎡ 目標的測距離約 25 公里，但被典型的 ESM 系統偵測到有效距離為 250 公里，若是高性能的 ESM 系統，則在 2500 公里遠就會被偵測到！由此可見 FMCW 優越的 LPI 特性了。現今已有 Pilot、Scout 等 LPI 雷達部署，其對低 RCS 目標之偵測距離約為 20 公里，因這類威脅日增，所以受到 ESM 系統設計者的重視而開始研究反制之道。從課程關切的程度可以領略到 LPI 雷達已是設計主流。

第二堂課程[CROSS-EYE and other angle jamming techniques]：講授 CROSS-EYE ECM 的優越性能，課堂上還播放此 jamming 技術在直昇機及戰機上的運用效果，當 jamming on 時，很清楚的看到追蹤雷達立即偏向鎖到假目標，這是因為 CROSS-EYE angle jamming 技術是應用 wavefront distortion 原理，製造位置偏差而達其目的，是非常有效的 ECM 方式。課程指出 angle jamming 的必要性，一般追蹤雷達採用的追蹤技術，被追蹤目標都有其因應的電戰對抗方法，惟 leading edge 追蹤技術，非常難 jamming，除非是用 angle jamming 才會有效果。常見的 angle jamming 技術有 angle blinking、cross polarisation、expendable decoys、towed decoys 等，各有其應用上之限制。CROSS-EYE 是最有效的反制雷達追蹤之技術，其所'製造'出的位置誤差(假目標位置)能於終端期有效地誘使威脅(如飛彈)擊向此假目標。
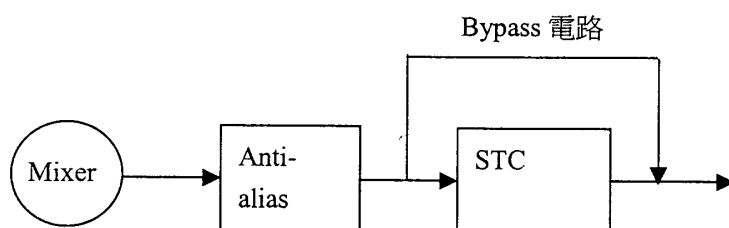
二、參訪部份

重點整理如下：

技術合作議題：

Dr. Sih 認為台灣穩懋公司 6 吋砷化鎵製程能力比德國 UMS 公司 4 吋晶圓佳，更可以 Cost down。UMS 掌控技術不可能釋出，惟培植另一家才有可能。穩懋公司正一切備便，如台灣有市場，MMCOMM 也會到台灣設立公司，It's time to cut in to market。一般而言，從 T/R Chipset 到 Prototype 到 Product 每 phase 研發費用分配約為 8 萬美金、100 萬美金、500 萬美金。所以從開發到市場 for 77GHz 期程三年總花費約 600 萬美金。如此技術可在國內生根以及低於此頻段的 T/R 模組也不會有問題。技術更可用到 ka、ku、x-band 等軍用產品上，投資效益很大，且技術已成熟風險不高，經費籌措上可由業界、經濟部、軍方分攤，降低各方財源負擔而成果共享。MMCOM 公司已一切就緒，隨時可以啟動。

John 從 1956 年服務於 B-52 雷達修護單位起已有 40 餘年雷達工作經驗，涵蓋系統設計、分析、教授雷達課程、雷達訊號處理分析等，適合納入顧問群，借用他豐富的雷達知識。他自己經營 Goleta engineering 公司，同時也是 MMCOMM 公司的系統顧問。

Long Bui 具有 FMCW 實作及巨細靡遺的測試經驗，在開發產品過程可幫助測試設計執行顧問，使開發產品之過程更順利。其經驗強調，FMCW 系統必須整體考量，從我們的需要訂出 DSP 需求及 T/R 的需求必須緊緊的結合在一起。若分開考量將引起若干系統無法解決的問題，如果沒遇到問題算你走運！

RA 診斷：

一、所有提供的測試圖包含所有可能的 Noise 來源，無法判讀。

二、需要 LPF(MHz)，設計建議：如下示意圖，IF 輸出端要有 Bypass STC 的電路設計，方便測試時 Isolate 問題。如果沒有這樣的設計，要是測試時出現問題就很難除錯了。

Bypass 電路

```
   ┌──────┐     ┌──────┐     ┌──────┐
   │      │     │ Anti-│     │      │
   │Mixer │────▶│ alias│────▶│ STC  │────▶
   │      │     │      │     │      │
   └──────┘     └──────┘     └──────┘
```

T/R subsystem 測試是非常重要的課題。

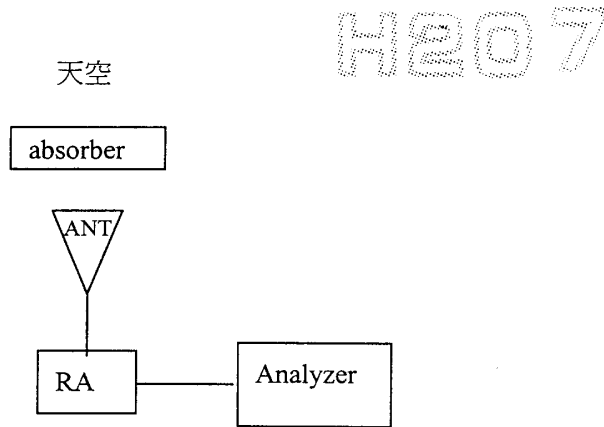三、天線指向天空，Bypass STC，觀察 IF 測試點，可以知道 Noise floor，將此結果與 corner reflector 關聯起來以找出我們的問題所在。

四、CW & FM will have the same noise floor。(絕對要好)

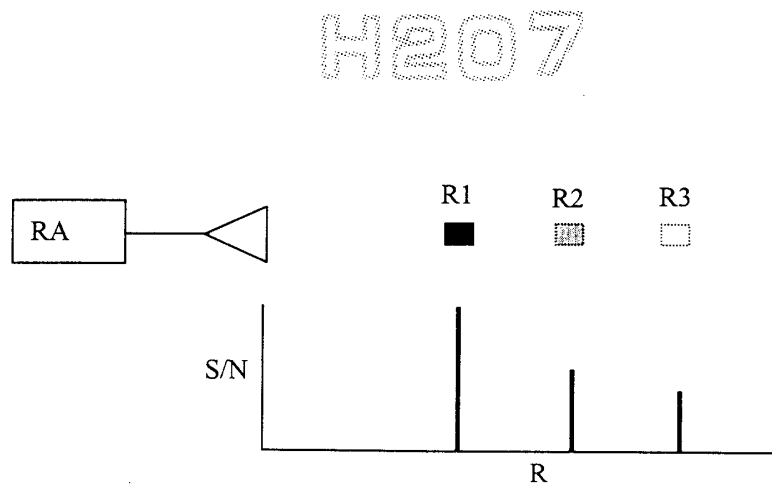五、需要執行大量的測試，make sure they are not saturated by anything，亦即發射及接收電路的元件都必須在 linear 範圍內工作，不可落入飽和區。

另改變已知 RCS 待測物距離 R，觀察 S/N 與 R 的變化關係是否符合雷達方程式，

若是，則表示系統處於 linear 工作區。

測試場景示意圖如下：

天空

```
┌──────────────┐
│   absorber   │
└──────────────┘
       ╲ANT╱
        ╲ ╱
         V
         │
┌──────┐   ┌────────────┐
│  RA  │───│  Analyzer  │
└──────┘   └────────────┘
```

觀察 S/N 與 R 的變化關係示意圖如下：

六、Acceptance test：應完整訂定，接收時逐項驗證，應該可以且必須能重複。

七、Design scenario：考量 RCS、Range。RA 對地，地面雜波是目標。S-1 對船，船是目標，地面雜波是干擾。規格內要放入 scenario，確實訂出需求，比如說對空或對地應用環境不同，規格也不同。

八、T/R 模組測試要點：

(a).waveform (input signal)測試需求

(b).Rx path test 、gain、mixer saturation、linear

(c).Tx path test、gain、linear

LEGO(樂高)法：提高效率

(1).MMCOMM 通訊裝備之 T/R 模組即用此方法完成開發，裝設一套顧客系統用來測試 T/R 設計，更換元件，很快便能找到符合需求之最佳解。

(2).具有完整 subsystem 開發能量，從 2.4GHz 到 E、W Band 都能開發，並包含天線，有溫箱測試，震動測試外包，最近也接些軍方案子。

Ka-band FMCW T/R 模組早在幾年前就開發完成，但沒有組成系統。若 MPQ-562 雷達採用 Dual band 設計，可以考慮這個商源。

九、找尋適當測試環境，避免 multipath，例如兩山頭，一邊放雷達另一邊放待測目標，並且要避免目標支撐物的回波。

十、測試裝備用現有的，自己兜出需要的以降低成本。

討論分四大系統：

（一）、RA 既有系統。

（二）、RA 更新設計系統。

（三）、S-1 將進行之系統。

（四）、DVS 系統。

(1). RA 既有系統：方塊圖及內部元件規格欠缺及系統測試如此測法，其結果無法判讀問題出在哪兒？

(2). RA 更新：缺內部細部元件資料。

(3).S-1：組長分析者系統幾乎沒有 margin，John 計算 S/I = 12 dB @ 15km without I-gain，懷疑 Clutter 亦將因 integration 而增大，所以組長放入 DSP 的 I-gain 需再檢討。

(4).Long Bui 建議提高頻段到 Ku，我認為將影響搜索時間等相關因素，不宜貿然行之。

(5).組長分析所用公式與 John 者相同，故結果相近。John 認為基本上 ok。Dr. Sih 及 Long Bui 認為 S/I=12dB 沒有 margin，硬體商源必須非常小心，稍有不慎即可能使系統失敗。但若降低 Range 需求至 10km 可以額外獲得 7dB，那就安全多了。
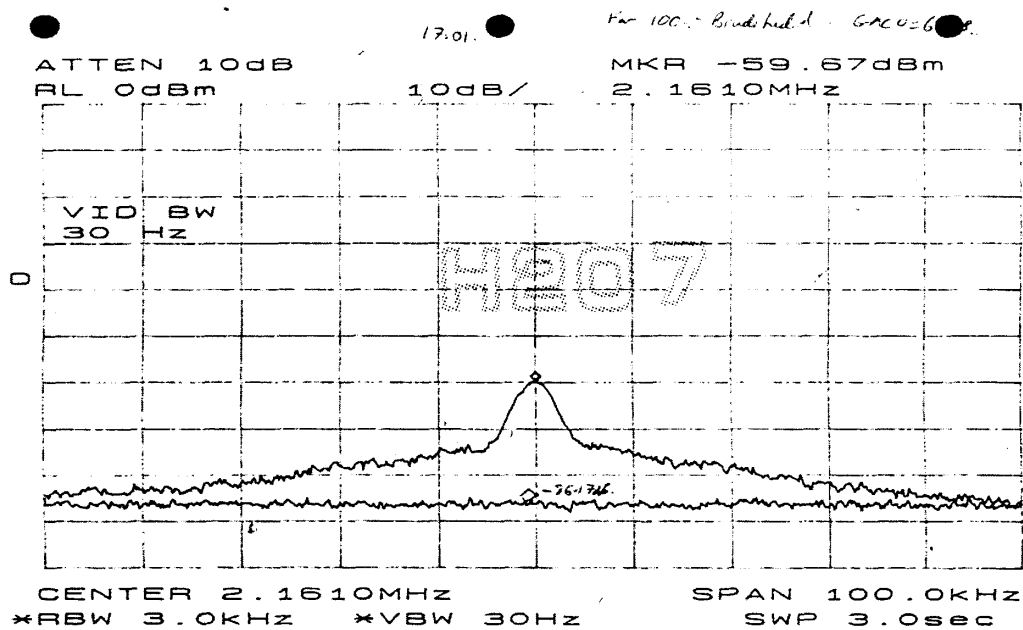
(6).DVS 目前 sweep 使用參數為 400MHz/5ms，如此回收之能量不足故無法達到 detection performance 1km 的設計規格。訊號估約損失 27dB。按第一次飛試

初估系統目前 detection range 約可達 200m 的情形看來，訊號增加 27dB 亦即系統也能達到 1km 性能。其它看來如 sweep trigger 之前 CW 與之後 FM 其 noise floor 相近，故系統大致上 ok。

Long Bui 建議 FMCW 雷達系統 Noise floor 量測基本步驟及判斷如下：

1. 天線指向天空

2. 天線前放吸收體

3. Terminate at Tx with a dummy load

4. Turn off the DC of PA

5. 天線指向真實目標（已知 RCS）

6. 天線指向模擬目標（已知 RCS）

7. 於目標前放吸收體

只需使用頻譜分析儀，從 STC 之前接出訊號測量之，2.、3.、4.、7. 項應該得到一樣的系統 Noise floor。6.、7. 項則能觀察到 RCS 及 Clutter 影響情形。（參考下圖：典型的 Noise floor 及指向已知 RCS 目標的頻譜，Long Bui 提供）

ATTEN 10dB
RL 0dBm 10dB/

17.01.

MKR -59.67dBm
2.1610MHz

VID BW
30 Hz

0

CENTER 2.1610MHz
✳RBW 3.0KHz ✳VBW 30Hz

SPAN 100.0KHz
SWP 3.0sec

參、效益分析

參加世界知名之 AOC 年會期間頂尖雷達專家講授之課程，藉此得以吸收 FMCW 雷達核心技術知識並收集相關資料以作為先進機載航電案高度計分析設計之重要參考依據。同時藉由參訪專業公司討論技術合作與引進事宜，應可獲得有助於目前計畫執行之相關資訊。此外，收集之資料對於後續建案及 FMCW 雷達技術相關應用都具有參考價值，並可增加計畫執行的前瞻性與整體效益。

此次出國獲得之效益總結如下：

（1）確定具 LPI 特性之 FMCW 雷達將成為雷達系統架構的主流。

（2）ESM 系統攔截及參數解算低功率之 FMCW 雷達訊號更加困難。

（3）已有 X-band FMCW 雷達部署服役，對低 RCS 目標的偵測距離可達 20 km，這樣的性能已具備廣泛應用價值。

（4）雷達設計者最需考量的 ECCM 技術為對抗 CROSS-EYE angle jamming。

（5）專業廠商工程師建議的測試步驟可作為律定雷達高度計商品化生產測試步驟之參考。

（6）為提昇 FMCW 雷達性能，其 T/R 次系統的設計架構有多種選擇，造價是重要因素，端視系統的應用需求而定。

肆、國外工作日程表

91.10.29-30	去程及轉機
91.10.31	ELINT and Modern Signals 課程、蒐集 FMCW 雷達核心暨關鍵技術最新之發展趨勢及資訊
91.11.01	Cross-Eye/Angle Jamming 課程、蒐集 FMCW 雷達核心暨關鍵技術最新之發展趨勢及資訊
91.11.02	轉機到洛杉磯。整理研討、合作與引進相關技術之資料

91.11.03	參訪 Goleta Engineering 公司、研討 FMCW 雷達系統分析設計及模擬等技術 (a). to introduce Goleta Engineering Company (Goleta) (b). to introduce the progress of FMCW tech. application in RA and problem encountered and then discussing (CSIST & Goleta) (c). introduction to the current FMCW application around the world (Goleta)
91.11.04	研討 FMCW 雷達系統分析設計及模擬等技術及洽談合作與引進事宜 (a). introduction to the state of art in RF front end design and system design (Goleta) (b). to introduce the new program being going to open (CSIST) (c). to discuss the possibility of creating new cooperation project in next year (CSIST & Goleta)
91.11.05	回程。

伍、社交活動

本次出國行程分兩部份：一為參加第 39 屆 AOC 年會 modern radar signal 及 CROSS-EYE angle jamming 技術的課程，收集 FMCW 雷達技術相關資訊；另一為參訪技術合作顧問公司，獲取工作上所遇問題的解決方法。除此之外並無其它之社交活動。

陸、建議事項

參見心得報告及收集到的資料不難看出 FMCW 雷達已然成為雷達設計技術主流之一。由於科技之進步，近年來，雷達技術之發展已明顯地朝向具

低功率、高偵測性能、體積小、重量輕、低價位、LPI 等優勢的頻率調變連續波(FMCW)雷達架構設計。其中又已 T/R 次系統技術最為關鍵。本組已具有雷達系統設計、軟體開發、系統整合測試等能量，但在 FMCW RF front end 部份尚須與國內外擁有這些技術的公司合作，從國外引進先進技術，厚植於國內產業，期望藉此構成完整之技術研發體系。同時按此次出國取得的資料研判，此類技術已經應用於國防上，例如 PILOT、Scout 等 FMCW 雷達。因此，建置 FMCW 雷達技術，實質上也等於建置了國防自主的重要基礎。基於此，建議：

國內(或院內)宜留意此一雷達技術發展趨勢，及早整合國內(或院內)相關技術，成立研究中心，統合國內(或院內)相關資源，適時切入 FMCW 雷達市場，並就產品創新、應用面深入探討。

RAS

ELINT and Modern Signals

39th Annual AOC International
Convention and Symposium

October 31 2002

Richard G. Wiley

Research Associates of Syracuse, Inc.

6780 Northern Blvd., E. Syracuse, NY 13057

315-463-2266 dickwiley@ras.com

RAS

ELINT and Modern Signals

39th Annual AOC International
Convention and Symposium
October 31 2002
Richard G. Wiley

Research Associates of Syracuse, Inc.
6780 Northern Blvd., E. Syracuse, NY 13057
315-463-2266 dickwiley@ras.com

RAS

Radar Signal Evolution

- The period since WWII has seen the deployment of large number of pulsed radars, seekers and other threat systems in the microwave bands
- Recently newer, high duty factor or CW systems have been deployed.
- The reduction in peak power makes EW more difficult (but not impossible)

1

Tomorrow's Radars plus Yesterday's and Today's

RAS

- There is a trend to long duration, low peak power signals to make them less vulnerable
- But older systems will still be used, too.
- Therefore EW systems must operate when both the high power, short duration signals as well as low power long duration signals are present
- Today's EW Receivers are optimized for Yesterday's Threat Environment

Radar and Interception Current Situation

RAS

- From the interceptor's point of view, there are only a few generic radar signal types to be intercepted now
- Likewise there are only a few different types of ESM receives in use
- To set the stage of considering the LPI problem, a review of the current situation is needed

Generic Radar Signals and Intercept Receivers

⬛ RAS

- There are only a few different types of radar signals in use today. (These generic types have many variations in specific detail.)
- Likewise there are only a few different types of Intercept receivers which are generally useful today. (There are also many variations and combinations of these.)
- Receivers must be selected to match signals.

⬛ RAS

Generic Radar Waveforms I

- 1. Unmodulated Pulsed Radar with nominally, constant RF. Usually modulated PRIs for MTI. High peak power.
- 2. Pulse Doppler—as above, but with Coherent RF and constant PRI bursts. (Typically 6-8 different PRIs as the beam passes a target) RF constant during the coherent processing interval. Modest Peak power.

Generic Radar Waveforms II

- 3. Similar to 1, but with Pulse Compression and lower peak power. Often has MTI and Modulated PRI Sequences.
- 4. Similar to 3, but with Frequency agility added. Frequency is constant during each MTI/ PRI Sequence.

Generic Radar Waveforms-III

- 5. Similar to 4 but with coherent RF to allow MTD processing (MTI plus Fourier Filtering)
- 6. CW or High Duty Factor for LPI. Low Peak Power. Modulation for Range Resolution (Bandwidth 1-10 MHz Typical) Repeat rate for max Ambiguous range. May be Frequency Agile from CPI to CPI

Generic Receivers

- The most common receivers today are
  - Superheterodyne (Narrow Band and tunable)
  - IFM (Crystal Video characteristics with frequency measurement on a single pulse basis if there is only one pulse present at the time of the measurement)
  - Channelized (Narrowband filter banks implemented in various ways, possibly acousto-optic) Processing problems at the outputs.

Superhet Receivers vs Generic Radar

- Narrow band. Must be Tuned to the Center Frequency
- Frequency agility is a problem.
- Nearly matched to type 1 radar if IF BW is about 1/PD. Good for types 2 and 3 radars if IF BW matched to Pulse compression code BW. (Discriminator or other intrapulse demodulator needs high SNR.)

IFM Receivers vs Generic Radars

- Lower sensitivity, but responds well to Freq. Agility. Can also demodulate pulse compression waveforms in high SNR cases.
- Misleading outputs if there are multiple pulses present at the same time (Pulse overlap)
- Poor performance vs Modulated CW in a crowded environment. No Coherence Measurement capability for Pulse Doppler.

Channelized Receivers vs Generic Radars

- Superhet replacement with wideband coverage useful for Frequency agility.
- Straddling of filter bands causes distortion
- Dynamic range limitations for signals nearby in Frequency.
- Costly. Also presents processing problems. (Strong signals enter multiple filters.)

Present Receivers

- Present Receivers generally do not match bandwidth to signal characteristics.
- Typical RF Bandwidth is 10 to 20 times the reciprocal of the PD to preserve pulse shape.
- This trades sensitivity for fidelity, but is unwise if the peak power of the signal is below the detection threshold

Generic Receivers vs Radars

Radar	Superhet	IFM	Channels
1.Simple	Best	Good	Good
2.P. Dopp.	Best	Good	Good
3. PC	Best	High SNR	Maybe
4. FA+PC	?	High SNR	?
5. 4+Coh	?	?	?
6. 5+CW	?	?	?

Threat Identification Table

- In early Threat warning systems with wide open receivers, the PRI was the first parameter used for ID. It is still a powerful threat recognition parameter
- Inverted files are used in which one enters the PRI and the possible threats are named
- If there are multiple threats for the observed PRI, other parameters are used to "break the tie"

Today's ESM Identification Strategy

- Today's systems rely on processing each received radar pulse. Measurements typically include Pulse width, RF, Time of Arrival (TOA), and Angle of Arrival (AOA)
- Pulses are sorted into "clusters" believed to have come from the same transmitter by matching PW, RF, AOA
  - note RF is not constant for Frequency Agile signals. These require added processing.

Forming Pulse trains

- Based on the clustering results, pulses are placed into pulse trains if they have "sensible" TOA sequences
- Then PRI parameters are determined
  - PRI value
  - PRI Jitter values
  - Stagger sequence and period or "stable sum"

Tie breakers

- A narrow band receiver may be used to search the frequency band used by the possible threats. For overlapping RF limits, there may still be a tie
- If threats operate with other related transmissions, the narrow band receiver may look for the associated signals
  - note: To save time, only the bands where the possible threats operate are searched

RF Agility and AOA

- Often, histogram techniques are used in clustering. If pulses have the same PW and AOA but differing RFs, one may conclude that it is a frequency agile threat
- AOA is normally a fixed value over many pulses even for moving threats
  - note: multipath effects may produce apparent AOA agility!

ESM Threat Recognition

- The ID tables used in ESM systems are built using the results of Electronic Intelligence (ELINT) efforts over long periods of time
- The ESM user customizes the world wide threat data to his region of operations
- Non-threatening signals must be handled, too (Own-ship blanking)

Reliance on Single Pulse Processing for ESM

RAS

- Today's ESM systems rely heavily on processing each individual pulse
- This is possible because the pulsed radar signals are strong enough to cross the detection threshold at tactically useful ranges
- The whole strategy breaks down if the signal is too weak to cross the threshold

Radar Vulnerability to ESM Detection

RAS

- ESM often uses peak power detection
- ESM may resort to energy detection for low peak power radars in the future
- Pulsed Radar capable of long range target detection is easily detected by ESM

Radar Vulnerability to ESM Identification

RAS

- Threat Identification is done by measuring signal parameters and using table look up
- ID Table data (initially) comes from Intelligence holdings
- Parameter variations and mimicking other signals are ways to degrade ID
- Generic Threat ID is a possibility

Generic Threat ID

RAS

- Radar performance considerations place restraints on the waveform characteristics
- Generic threat types go with certain waveform characteristics
- ESM may identify an unknown signal as a potential threat (e.g. SAM) even if the parameters do not match the specific threats in the ID table using measured parameters

What is LPI Radar Today?

- LPI Radar designers often use this term to describe radars which are not easily detected by today's ESM systems
- BUT newly designed ESM Systems may be able to detect and process today's "LPI" radar signals
- During this class we will quantify "LPI"
- You will know how "low" is "low!"

**What is the purpose
of LPI Radar?**

**Can this be done?
Under what conditions?**

Brief History of LPI Radar RAS

- Hughes/MICOM 1980s CW/Phase coded with separate antennas for Tx and Rx. Dev. model only (17Km for 3 sq m target) Later versions were built by other companies.

- Phillips Laboratory-UK devised FM/CW scheme for cancellation of leakage to allow simultaneous Tx/Rx (late 80s)

- Phillips broken up in early 90s. CelsiusTech in Sweden and Signaal in Holland market FM/CW systems

Today's LPI Radars RAS

- Netherlands
  - Signaal: Squire Portable Battlefield Surv. (Man @10km, jeep@16 km); Scout FMCW Naval/Coastal Border Surv. (Ship/Truck mount); Page FMCW Gap filler SHORAD (manpack and other platforms available) (fighter at 16 KM)

- Sweden
  - Saab (was CelsiusTech) Pilot FMCW, Shipboard, RF Switch to use existing T/R and Antenna or LPI (1MW-1W)
  - Ericsson: HARD (60W peak power in Whispering mode) used for SHORAD

- FGAN (Germany) OLPI-- Dev. Model

Random Signal Radar

- Chinese authors publish IEEE-AES paper, July 1999. Reviews history since 1960
- Reviews types of random signal radar
- Author Guosui holds a Chinese patent on a Random FMCW fuse issued in 1987.
- Projects future growth due to availability of DSP and the need for counter-ESM

LPI Radar Sensor

- April 2000 AES Systems Magazine
- Authors from Spain
- Propose Frequency Hop waveforms as better for LPI than LFM or PSK when the intercept receiver uses cyclo-stationary spectrum Analysis

Deployed LPI Radars(1998) RAS

- Scout: over 130 deployed (per MSSC)
- Squire: Development being completed.
  Project over 1000 units in 5 years (MSSC)
- Page: Production expected in 2002 (MSSC)
- Pilot: less than 50 deployed (CelsiusTech)
- Hard: (Ericsson)
- MICOM: Laboratory only
- FGAN: OLPI, Laboratory only

Squire FMCW LPI Radar RAS

Celsius

Mk2

Comparison, main principle FMCW
and Pulsed radar
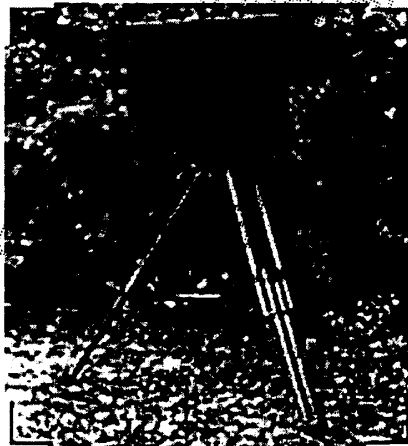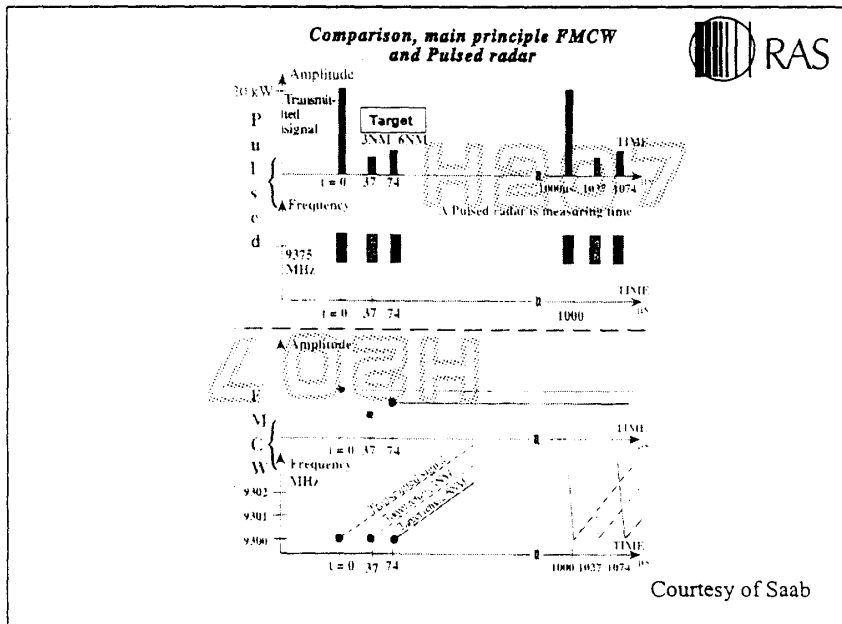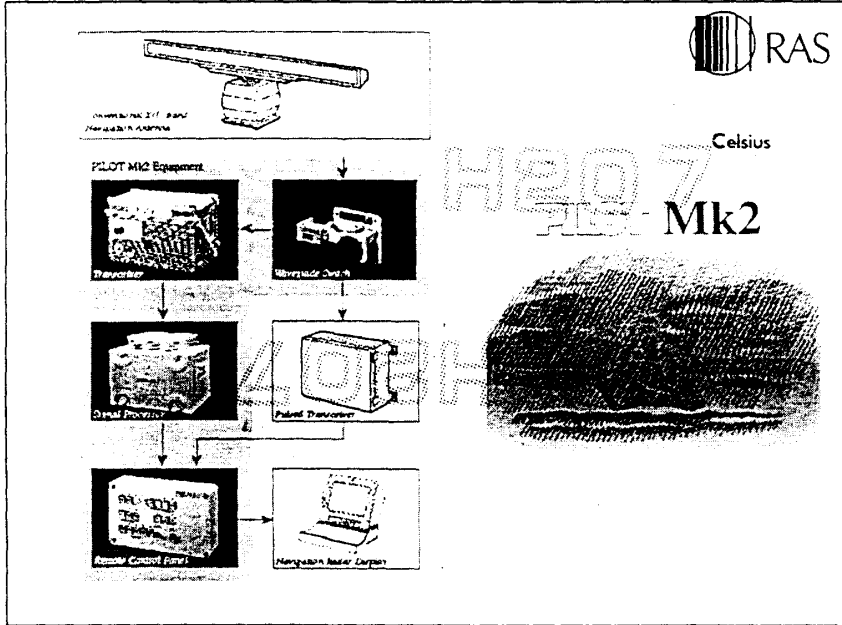
Courtesy of Saab

FMCW Range Measurement

Frequency

Transmitted Signal

Received Signal

Δ f

δ f

Delay

0

t_d

T

Time
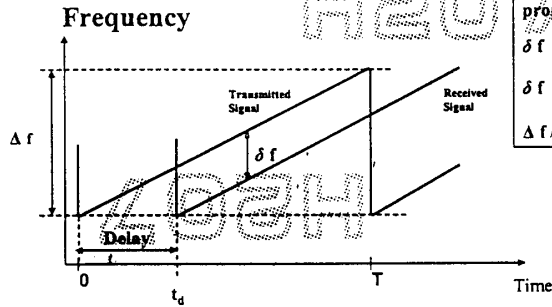
Frequency difference proportional to Range:

$\delta f = d f / d t * t_d$

$\delta f = \Delta f / T * 2R / c$

$\Delta f / T$ is called Sweep rate

The deviation Δf determines the range resolution : $d R = c / 2 \Delta f$

Courtesy of Saab

Main principle
Linear FMCW Radar

frequency

Δf

t = 0   37 74

Amplitude
After the mixer
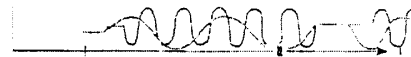
1 MHz and 2 MHz
difference frequency

$\delta f = \dfrac{\Delta f}{T} \cdot \dfrac{2R}{C}$

$\Delta f = 28 \text{ MHz}$
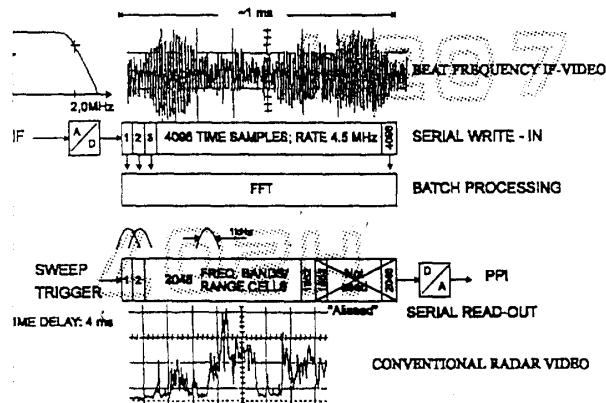
$T = 1 \text{ ms}$

$\delta f_{target 6NM} = 2 \text{MHz}$
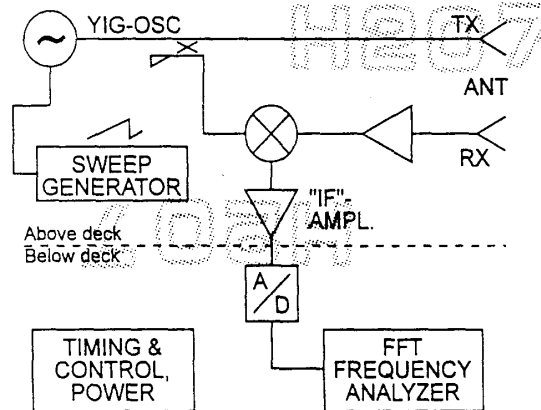
Signal processing
fast spectrum analysis

delay
4 ms

Amplitude

t = 0   37   74

Courtesy of Saab

18
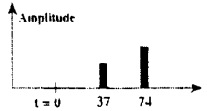
Principles of Signal Processing

~1 ms

2,0MHz

BEAT FREQUENCY IF-VIDEO

IF — A/D — 1 2 3 | 4096 TIME SAMPLES; RATE 4.5 MHz | 4096 | SERIAL WRITE - IN

FFT | BATCH PROCESSING

SWEEP
TRIGGER

TIME DELAY: 4 ms

1 2 | 2048 FREQ. BANDS/RANGE CELLS | | | PPI

SERIAL READ-OUT

CONVENTIONAL RADAR VIDEO

Courtesy of Saab

FMCW Radar Transceiver

RAS

YIG-OSC — TX

ANT

SWEEP GENERATOR

RX

Above deck
Below deck

"IF" AMPL.

A/D

TIMING & CONTROL, POWER

FFT FREQUENCY ANALYZER

Courtesy of Saab

Single Antenna Operation
Reflected Power Canceller

VECTOR MODULATOR

COMMON ANTENNA

VECTOR MODULATOR

CONTROL AMPLIFIER

LNA

LO

IF

$$\frac{RF}{IN} \quad 90° \quad 0° \quad \frac{RF}{OUT}$$

I

Q

BI-PHASE MODULATORS, ANALOG DRIVE
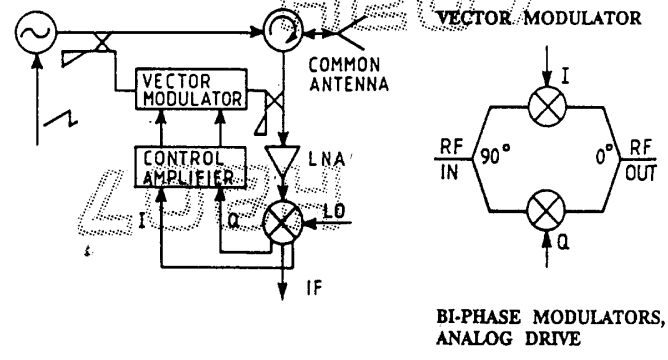
Courtesy of Saab

EW Receiver — Intercept Range

R

P

G

λ

MDS

Radar

ESM

$$R_{ESM,0} = \sqrt{\frac{PG\lambda^2}{(4\pi)^2} \cdot \frac{1}{MDS}}$$
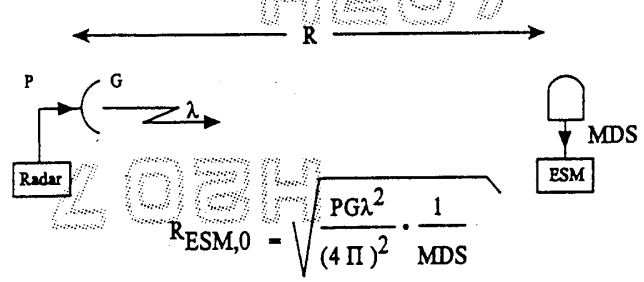
Sensitivity is expressed as MDS:

Minimum Detectable Signal, measured in "dBmi",
which includes antenna gain (a convention)

Courtesy of Saab

Radar detection and ELINT/ESM intercept ranges

⬛ RAS

(Assuming "Free space" propagation and that the (rarely occurring) case exists that the FMCW radar and ELINT/ESM antennas have their main beams pointing at each other and also that the FMCW frequency lies within the BW of the ELINT/ESM receiver)

Radar Output Power	Radar Detection Range(km)		ESM Intercept Range (km)		
	100 m² Target	1 m² Target	Radar Warning Receiver -40 dBmi	Typical Tactical ESM -60 dBmi	High Performance ESM -80 dBmi
FMCW Radar					
1 W	28	8.8	0.25	2.5	25
0.1 W	16	5	0	0.8	8
10mW	9	2.8	0	0.25	2.5
1 mW	5	1.5	0	0	0.8
Conv. Pulsed 10 kW	25	7.9	25	250	2500

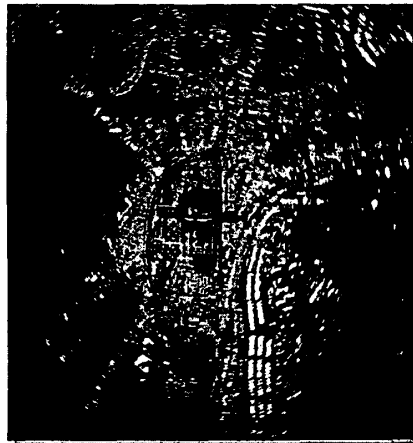Courtesy of Saab

---

Radar - ESM ranges

⬛ RAS

	1 mW	10 mW	100 mW	1W
RR 100 sqm target	5	9	16	28
ESM -40 dBmi	0	0	0	0.25
ESM -60 dBmi	0	0.25	0.8	2.5
ESM -80 dBmi	0.8	2.5	8	25
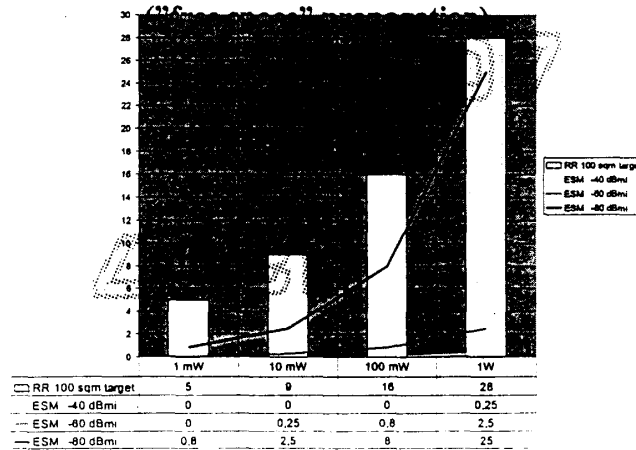
Courtesy of Saab

Advantages and disadvantages of FMCW radar

RAS

+ Low output power achieving LPI by ESM systems and ARM (Anti Radiation Missile)

+ Solid state, no warm-up time

+ Excellent close range resolution

- Limited usable output power when using single antenna due to transmitter noise leakage to the receiver

RAS

PPI picture from Saab roof in Järfälla

Modern Radar Signals

- "LPI" Radars are being deployed which use long duration pulses (or CW) and pulse compression
- CW radar must receive and Transmit at the same time--isolation problem
- The next generation of ELINT equipment must cope with these signals
- The community needs a quantitative measure of "LPI"

Low probability of Identification Radar (LPID)

- The ELINT threat recognition process can clearly be disrupted by transmitting unexpected parameters.
- Using parameters similar to another non-threatening radar is one example
- Introducing parameter agility is another
- These will probably deceive the opponent only for a short time

Low Probability of Interception

- Another is to try to make the signal so weak that the ELINT system cannot detect it.
- As we will see, for radar this can be difficult. It is this aspect that we will spend most of our time examining
- Spread Spectrum is a term used in communications. (I say it does not apply to radar!)

Radar Fundamental Principle

- Range resolution is determined by the BANDWIDTH of the transmitted signal

$$\Delta R = \frac{c}{2B}$$

Range resolution is about
150m for B=1 MHz, 15m for B= 10 MHz,
1.5m for B= 100 MHz, 15 cm for B= 1GHz

What Range Resolution is Needed for a Radar? RAS

- If the range resolution is too coarse, the returns from multiple targets will be merged together into one echo

- If the range resolution is too fine, the return from one target will be spread among many range "cells," reducing the echo power in a single range cell--making the target harder to detect in noise (but not "clutter")

Radar Function determines Range Resolution RAS

- For many military search or track radar applications, the range resolution should be on the order of the range extent of the target

- All of the echo power is in one range cell

- Thus radar signals have bandwidths of 1 to 10 MHz. For big targets like ships, the bandwidth is narrower than for small targets like missiles and fighter aircraft

Spread Spectrum

- Communications systems are referred to as "Spread Spectrum" when their modulation scheme spreads the transmitted signal over a band much wider than required by the information

- This makes the interception of the signal more difficult since the spectral density can be below that of thermal noise at the would-be intercept receiver

Generally, Radar Today is not "Spread Spectrum"

- In communications, the spreading is removed in the receiver and the message is recovered.

- In radar, the transmitted bandwidth determines range resolution. Wideband signals smear the echo across many range cells and thus reduce target detectability
  - what you transmit is what you get back
  - synchronizing the receiver *is* the ranging process

Tomorrow's Radar Techniques

- Future radar systems could be called "Spread Spectrum" if they *coherently* combine the echoes in several range cells prior to making target detection decisions
- Coherently combining the echoes means adjusting the phase of the echoes in adjacent range cells prior to adding them together.
- This requires more signal processing and cost, but could happen

Consider the Effect of a Moving Target on Bandwidth

- If the radar target is moving radially toward or away from the radar, it will be in one range cell for only a certain amount of time
- The wider the bandwidth, the smaller the range cell and the less time the radar has to accumulate echo energy

Limit on Time Bandwidth Product

- Bandwidth is related to Range Resolution
- Integration time is limited by range resolution and target radial velocity

$$B = c / 2\Delta R \qquad V = 300\,m\,/\,s$$

$$T = \Delta R / V \qquad c = 300\,m\,/\,\mu s$$

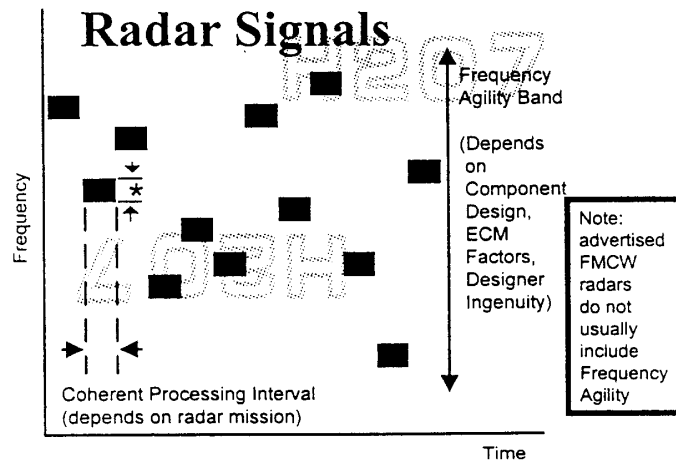$$BT = c / 2V \qquad B T < 500,000$$

Modern Radar Waveforms

- Energy on target, not peak power determines radar performance
- A CW radar has peak power 30 dB lower than a pulsed radar with a duty factor of .001, e.g. 1 microsecond Pulse Duration and 1 millisecond PRI.
- Frequency or Phase Modulation is needed to obtain the desired Range Resolution

CW Radar Reduces Peak Power

Power

Pulse-High Peak Power

CW–Low Peak Power
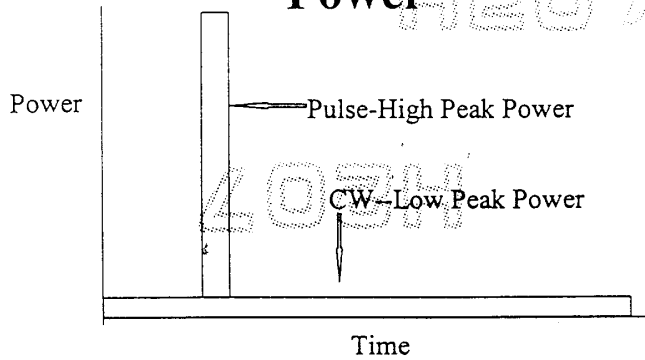
Time

Frequency/Time for Modern Radar Signals

Frequency

Frequency Agility Band

(Depends on Component Design, ECM Factors, Designer Ingenuity)

Note: advertised FMCW radars do not usually include Frequency Agility

Coherent Processing Interval (depends on radar mission)

Time

* Bandwidth Determines Range Resolution Which Depends on Radar Mission

Intercepting Modern Radar

- Lower Peak Power helps the radar
- Earlier Radar designs were concerned with target detection and with ECM
- Today's radar designs are also concerned with Countering ELINT/ESM (Intercept Receivers)
- Tomorrow's Intercept Receivers must cope with new types of Radar Signals

Types of "LPI" Radar Modulation

- FMCW ("Chirp")
- Phase Reversals (BPSK)
- Other Phase Modulations (QPSK, M-ary PSK)
- In short, any of the pulse compression modulations used by conventional radar.

Radar and Intercepting its Signal

- Now that we understand some of the constraints on time and bandwidth, we can explore how "low" is low

- Developing a Quantitative measure of LPI requires examining the radar and interception range equations

Range Equations

Signal received from the target by the radar receiver varies as range to the -4 power

$$S_R = \frac{P_t G_t G_r \lambda^2 \sigma}{(4\Pi)^3 R^4}$$

Signal received at the ESM receiver varies as range to the -2 power

$$S_E = \frac{P_t G_t G_E \lambda^2}{(4\pi)^2 R_E^2}$$

Receiver Sensitivities Compared

RAS

The radar receiver needs certain minimum signal level to do its job.

Likewise the ESM receiver needs a certain minimum signal level to do its job. We can compare these:

$$\delta = \frac{S_{E(min)}}{S_{R(min)}} \approx \frac{NoiseBWofInt.Rx.}{NoiseBWofRadarRx}$$

The term on the right assumes the same noise figure and SNR is required at both radar and intercept receivers.

Intercept Range/Radar Range

$$\frac{R_E}{R_R} = R_R \left[\frac{4\pi}{\delta} \bullet \frac{1}{\sigma} \bullet \frac{G_{TE}G_E}{G_T G_R} \bullet \frac{L_E}{L_R} \right]^{1/2} \quad (1)$$

Note that the ratio of the radar receiver sensitivity to the ESM receiver sensitivity is in the denominator. *If the radar receiver is more sensitive, the ratio of the ESM range to the Radar range is reduced*

Quantitative LPI Measure

- The ratio of the Intercept range to the radar range is the best measure of "LPI-ness"
- If this ratio is 1, then the radar detects the target at the same range that the target can detect the radar's signal
- A radar achieving a radar range to intercept range ratio of 1 could be called "Quiet"-- this term would have a precise meaning

Example for Existing Designs

- RCS =1 sq meter
- Rx Ant Gain =1, Sidelobe Tx Ant. Gain=1
- ESM Rx 20 dB less sensitive than Radar Rx
- Then the Sidelobes of the Radar can be detected at a range of over 30 times the range at which the radar can detect a target
- Main beam detection over 1000 times Radar Range

Plot of the Range Ratio

ELINT Range Advantage
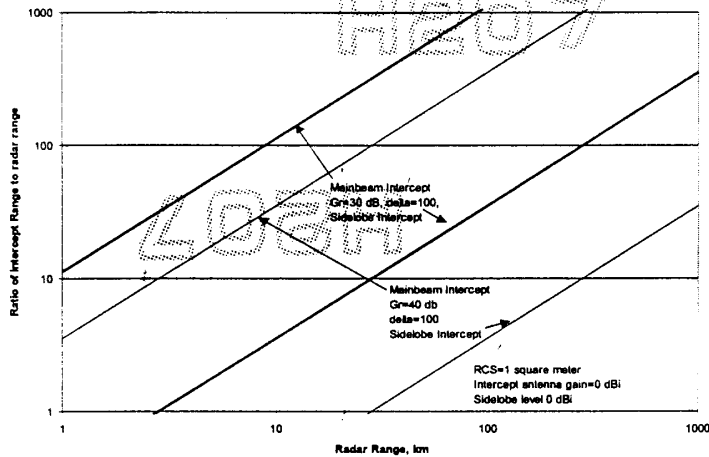
Warning Time and Range Equations

$$\frac{R_E}{R_R} = R_R \sqrt{4\pi \frac{G_{TE} G_E}{\delta\sigma G_T G_R}}$$

(From Range Equations)
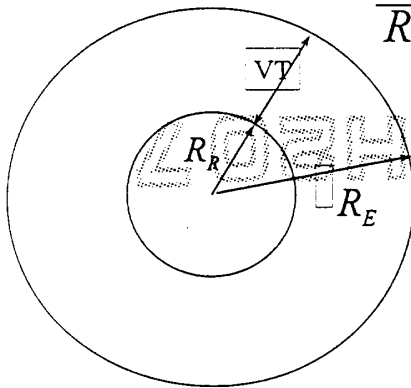
$$\frac{R_E}{R_R} = 1 + \frac{V T}{R_R}$$

(From Diagram)

Receiver Sensitivity as a function of Warning Time

$$\delta = \frac{4\pi R_R^{\,4}}{(R_R + VT)^2} \frac{1}{\delta} \frac{G_{TE} G_E}{G_T G_R}$$
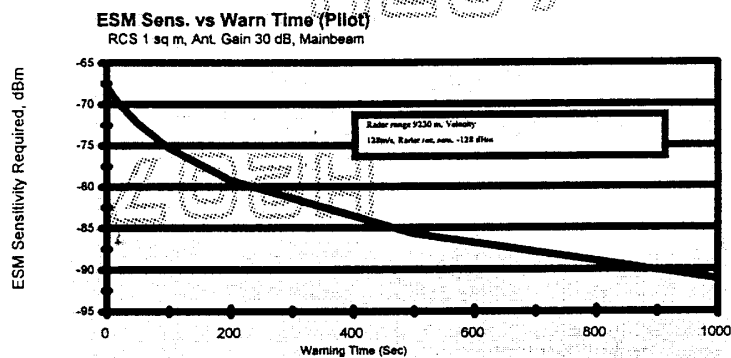

Warning Time and ELINT Receiver Sensitivity, Ship ESM

ESM Sens. vs Warn Time (Pilot)
RCS 1 sq m, Ant. Gain 30 dB, Mainbeam

35
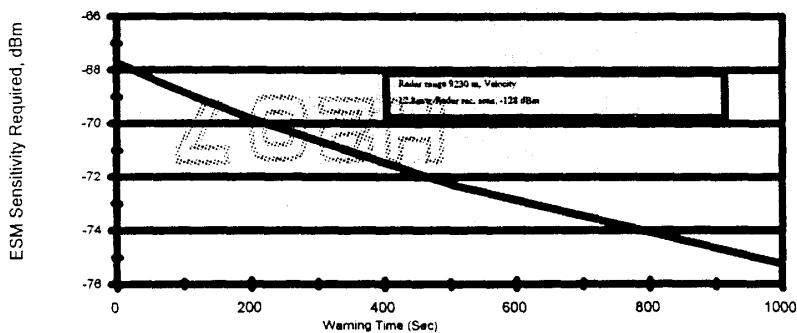
Warning Time and ESM Sensitivity, Aircraft ESM

ESM Sens. vs Warn Time (Pilot)
RCS 1 sq m, Ant. Gain 30 dB, Mainbeam

Radar Rx Sensitivity Limit

- The best the radar receiver can do is to perform a matched filtering operation on the received echoes.
- A well known result is that the SNR after matched filtering is equal to the signal energy to noise energy ratio at the receiver input

36

Signal to Noise Energy Ratio at the Radar Receiver

- Energy at the receiver input is the product of the average power times the time during which the echo is coherently integrated.

- Noise "energy" at the receiver input is the product of Boltzman's constant and the noise temperature (nominally 290 K), or -174dBm/Hz

Radar Rx Sensitivity

- For reliable detection, the ratio may need to be at least 13 dB, so the signal energy must be at least -161 dBm/Hz. (13 dB provides 90 % probability of detection and .0000001 probability of false alarm

- This means the signal energy must be at least -161 dBm/Hz

Minimum Signal Power

- The minimum Signal Power is determined by dividing the energy by its duration
- The reciprocal of its duration is often referred to as the *radar receiver's noise bandwidth*
- For coherent integration of 1 ms, the required received signal level is -131 dBm (a noise bandwidth of 1 kHz)

Can the limit be reached?

- Ideal matched receiver processing is rarely achieved in practice; also there is the noise figure of the receiver to consider. In dBs, these must be added to the minimum signal level which the radar can detect, and may increase it by 10 dB.

Generic Receiver Sensitivity

- Typical RF/IF Bandwidth 20 MHz
- Noise Floor -114+10log20+NF~-101dBm+NF
- Minimum Required Signal= noise Floor +13 to 15 dB, or~-85 dBm+NF at antenna output (Antenna gain provides additional signal level.)
- Today's typical ESM sensitivities ~-70dBm

Modern Receivers vs Generic Radars

- Digitizers can process most types of signals if the rates are fast enough.
- Different algorithms needed to match different radar signals and to do different jobs
- Parallel processing paths needed to search for different signal types in noise and interference. Each path optimized for a different generic signal

Required Transmitter Power

- Minimum ERP of Transmitter to be intercepted at 40kM @10 GHz by a receiver with -70 dBm sensitivity is +45dBW
- For sidelobe interception (0 dBi SLL), required transmitter power is 45 dBW (This is 32 KW)
- But reduced by antenna gain on the ESM receiver

Intercepting LPI Signals
at -70dBm

- Sidelobes of 1 W FMCW Radars are 45 dB below the Receiver Threshold
- Typical antenna gain of main beam is 30 dBi, therefore the mainbeam is still 15 dB below the receiver threshold at 40 kM

Receiver Strategies

- In communications and radar, it is customary to match the receiver bandwidth to that of the signal being received (best sensitivity)
- For ELINT/ESM systems, it is customary to match the RF or pre-detection or RF/IF bandwidth to the widest signal bandwidth expected and to match the post-detection or Video bandwidth to the reciprocal of the shortest pulse expected

Wideband ESM Receiver Strategy

- To achieve good probability of Intercept, ESM Receivers often choose to sacrifice sensitivity and widen the pre-detection (RF/IF) bandwidth to cover a much wider band than that occupied by one an expected radar signal
- BUT the noise bandwidth does NOT increase in proportion to the RF bandwidth if the Video bandwidth remains narrow

Wideband ESM Receivers

RAS

- Although not covered in standard radar or communications literature, wideband receivers are very common in ESM
- Sensitivity can be estimated using simple approximations; however exact computations are difficult
- One approach is to use the equations published in the 1960s by Klipper

---

Klipper Equations

RAS

A way to relate Pre-Detection SNR at the input and Video SNR at the output for wideband ESM receivers:

$$SNR_{out} := \frac{\left(SNR_{in}\right)^2}{2\cdot\left(\frac{B_v}{B_r}\right) - \left(\frac{B_v}{B_r}\right)^2 + 4\cdot\left(\frac{B_v}{B_r}\right)\cdot\left(SNR_{in}\right)}$$

$$SNR_{in} := \frac{2\cdot SNR_{out}}{\frac{B_r}{B_v}}\cdot\left[1 + \left[1 + \frac{2\cdot\frac{B_r}{B_v} - 1}{4\cdot SNR_{out}}\right]^{\frac{1}{2}}\right]$$

Klipper Equation Example

$$SNR_{in} = -1.8 \quad dB$$

$$B_v = 6.25 \cdot 10^6 \quad Hz$$

$$B_r = 1 \cdot 10^9 \quad Hz$$

$$SNR_{out} = 11.78 \quad dB$$

Amazing Performance?

- A signal weaker than the noise at the input is now nearly 12 dB stronger than the noise at the output--just by using a low pass filter!

- No magic: the output SNR would be even better if the RF bandwidth were reduced-- until it matched the bandwidth of the signal

- The video bandwidth must be wide enough to pass the signal envelope (or about one over the pulse duration, 1/PD)

Klipper Equation Comments

- Output SNR is the ratio of the signal envelope power to the noise power at the output of the detector

- Output SNR is not directly useable to obtain Pd and Pfa values from the usual curves

- The Tsui/Albersheim approximations provide the input SNR required to obtain specified Pd and Pfa values.

Klipper Equation and Noise Effective Bandwidth (NEBW)

- Consider the case where (SNR in) is much less than one and RF Bandwidth is much larger than Video Bandwidth:

$$SNR_{out} = SNR_{in}^2 \cdot \frac{B_r}{B_v} \qquad SNR_{out} := \left(\frac{S_{in}}{FkTB_r}\right)^2 \cdot \frac{B_r}{2 B_v}$$

$$SNR_{out} := \frac{\left(S_{in}\right)^2}{\left(FkT \cdot \sqrt{2 B_v B_r}\right)^2}$$

For a Square law detector SNR out is proportional to the square of SNR in

Post-Detection Filtering
Improves Output SNR

- Improvement is approximately the square root of the ratio of the pre-detection bandwidth to twice the post-detection bandwidth (Linear Detector)
- Improvement is relative to the SNR in the Input Band
- Noise Effective Bandwidth (NEBW) is often approximated as the square root of twice the product of the RF and Video Bandwidths.

Range Ratio Calculations

- ESM NEBW can be compared to the Radar Noise Bandwidth to estimate the ratio of the sensitivity of the radar and ESM receivers
- We may not choose to use a receiver with wideband RF and narrow band video-- surely we can do better. But it can help bound the LPI radar problem

Sensitivity Ratio

- For the LPI radar problem, assume that the intercept receiver must cover a wide RF band (say 1 GHz) because the signal is weak and because it may be frequency agile (more on this later)
- Also assume that the ELINT/ESM designer knows the radar signal will be present for several ms-- allowing use of narrow band video (say 1 kHz)

ESM NEBW

- Using the simple approximation, the NEBW of the ESM receiver for a 1 GHz predetection bandwidth and a 1 kHz post detection bandwidth is:

$$NEBW = \sqrt{2B_{RF}B_v} = 1.4MHz$$

Receiver sensitivity ratio

- The ratio of the radar to ESM receiver sensitivities is equal to the ratio of their noise bandwidths if both have the same NF, losses and require the same SNR to do their respective jobs

$$\delta = \frac{NEBW_{ESM}}{NEBW_{Radar}} =\sim \frac{\sqrt{2B_{RF}B_v}}{1/T_c}$$

Tc is the radar's coherent integration time

Partially Matching ESM to Radar

- If the ESM receiver matches its video bandwidth to the radar's coherent integration time, the sensitivity ratio becomes

$$\delta = \frac{NEBW_{ESM}}{NEBW_{Radar}} =\sim \frac{\sqrt{2B_{RF}B_v}}{1/T_c} = \sqrt{2B_{RF}T_c}$$

For 1 GHz RF BW and 1 ms integration time, this is 31.5 dB
For 100 mHz RF BW and 1 ms integration time, this is 26.5 dB

What about measuring as well as detecting?

- For detection, the same 13 dB SNR may be required by both the radar and the ELINT/ESM system
- To make ELINT/ESM measurements (Time of Arrival, Frequency, Amplitude, Phase, etc.) an larger output SNR may be required
- Consider the ultimate limits to such measurements

Two Aspects Explored

- The limits of parameter measurement as determined by information theory compared to the limits imposed by typical SIGINT measurement techniques
- The probability of recognizing signals as a function of Signal-to-Noise Ratio (SNR)

Information Theory

- Information theory was suggested as a means for exploring the limits of parameter measurements in *Electronic Intelligence: the Interception of Radar Signals* (Artech House, 1985)
  - The energy to transfer one bit of information in the presence of thermal noise is given by

$$E_{min} = \frac{kT}{\log_2 e} = -175.6 dBm / Hz$$

Radar/SIGINT Measurements

- In Radar and SIGINT parameter measurements, the fractional accuracy is often found to be related to the Signal-to-Noise Energy ratio
  - Here M is the value and (delta M) is the uncertainty after the measurement is made

$$\frac{\partial M}{M} = \frac{\sim 1}{\sqrt{2E / N_0}}$$

Relating these Limits on Accuracy

- Information Theory gives the minimum energy needed to for each bit of information obtained and Radar theory gives us the uncertainty in the parameter being measured
- Suppose the emitter purposely transmits its parameter value to the SIGINT Receiver!
- How does the normal SIGINT accuracy compare to the Information theory limit?

Quantitative Relationship

- Prior to the measurement, we have some uncertainty in the parameter value (U1) and after the measurement, we have some lesser uncertainty (U2). The information gained is (bits)

$$\log_2 \frac{U_1}{U_2}$$

Quantitative Relationship-2

- For radar and SIGINT measurements, the uncertainty (delta M) in the measured value (M) can be expressed in terms of the signal energy and noise density as

$$\frac{\partial M}{M} = \frac{\sim 1}{\sqrt{2E/kT}}$$

Quantitative relationship-3

- The initial uncertainty can be associated with M and the final uncertainty with delta M.

  - For example, if a receiver of bandwidth M Hertz receives a signal, we know it is somewhere within the band M. If we then use a frequency discriminator to measure the frequency, we then know its value to within delta M.

Quantitative Relationship-4

- The energy required for SIGINT measurements is related to the initial and final uncertainty as follows

$$E = \frac{M^2}{2(\partial M)^2} kT(NF) = \frac{U_1^2}{U_2^2} kT(NF)$$

Quantitative Relationship-5

- Now we can find the ratio of the energy for SIGINT measurements to the information theory lower limit

$$\frac{E}{E_{min}} = \frac{U_1^2 \log_2 e}{2U_2^2 \log_2(U_1 / U_2)}$$

Plot of E/Emin vs No. Bits of Information

RAS

Minimum occurs at about 0.7 bits, where SIGINT is 5.7 dB less efficient than the theoretical limit

For 10 bit measurements, SIGINT requires about 50 dB more energy than the information theory limit

Ratiodb

bits

.10.966
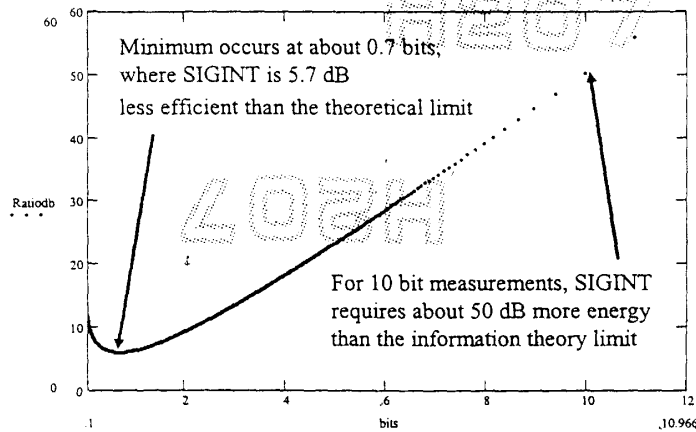
SIGINT Accuracy for Other Parametric Measurements

RAS

- The measurement accuracy for amplitude and time as well as frequency can be found in the radar literature

- The next three slides show the SIGINT measurement accuracy as a function of SNR for four important cases

Percent Amplitude Error

Phase Error (Degrees)

PW or PRI Error

Frequency Error (kHz)
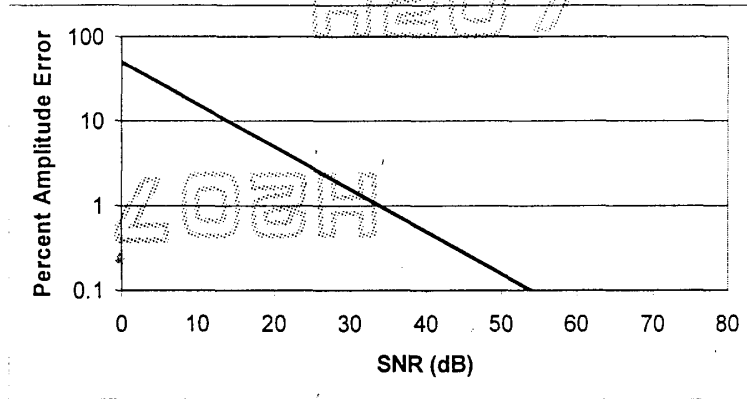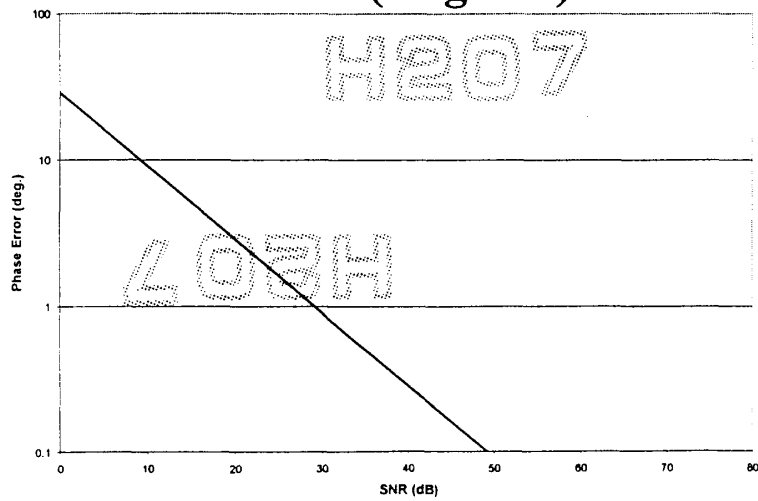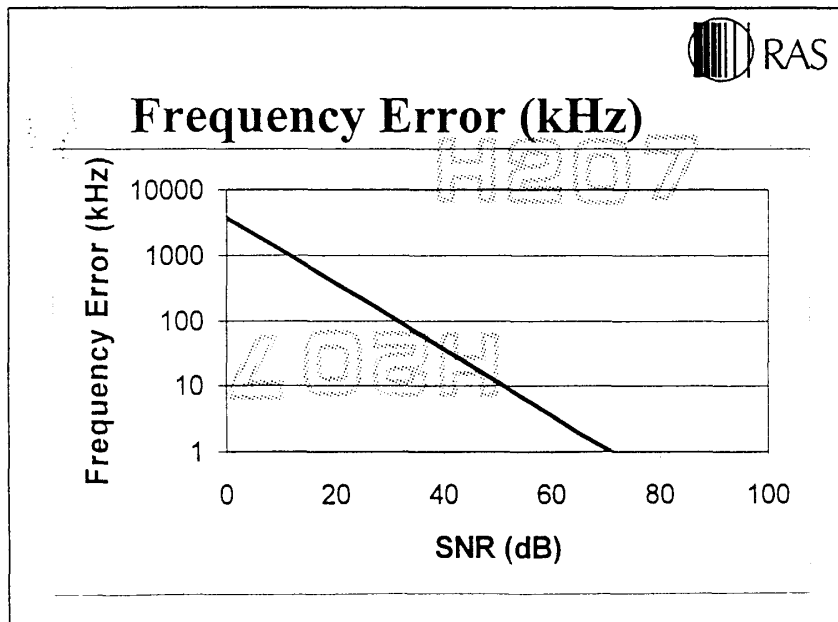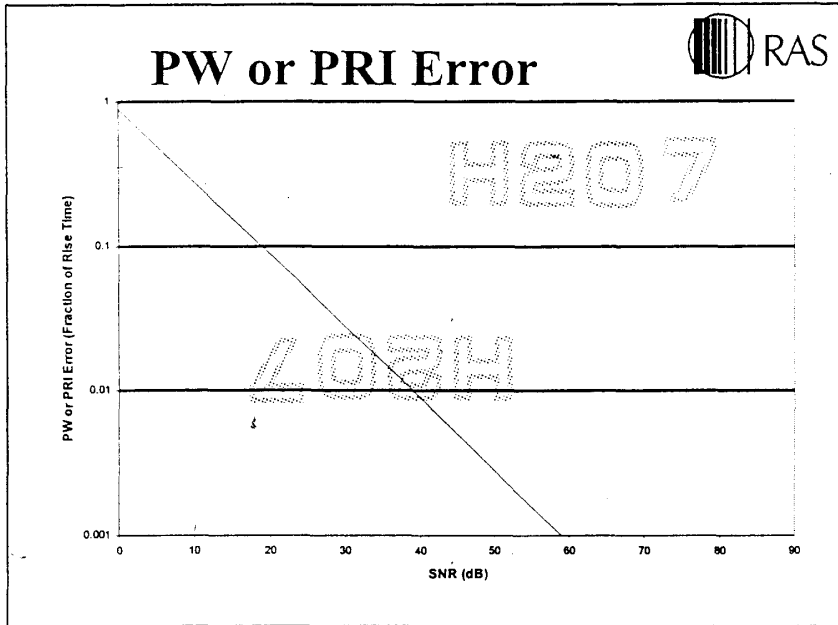
Application to Frequency Measurement ⦿ RAS

- For measuring the frequency of a segment of a signal of duration tau, the frequency uncertainty (from Skolnik, 1962) is

$$\partial F = \frac{\sqrt{3}}{\pi\tau\sqrt{2E/kT(NF)}}$$

Application to Frequency Measurement-2 ⦿ RAS

- The initial uncertainty may be taken as approximately the reciprocal of tau; that is, we need a bandwidth that wide to pass pulses of duration tau
  - Expressed in terms of initial and final uncertainty, the energy required is

$$E = \frac{3U_1^2}{2\pi U_2^2} kT(NF)$$

Application to Frequency Measurement-3

- Interpretation?
  - If you want to measure the frequency of a signal segment 0.1 Microseconds long with 10 bits of accuracy, you need 50 dB more signal strength than you would if the purpose of the signal were to transmit its carrier frequency value to you every 0.1 microseconds
  - 10 bits is one part in 1000 out of 10 MHz or to the nearest 10 KHz

What about Frequency Agility?

- With Frequency agility from one coherent processing interval to the next, the radar signal occupies a wider bandwidth and may require the ESM receiver to use a larger RF bandwidth than with no frequency agility

- As we have seen the sensitivity ratio changes in proportion to the *square root* of the RF bandwidth

Frequency Agility Effect on LPI

RAS

- Frequency agility may require the RF bandwidth of the ESM receiver to be larger than the radar's pulse compression bandwidth
- The sensitivity ratio increases by the square root of the bandwidth increase; and the range ratio decreases in proportion to the 4th root of the bandwidth increase
- FA of 10x the radar's PC bandwidth decreases the range ratio by 2.5 dB (which is a factor of ~.56)

Future ESM Receivers

RAS

- 10-30 dB Sensitivity enhancement needed to cope with modern FMCW radar threats
- One way is to use narrow beam, high gain antennas
  - then a number of receive channels is needed to cover a given angular sector. Number of receivers and antennas is equal to the antenna gain, i.e. 10 to 1000
- Another way is through signal processing

Basic ESM Enhancements ⬛ RAS

- Higher Antenna Gain
  - Payoff: Improves direction finding
  - Problems: Limits Field of View, Physical size limits some applications
- Low Noise Front Ends: High Temperature Superconductors may be practical soon.
  - payoff: system noise figures of 1 dB, sensitivity improves by 5-10 dB
  - Problems: Cost, limited sensitivity enhancement, radar can use them too!

"LPI" Radar "Codes" ⬛ RAS

- True Noise (From a noise source, stored for later correlation in the radar receiver)
- Pseudonoise (nearly unpredictable unless the interceptor has the algorithm and key)
- The code must have good ambiguity properties in range and Doppler. Unpredictability is a plus.

Correlation Random Signal Radar

- RF Correlation uses microwave delays and mixers. AM, FM or PM modulation schemes are possible (AM not used.)
- Video correlation is done after downconversion to baseband--possibly digitally
- Range is determined by the correlation delay needed to achieve a peak output

Spectrum Analysis Random Signal Radar

- For detecting stationary targets, the echo is added to the transmitted signal and the result is periodic interference patterns.
- Spectrum analysis reveals the frequency of the interference pattern, which is proportional to the range
- Problems with moving targets and other artifacts limits the use of this technique

Random Noise FM radar-1

- Noise is used to frequency modulate the transmitted signal. Then the rms difference frequency between the transmitted signal and the echo is a function of the delay to the target
- The known correlation function of the noise is compared to that obtained from the rms frequency difference to find target range

Random Noise FM radar-2

- The same FM by noise signal is transmitted and mixed with the transmitted signal. A moving target at zero range has a line spectrum at the Doppler frequency
- According to Guosui, longer range widens the spectrum and range is proportional to the power difference in the frequency range (FDmin to FDmax) compared to the power in the band (FDmax to 3FDmax)

RAS

ESM Receiver Strategies

- Detection of a random signal radar using only the energy has the advantage that the detection performance is largely independent of the radar waveform
- Detection based on specific properties of the radar signal can be more efficient
- Radar usage of code/modulation diversity may defeat ESM designed for specific signal properties.

RAS

Signal Processing Techniques

- Non-coherent methods (radiometer) use average power over times comparable to radar's integration time, e.g., milliseconds (10-15 dB improvement)
- Coherent methods which use "nearly matched" filters, e.g., Wigner Hough Transform for linear FM signals (15-25 dB improvement)
- Cross Correlation method

Non-coherent Approach RAS

- Rapid Sweep Superhet Receiver (RSSR) proved usefulness of noncoherent or post-detection integration against LPI signals
- Technique should be routinely applied to processing wideband receiver outputs for discovering LPI signals
- Sensitivity improves with square root of n, number of sweeps per pulse
- Hough transform can be applied when chirp exceeds processor IF bandwidth

Frequency Versus Time: RAS Environment and RSSR Sweeps
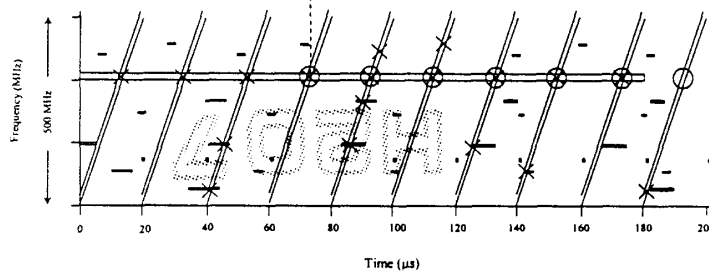
Note: 1 This shows one long pulse/CW (pulse compression) of low SNR with eight low duty cycle pulse trains of high SNR
2 RSSR outputs for M=4, N=8 begin at the fourth sweep ⊗ or ○ X provides no output.
3 Microscan outputs occur for all of the strong short pulses but not the weak long pulses

63

Envelope Techniques

- RSSR uses many samples of the envelope prior to making a detection decision
- Various M/M, M/N and other statistical techniques for sensitivity enhancement can be used
- The past analog implementations could be done digitally in software and applied to a widband digital data stream

---

Required IF SNR
Pd=.9, Pfa=1E-6 (single Pulse SNR=13.2dB)

- M/N integration; N determined by signal duration during its Coherent Processing Interval or Pulse Width (M optimized).
- Note: PW values shown are for 512 MHz Sweep Band. Reducing the Sweep to 256 MHz reduces the minimum PW by a factor of two.

N=8	N=16	N=32	N=64
PW>160us	PW>320us	PW>640us	PW>1320us
M=4	M=6	M=8	M=12
SNR=7.3dB	SNR=5.4dB	SNR=3.4dB	SNR=1.7dB
Gain=5.9dB	Gain=7.8dB	Gain=9.8dB	Gain=11.5dB

M/N Integration; N Large

Detection and False Alarm Probabilities
IF SNR=-1.5 dB

Pd,1=.118; Pfa,1= .0298
Pd, 256=.9; pfa, 256=.000001
Threshold =2.65
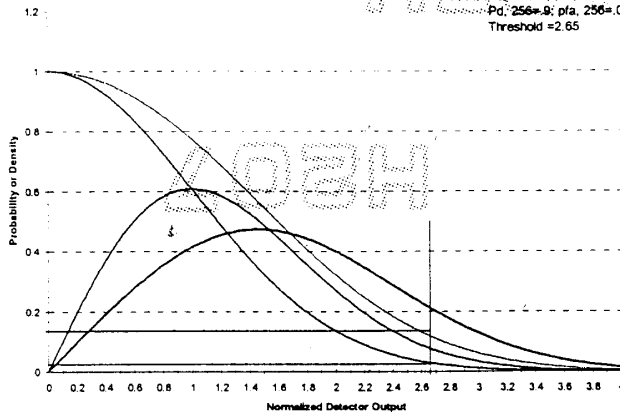
RSSR Display Example
Operator Threshold Set Aid
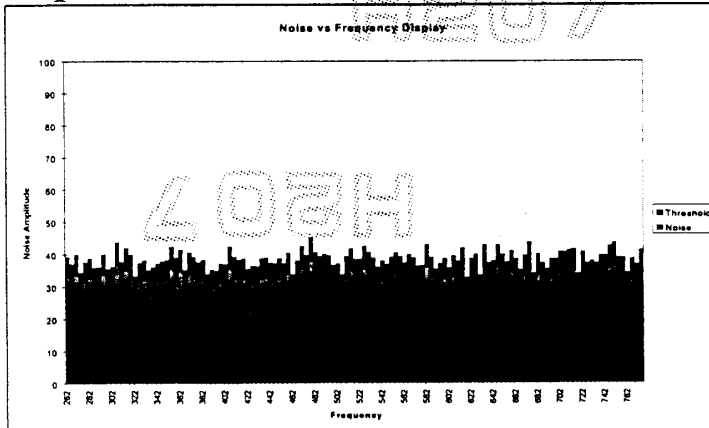
RSSR Display Integration
Count vs Frequency
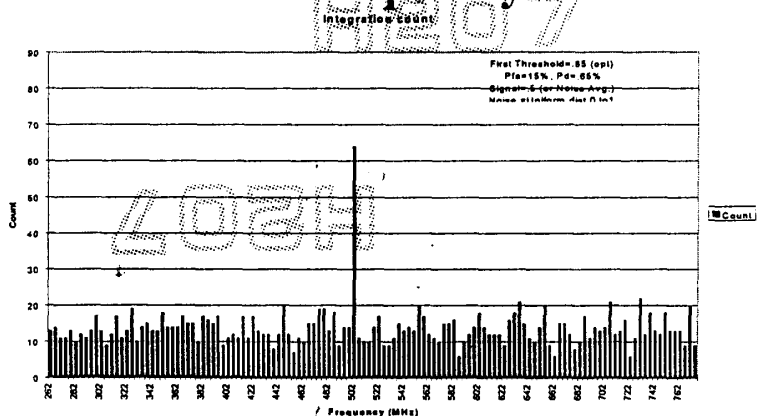
RSSR Raster Display
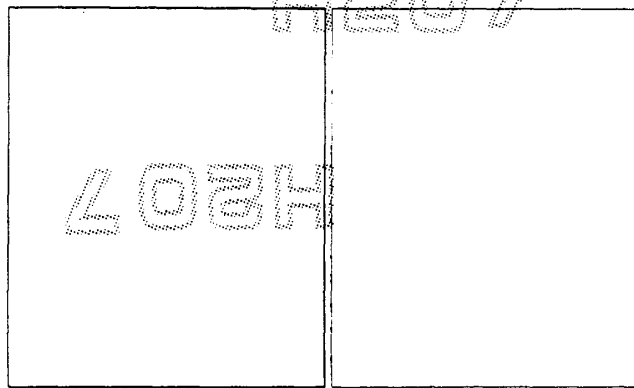
RSSR Raster Display

RSSR Raster Display

67
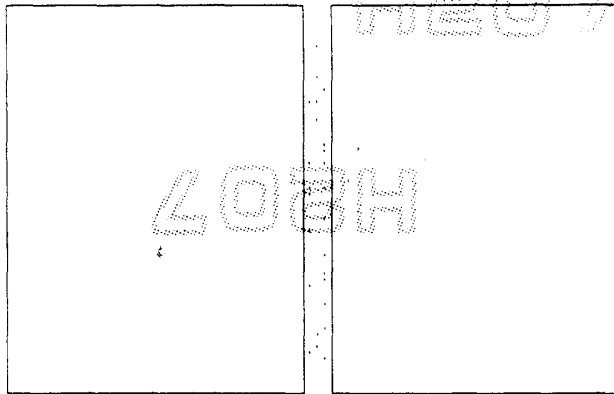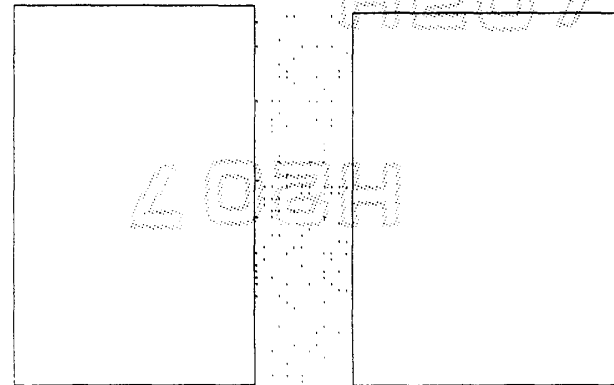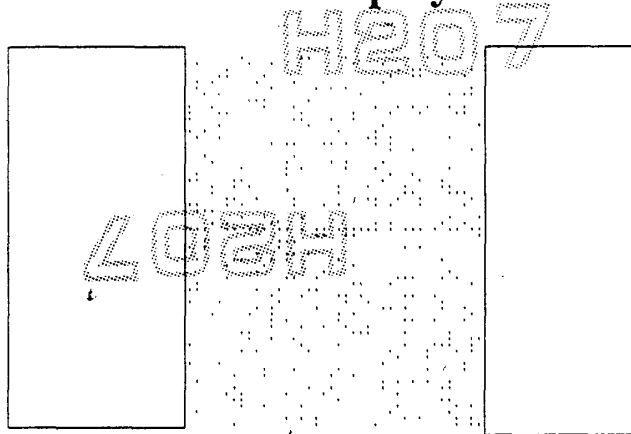
Typical LPI and Conventional Radars

	LPI Radar	Conventional Radar
Peak Power	0.1W - 10W	10 KW to 100 KW
Duty Factor	~1	.001 - .0001
Time x Bandwidth	1,000-10,000	1
Antenna Gain	30 dB	30 dB
Antenna Sidelobes	-50 dB	-30 dB
Range Resolution	50 meters	50 meters
Maximum Range	15 n. mi	15 n. mi
	(RCS 100m^2)	
Frequency Agility Bandwidth	10%	none

Example Problem
Radar and ELINT
Parameters
(Transmit Power 1 W)

FREQ	= 10000	MHz
ERPmb	:= 30	dBw
P_t	= 1	w
G_{tmb}	= 30	dB
ERPsl	= -10	dBw
P_t	= 1	w
G_{tsl}	= -10	dB
σ_{sqm}	= 10	RCSsqm
B_e	= 50	MHz
F_e	= 23.25	dB
G_e	= 22.3	dB
L_r	= 6	dB
L_e	= 0	dB

SNR at Radar
and ELINT Rx
for Sample
Problem

Range in km

——— Radar SNR on 10 sqm
——— SIGINT SNR on radar ERPmainbeam
——— SIGINT SNR on radar ERPsidelobes
— — Radar SNR in rain
— — SIGINT SNR on radar ERPmb in rain
— — SIGINT SNR on radar ERPsl in rain
— — threshold SNR for detection
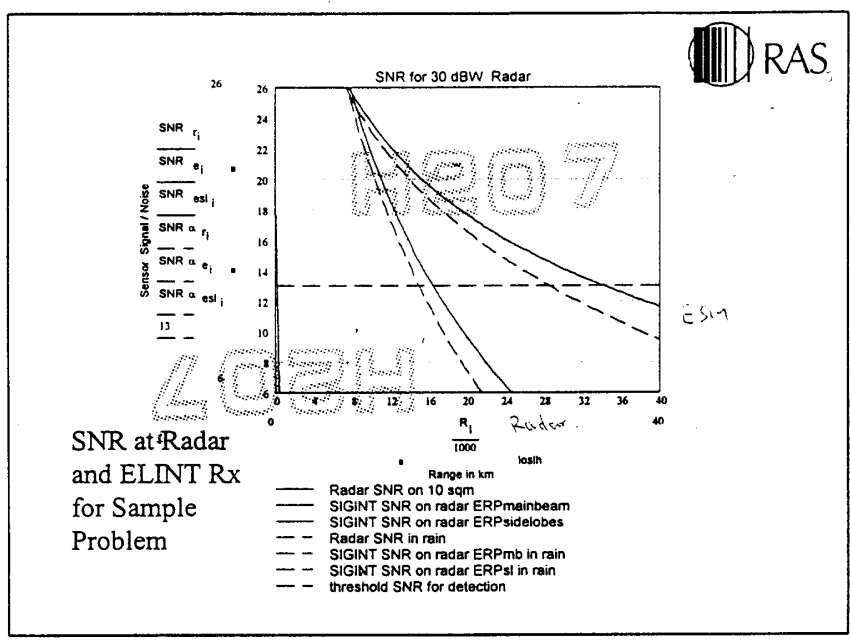
Range Comparisons for Pilot Radar

Target Cross-section	Radar Range (km)		ESM Sensitivity	ESM Range (km)	
(m²)	10KW Pulsed Radar	1W FMCW Radar	-dBmi	10KW Pulsed Radar	1W FMCW Radar
10	15	16	-60	250	2.5
100	26	28	-80	2,500	25
1,000	46	0			

Intercept Range/Radar Range=2.5/16=.156
=25/28=.893

Optimized Intercept Rx Regains Range Advantage

[logo] RAS

Sensitivity prior to Non-coherent Integration

-114 dBm/MHZ + 10 log 10 MHZ + NF + SNR

= -87dBm for NF=4dB and SNR=13 dB

Sensitivity with non-coherent integration
for one beam dwell of 8.3 ms
and Rx Sweep time of 10 microseconds:

$$IntegrationGain = (8300/10)^{.5}$$

$$Sensitivity = -87 - 14.6 = -101.6dBm$$

Intercept Range Increased from 25 to 134 km

Channelized Receiver Plus Non-Coherent Integration

[logo] RAS

- The RSSR IF bandwidth was chosen to include the energy of the entire pulse compression waveform
- This allows it to receive all types of modulations without knowledge of the particular waveform used
  - Suppose the interceptor knows the LPI radar uses Linear FM. Can the interceptor do better?

Emitter Signal Characteristics

- **LPI**
  - Surveillance radars (Scout, Squire, ...)
  - ASM Seekers (RBS 15 Mk 3...)

- **High PRF**
  - SA-10
  - Air Intercept (APG-63/65/66/70)
  - SPQ-9B

- **Agility**
  - PRI
  - Wideband Frequency

Time-Frequency
View of RF
Environment
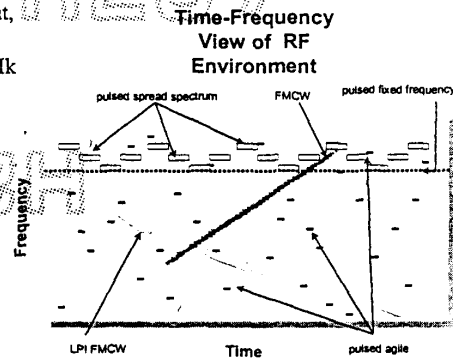
(Courtesy of NRL)

Optimum Receiver Channel Bandwidth for Linear FM

- Linear FM is a common choice for LPI radar waveforms

- Is there an optimum choice for achieving the best sensitivity for a channelized receiver?

- Instantaneous Frequency for Linear FM:

$$f(t) = f_c + at$$

72

Channel Response Time

- For a channel bandwidth of B, the signal must be present for approximately 1/B seconds to reach full output amplitude
- For a signal with frequency *vs* time slope of "a" Hz/s, the time the signal is present in a channel of bandwidth B is

$$\tau = B / a \geq 1 / B$$

Bandwidth choices for LFM

- The minimum channel bandwidth is therefore

$$B \geq \sqrt{a}$$

For a slope of 1 MHz per ms, the min. bandwidth is 31.6 KHz. (Regardless of the extent of the frequency ramp!)

NEBW independent of Bandwidth!

- If channel bandwidth larger than the minimum is used, the number of channels excited by the LFM sweep is reduced, but the signal dwells in each channel for a longer time.

- As a result the NEBW is unchanged as the channel bandwidth is increased!

- The max. bandwidth is determined by the extent of the FM, "DF" *This is the RSSR case*

Wider Channel Bandwidths

- When the bandwidth of the channel is "b," the signal dwells in that bandwidth for a time equal to b/a

  - If the channel envelope detector is followed by a low pass filter whose bandwidth is half the reciprocal of that time, the channel NEBW is independent of b!

$$NEBW = \sqrt{2b(a/2b)} = \sqrt{a}$$

Channel BW choice can be based on factors other than slope

- LFM radar signals can be detected with a NEBW which is independent of Channel BW:

$$NEBW = \sqrt{a}$$

For a=1 Mhz per ms, proper Rx design yields NEBW=31.6 KHz, with channel BW up to DF, using post-detection integration.

Note: This is the NEBW for a single channel. Wide band Channels obscure the frequency.vs time waveform.

Post Envelope-Detection Channel Combining

- If the extent of the LFM is "DF" and the slope is "a," the duration of the ramp is DF/a. A receiver with the minimum bandwidth will have "n" channels excited as the frequency ramp sweeps through the channels:

$$n = DF / \sqrt{a} = aT / \sqrt{a} = \sqrt{aT}$$

Sensitivity after combining

- The sensitivity improves approximately as the square root of "n," making the NEBW equal to

$$NEBW = \frac{\sqrt{a}}{\sqrt{n}} = \frac{a}{\sqrt{DF}} = \sqrt{\frac{a}{T}}$$

Combining the Channel Outputs

- For Linear FM, the best approach is to combine the channel outputs along a line that traces the frequency *vs* time modulation of the radar
- An algorithm that does this is the Hough Transform (used in image processing).
  - Without knowledge of the slope or the starting time, the computational load is heavy

Example for the Pilot Radar

- Assume a=1MHz/ms, DF =1 MHz
- Channel NEBW=31.6 kHz.
- Number of Channels excited per sweep=31.6
- After non-coherent addition, the NEBW is reduced by a factor of 5.6 to 5.6 kHz
- The NEBW of the Pilot radar is 1 kHz
- An optimized SIGINT Rx is only 7.4 dB less sensitive than the radar receiver

"Coherent" Approaches

- "Coherent" means processing prior to the envelope detector
- Frequency-Time Processing detects Linear FM signals in Noise
  - (Wigner-Hough Transform; puts the Hough transform before taking the magnitude of the Time-Frequency distribution
  - Time coincident pulses detected separately
- Cross-Correlation--performance is independent of waveform

Predetection ESM Sensitivity Enhancement

- Wigner-Hough Transform
  - Approaches Coherent Integration
  - "Matched" to Chirp and Constant MOP
  - Separation of Simultaneous Pulses
- Provides Parametric Information about Frequency and Chirp Rate

---

Filter Banks give T-F Distribution

Wavelet Transform $W_r(t,s) = \langle r, \tau, D, g \rangle$

Gabor Transform $G_g(t,s) = \langle r, e, \tau, g \rangle$
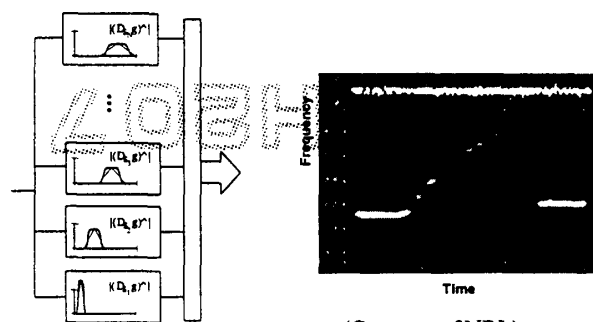
(Courtesy of NRL)

Wigner-Hough Transform

Wigner – Ville Transform

$$W_{x,x}(t,f) = \int_{\tau=-\infty}^{\infty} x(t+\tau/2) \cdot x^*(t-\tau/2) \cdot e^{-j2\pi f \tau} d\tau$$

Wigner – Hough Transform

$$WH_{x,x}(f,g) = \iint W_{x,x}(t,v)\delta(v-g\cdot t)dtdv$$

$$= \int W_{x,x}(t,f+g\cdot t)dt$$

W-H SNR Improvment

- Near Coherent Integration Performance
- If SNR*N>>1, within 3 dB of Ideal
  - Similar to expression for Cross-Correlation Performance

$$SNR_{OUT} = \frac{N^2 \cdot SNR_{IN}^2}{2 \cdot N \cdot SNR_{IN} + 1}$$

W-H Transform Example

- 20 Mhz Chirp
- 1 usec Pulse Duration
- 200 Mhz Sample Rate
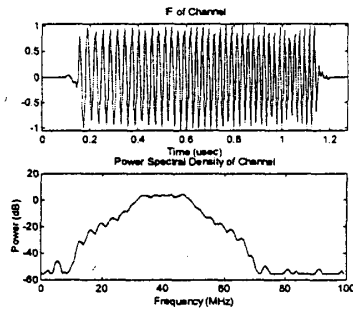
Time-Frequency Transforms
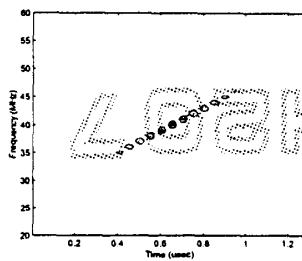
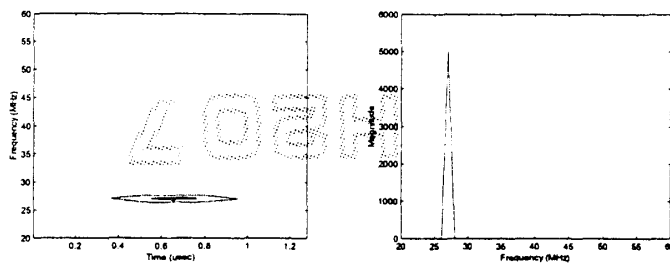- W-V Transform   Power Spectrum
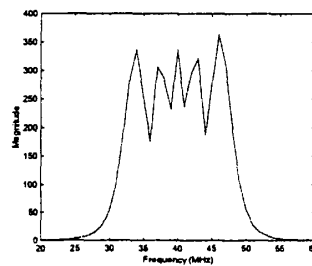
Spectrum Level ~300
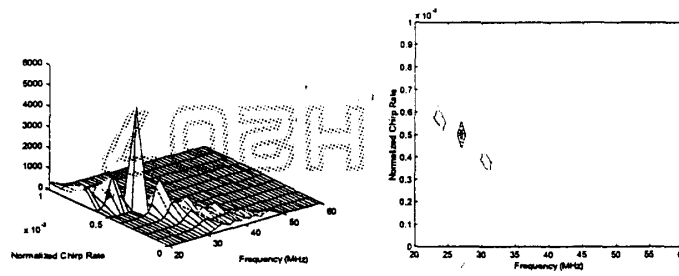
Intermediate Steps
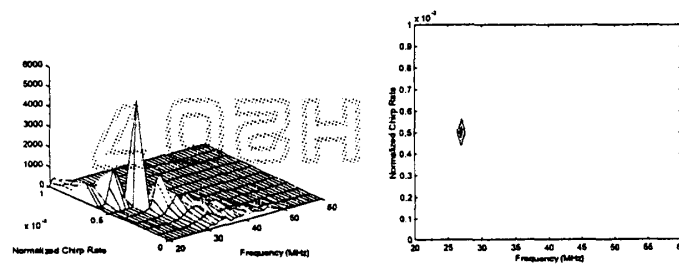# in W-H Transform
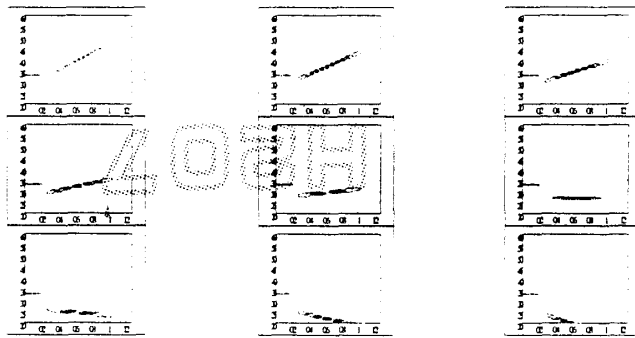
Chirp "Rotated"

Spectrum level ~5000
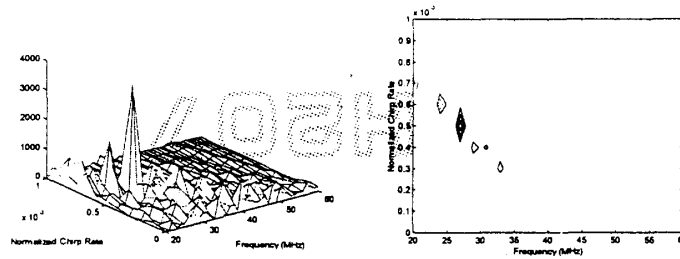or 12 dB higher

81

Wigner Hough Transform
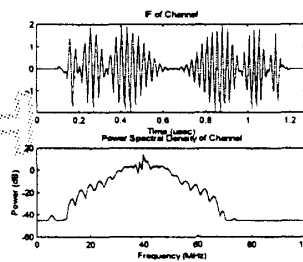

W-H Transform
(12 dB SNR)

8

W-H Transform
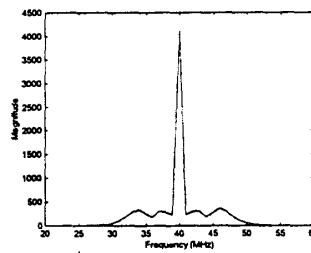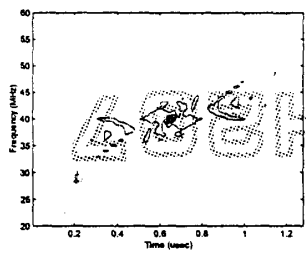# (0 dB SNR)

Simultaneous Signals

- 2 Pulses
  - Same Center Frequency
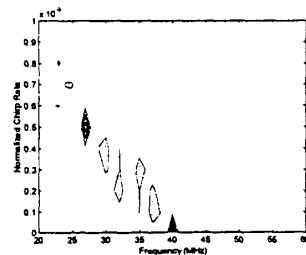 - Same TOA
- Pulse 1
  - 20 Mhz Chirp
- Pulse 2
  - Constant RF

Wigner-Ville Transform

W-H Transform-simultaneous signals
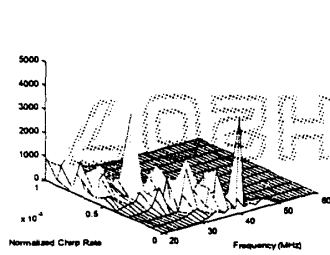
Time-Frequency Approach

RAS

Processing Model
(Courtesy of NRL)

RAS
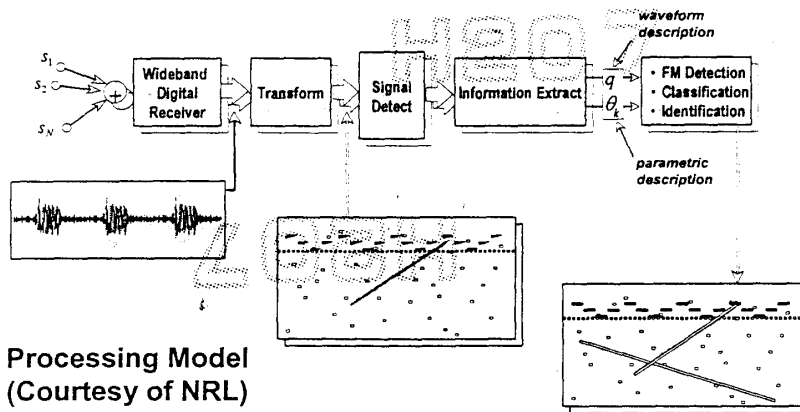
Cross-Correlation Method

- Requires two channels with two antennas
- Sensitivity enhancement can be sufficient to deal with modern LPI FMCW radars on the battlefield ("almost coherent")
- Processes all modulation types equally well (Phase codes as well as FM)
- Provides AOA, Frequency and Bandwidth information

Cross-Correlation Block Diagram
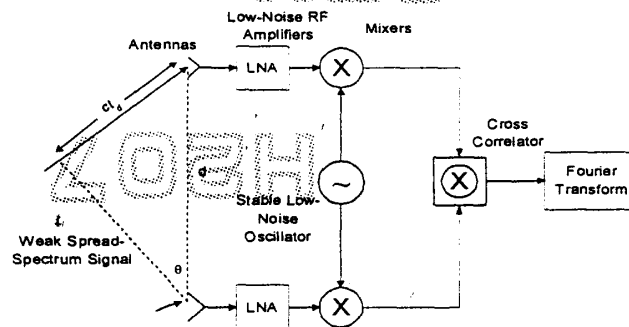
Cross-Correlation (con't)

- Does not provide knowledge of the modulation type
- Modulation may be determined via high gain antenna directed toward the AOA of the LPI signal (dedicated ESM Rx)
- Significant signal processing load
- Wideband Cross-Correlation (large BT) beyond the current State-of-the-art(?)

Cross-Correlation Performance

$$SNR(Spect.dens.) = \frac{z(B/b)^2 SNR^2(in)}{1 + 2(B/b)(SNR(in))}$$

B=Receiver Bandwidth
b=Signal Bandwidth (Assumed less than B)
z="Zoom factor"=ratio of Correlation time to duration
       of central part of correlation function (~10/b)

Note: For (B/b)SNR(in)<<1, this expression
        is approximately equal to the numerator.

Performance Example

- For B=100MHz, b=10MHz, T=1ms,
  z~1000, SNR(in)=0.1 or -10dB

- Sensitivity enhancement~25 dB;
  SNR(Spect. Dens.)=+15dB

- Cross-correlation calculation is intensive
  (2BT=200000 data points).

Choosing Corrrelation Parameters ⬛ RAS

- Correlation Time (T) is on the order of the radar's time on target or Integration time (Typically 1-10 ms) Long enough to provide integration gain but not so long that the signal changes "very much"
- Receiver Bandwidth (B): wide to minimize search time; narrow to minimize noise and A/D speed. (Several times wider than the likely modulation bandwidths.)

Modern Intercept Receivers vs LPI Radar ⬛ RAS

- Integration over times on the order of 1-10 ms over bandwidths on the order of 100 MHz. are required to cope with short range FMCW or Phase coded radars expected on the modern battlefield. (BT~1,000-100,000)
- Fast A/D conversion and DSP are the keys to implementation of these ESM strategies.

Implementation Problems

- Today's digital systems detect and measure signals with SNR=~13 dB (20:1)
- To detect signals at, say -7 dB SNR, the LSB of the A/D converter must be about 20dB lower than it is now. For an 8 bit A/D, there is ~48dB of dynamic range.
- Therefore, ~11-12 bit high speed A/D converters are needed in tomorrow's systems

The Future of LPI Radar-I

- Present LPI radar designs are effective against currently deployed intercept receivers (NEBW~10 MHz; ~30 dB advantage for the radar)
  - Even so, their Quiet range is of the order of 20 Km
- Next generation Intercept Receivers may decrease their NEBW to within 10 dB of that of the Radar receiver

Implementation Problems

- Today's digital systems detect and measure signals with SNR=~13 dB (20:1)

- To detect signals at, say -7 dB SNR, the LSB of the A/D converter must be about 20dB lower than it is now. For an 8 bit A/D, there is ~48dB of dynamic range.

- Therefore, ~11-12 bit high speed A/D converters are needed in tomorrow's systems

---

The Future of LPI Radar-I

- Present LPI radar designs are effective against currently deployed intercept receivers (NEBW~10 MHz; ~30 dB advantage for the radar)
  - Even so, their Quiet range is of the order of 20 Km

- Next generation Intercept Receivers may decrease their NEBW to within 10 dB of that of the Radar receiver

The Future of LPI Radar-II ◫ RAS

- LPI Radar may use
  - Hough-like integration across range, angle and Doppler to combine echoes coherently ("Track before Detect")
  - OLPI: main beam as low as today's sidelobes
  - Multistatic: may disperse Tx and Rx assets
- R-squared *vs* R-fourth
  - not changed by technology (LPI radar is very difficult if the interceptor adapts)

References ◫ RAS

- Wiley, R. G., *Electronic Intelligence: the Interception of Radar Signals*, Artech House 1985, Chapter two. "LPI radar and the Future of ELINT"
- Wiley, R. G., *Electronic Intelligence: the Analysis of Radar Signals*, Second Edition, Artech House, 1993, Chapter 1
- Kosinski and Wiley, "Information Theory Applications to SIGINT," 37th Annual AOC International Symposium and Convention, October 1-4, 2000, Las Vegas, NV
- Guosui, Hong, Weimin, "Development of Random Signal Radars,"*IEEE Trans. on Aerospace and Electronic Systems*, Vol. 35, No.3, July 1999
- Wirth, W. D., Long Term Coherent Integration for a Floodlight Radar, IEEE International Radar Conference Proceedings, 1995
- Burgos-Garcia, Sanmartin-Jara, Perez-Martinez, and Retamosa, "Radar Sensor using Low Probabilty Interception SS-FH Signals," IEEE-AES *Systems Magazine*, April 2000
- Leavers, V. F., *Shape Detection in Computer Vision using the Hough Transform*, Springer-Verlag, 1992,
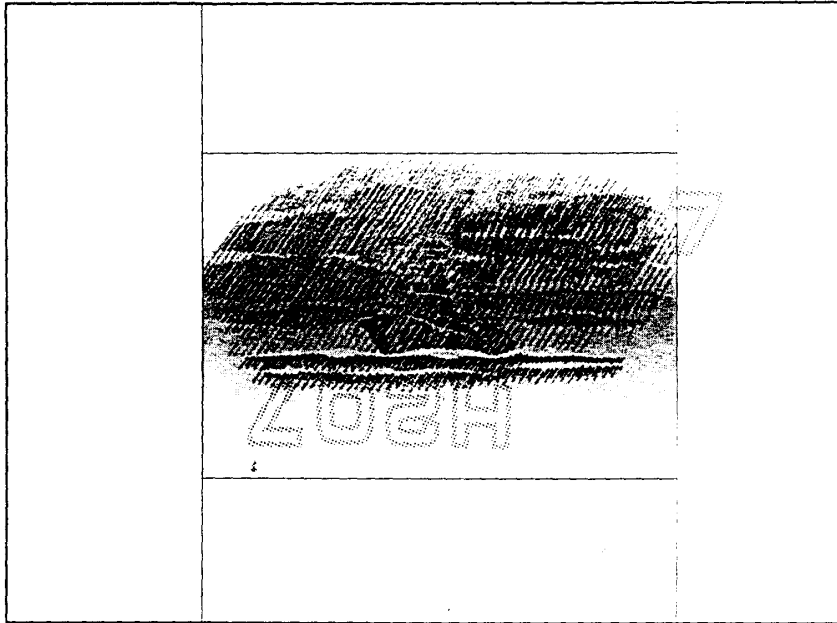
CROSS-EYE

and other
angle Jamming Techniques

By Dr Filippo Neri
Assistant to ELETTRONICA spa President
(e-mail: filippo.neri@elt.it)

CROSS-EYE

and other
angle Jamming Techniques

By Dr Filippo Neri
Assistant to ELETTRONICA spa President
(e-mail: filippo.neri@elt.it)

Summary

- Need for angle jamming
- Well known angle jamming techniques
    - angle blinking
    - cross polarisation
    - Expendable Decoys
    - Towed Decoys
- Cross-Eye
- Conclusion

Need for Angle Jamming Techniques

**Conical Scan
Tracking Radar:**

Angle information are
available only after
a scan period.

Thes type of radar can
be jammed by Amplitude
Modulation:
- Swept
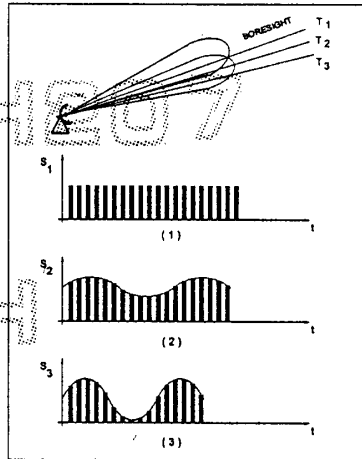- Inverse Gain

---

COSRO

COSRO and LORO radar perform
scan on receiving antenna lobe only

Jog Detection
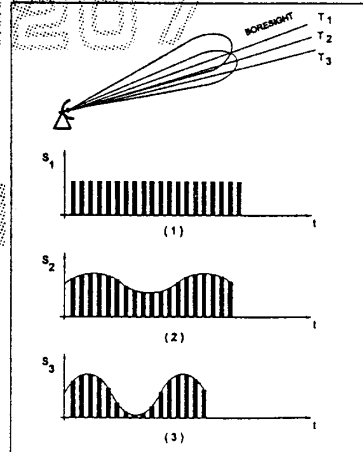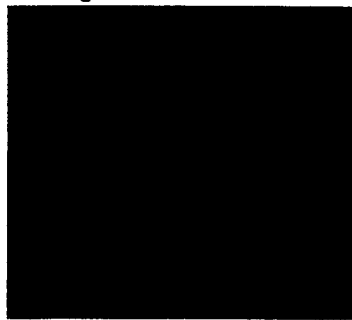
Monopulse Tracking Radar
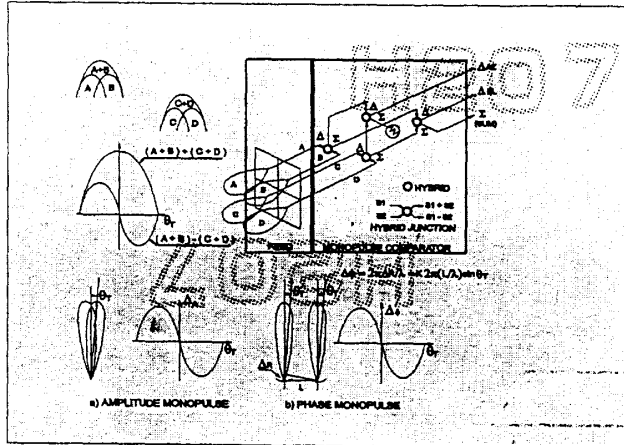
Monopulse Radar Block Diagram

3
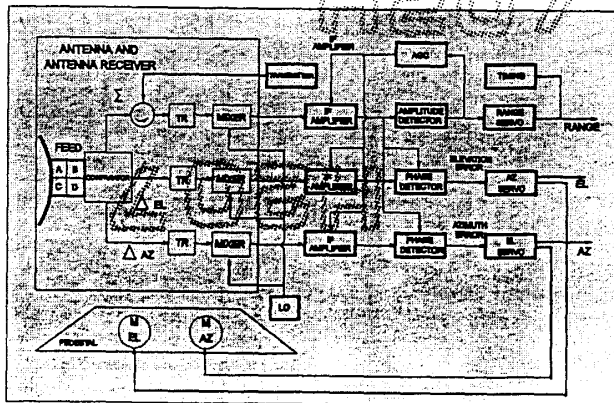
Angle Information in one pulse (Monopulse)
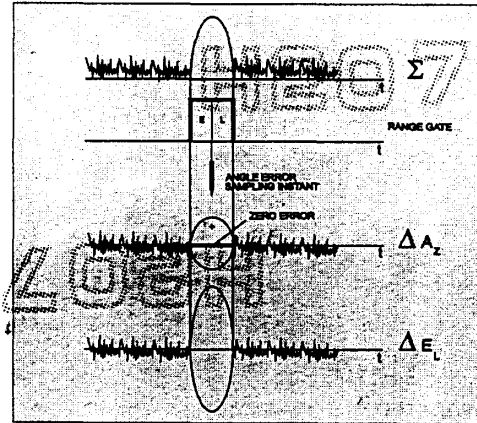
Pulse Doppler Radar
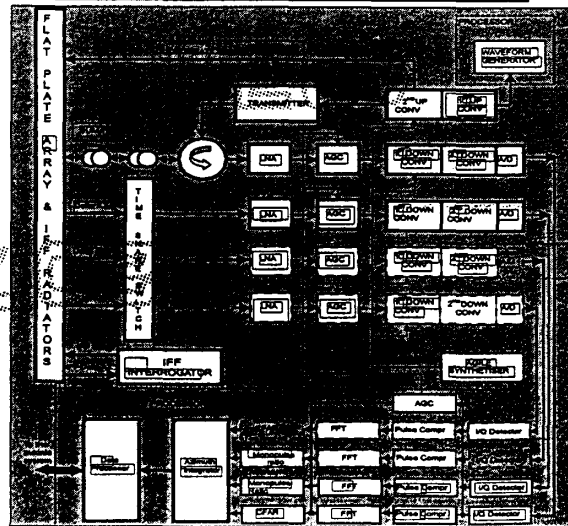
Pulse Doppler Radar ECCM capability

PD Processing can destroy the effectiveness of traditional RGPO Jamming

---

Tracking Radar Needs

1- Range gates

2- Velocity Gates (CW)

3 - Range & Velocity Gates (PD)

4- AGC or Log-Receiver to keep the received signals at the foreseen level (for tracking loops stability)

General Monopulse Jamming

1- **Noise Jamming**: to remove the capability of Range Tracking (useful to protect extended targets, like ships)

2- **Deception Jamming (RGPO or VGPO)**: to move the Range/Velocity gates in a wrong position.

But ...

ECCM EFFECTS

Frequency Agility strongly
reduces
Noise Jamming Effectiveness

f
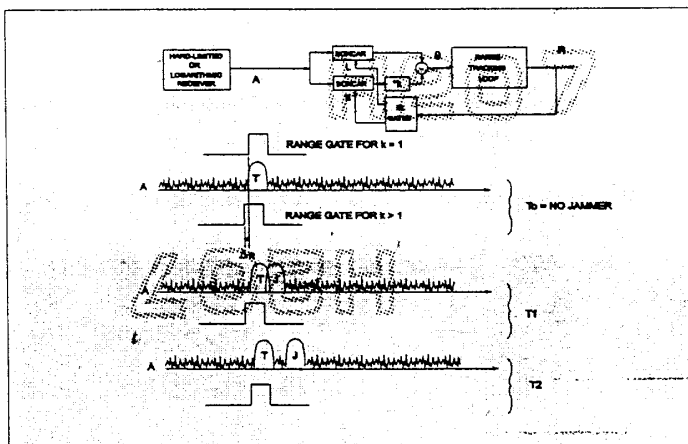
ARGS Prevents RGPO

ARGS Prevents RGPO
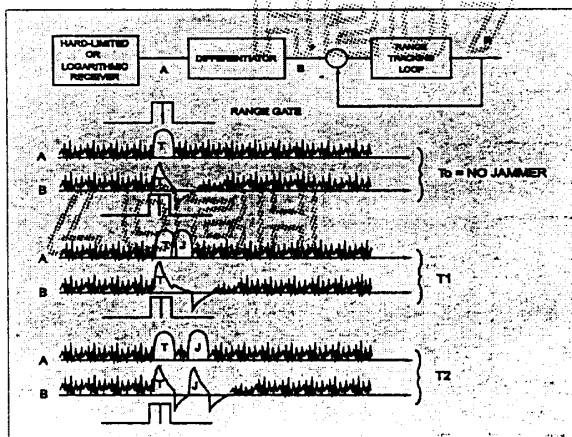
Need for Angle Jamming

For the above considerations, the conclusion is that it is necessary to:

1) Jam Monopulse Tracking Radar directly in ANGLE

2) Avoid the necessity of Range/Velocity Pull Off

Pag. 15

Well Known Angle Jamming Techniques

- Angle blinking
- Cross polarisation
- Expendable Decoys
- Towed Decoys

Pag. 16

8

ANGLE BLINKING

Angle Blinking

Many clever
solutions have
been studied to
avoid Range or
Velocity Gates
separation

Angle Blinking Performances
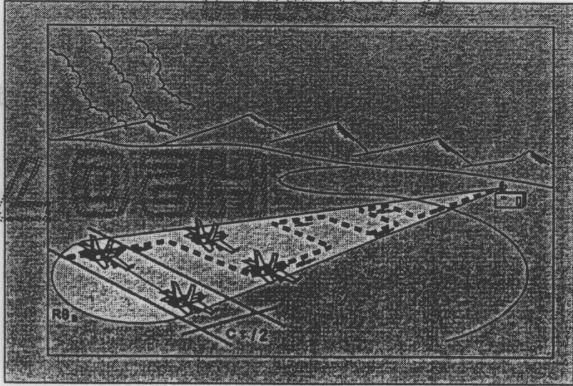
The angle blinking performances against missiles
depend upon:
- blinking period
- blinking duty
- sources distance
- missile loops time constants
- max lateral acceleration

Angle blinking Summary

- Good performances, but effectiveness linked to
many factors
- possibility of sources separation
- In the airborne case, two platforms are required

CROSS POLARISATION

Pag. 21

CROSS POLARISATION

Concept:

Pag. 22

Cross Pol - Basic theory
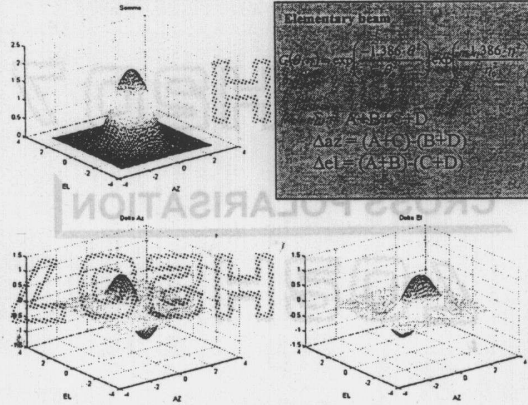
Antenna copolar Sum and delta channels

Cross Pol Basic theory
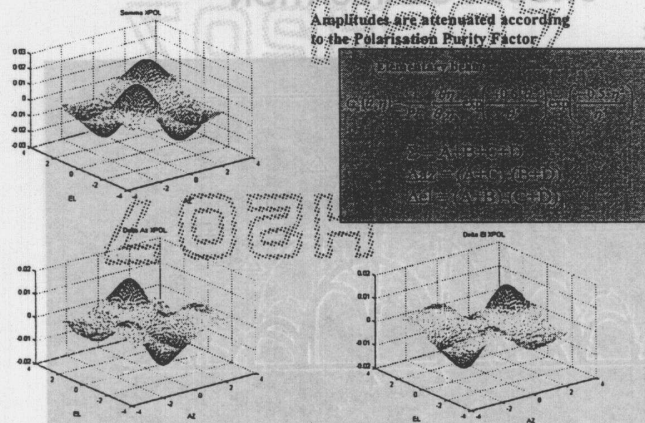
Antenna cross-pol Sum and delta channels   (See Appendix 1)

Cross Pol: equilibrium points

Polarization 90 deg. Pattern Gain
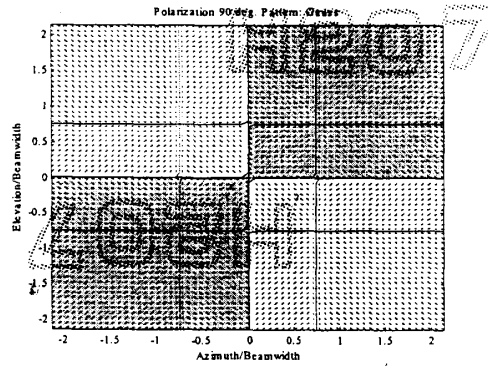
Jammer Cross plarised. Pol: 90°, PF: 20 dB

Pag. 25

Cross Pol: inaccuracies effects

Polarization 89 deg. Pattern Gain

Jammer Cross Pol. Pol: 89°, PF: 20dB

Pag. 26

13

Cross Pol: inaccuracies effects

Polarization 88 deg. Pattern: Gauss
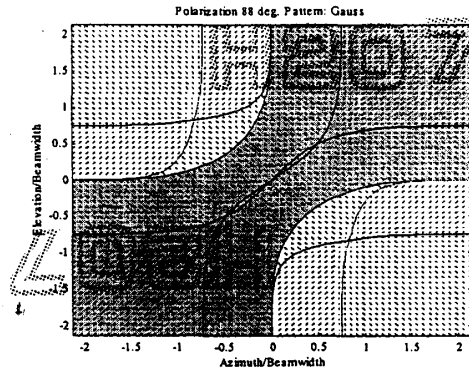
Jammer Cross Pol. Pol 88°, PF: 20 dB

Pag. 27

Cross Pol: inaccuracies effects

Polarization 80 deg. Pattern: Gauss
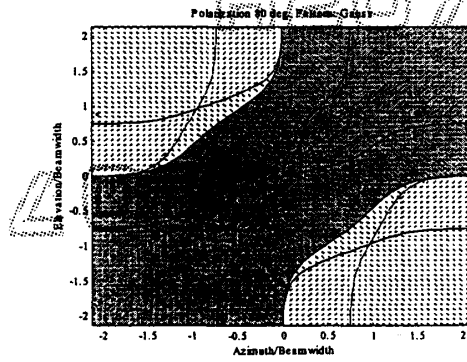
Jammer Cros Pol. Pol: 80°, PF: 20dB

Pag. 28

14

Cross Pol: inaccuracy and Purity Factor effect
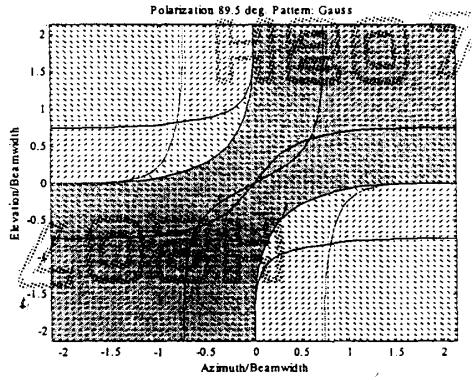
Jammer Cross Pol. Pol: 89.5°, PF: 30dB

Cross Pol: inaccuracy and Purity Factor effect
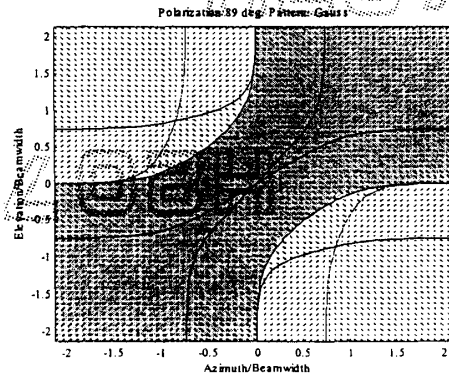
Cross Pol Jammer. Pol: 89°, PF: 30dB

Cross Pol Inaccuracies and Purity Factor effects
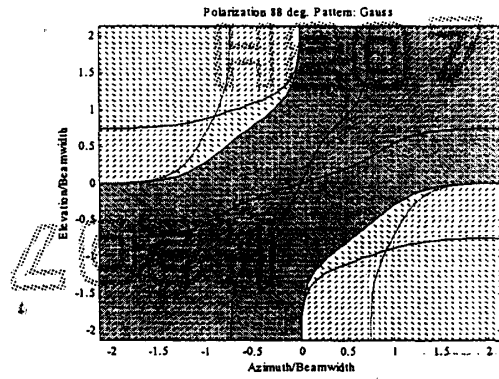
Cross Pol Jammer. Pol: 88°, PF: 30 dB

Cross Pol experimental results
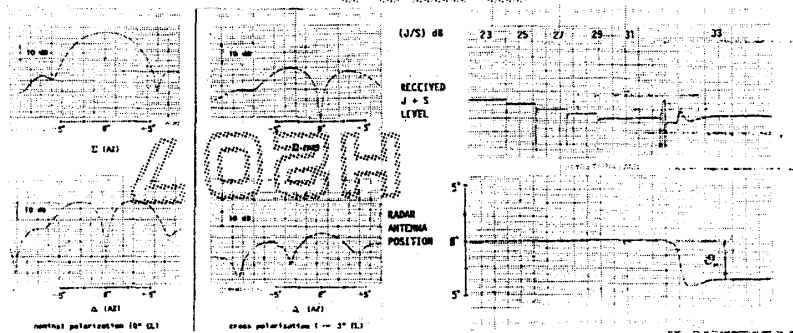
Cross Pol Implementation

1- Swept

2 - Adaptive

Pag. 33
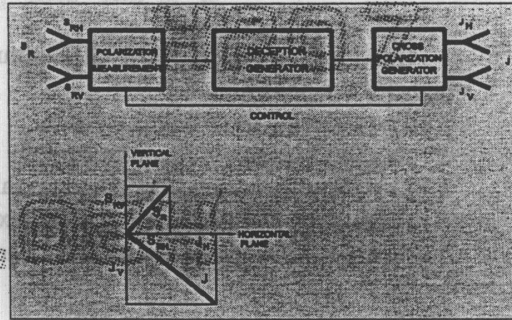
[handwritten right margin: Because we dont know the right direction signal comes]

[handwritten left margin: 90°]
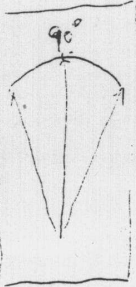
Cross Pol Exploitation

1 - Angle Jamming

2 - Reliable angle offset

Pag. 34

17

Cross Pol Summary

1 - Good for long distance ANGLE Jamming, where high J/S are possible
2 - Can generate large angular errors
3 - At short ranges may require RGPO!
3 - Lower performances against terminal threats
4 - Swept type does not require complex installation
5 - Strongly depends on radar Purity Factor

TOWED DECOY

Towed Decoy

Concept

NB: to avoid heavy weight winch, after use, the decoys
deployed by fighter aircraft are released.

Towed Decoy Implementation Challenges

1 - Aerodynamics: many manufactures show in 99%
of the time of their presentation how the decoy
deployment and flight are smooth.
2 - Payload: to accommodate in a small volume high
power transmitter
3 - Waveforms: so far only CW repeater. Since more
complex waveforms are required, next Towed Decoy
generation will use complex signals generated in the
aircraft ECM units. The signals are sent to the Decoy
through a Fibre Optic cable (FOTD)

Towed Decoy criticisms

Criticisms done in the recent past:
1 - "g" limitations
2 - manoeuvres limitations
3 - Deployment time

Towed Decoy Considerations

Achievable ERPs ensure good performances (J/S)
against semi-active missiles and low aircraft RCS.

Problems could arise for other weapon types:
- command missiles
- active missiles
- Anti Aircraft Artillery

Necessity of FOTD and High ERP.

Towed Decoy Limitations

Blind cone

BLIND CONE APERTURE (Degrees)			
FUSE SENS. RADIUS	TOWING CABLE LENGTH		
	50m	100m	200m
10	23.6	11.7	5.9
20	47°	23.5	11.7
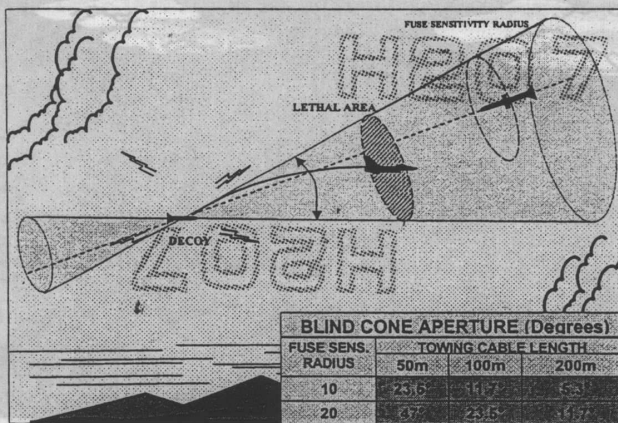
Pag. 41

Solution to Blind Cone

- Evasive manoeuvres (in what direction?) or

- Waving

Pag. 42
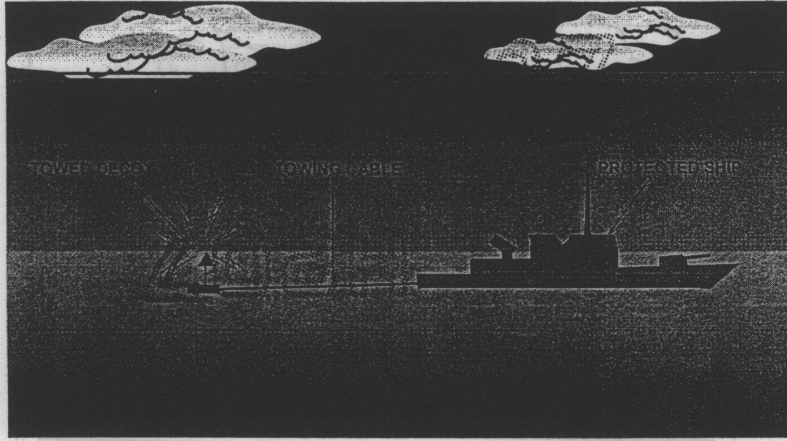
TOWED DECOY (NAVAL)

Pag. 43

Naval Towed Decoy

Problems:
- Multithreats
- sea state
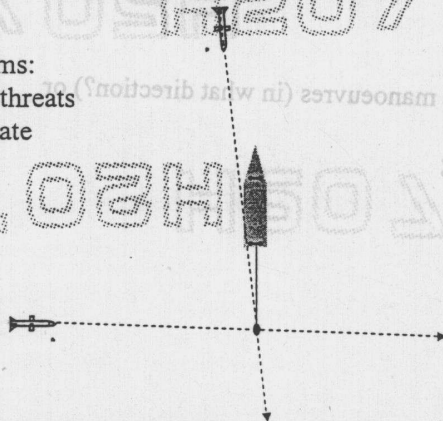
Pag. 44

Towed Decoy Summary

- It is capable of "POSITION" error

Airborne
- signals valid against semi-active missiles
- problems in front and rear sectors
- not easy installation
- Very high life Cycle Cost (one month of war operation can require thousand towed decoys)

Naval
- affordable solution
- sea state dependent
- low multithreats capability

Pag. 45

EXPENDABLE DECOY

Pag. 46

23

Expendable Decoys
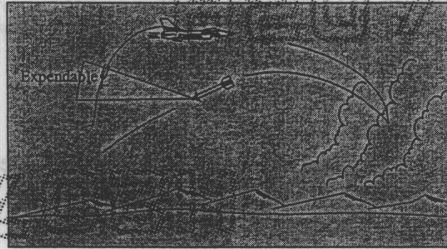
Concept

Airborne Expendables decoys are tailored to specific threats. We will consider only Naval Expendable Decoys

Naval Expendable Decoys

Concept: a low cost flying platform will carry a Repeater Jammer to attract the incoming missile.
It generates a Position error

Naval Expendable Decoy Requirements

- High ERP to seduce missile seekers
- Credible waveforms
- Multi-threats capability
- Very short reaction time to counter late seeker switch-on
- Long endurance

Naval Expendable Decoy Summary

- Provides Position error
- Difficult to get a low cost platforms
- Settling time can be too long
- Susceptibility to false alarms
- Dedicated crew could be necessary for platform control
- Very high Life Cycle Cost

CROSS-EYE

Cross Eye Concept

■ To exploit the same Phenomena of Multipath (Nodding)
to let the radar/seeker track the target is in a different position

TRUE
TARGET

IMAGE

26
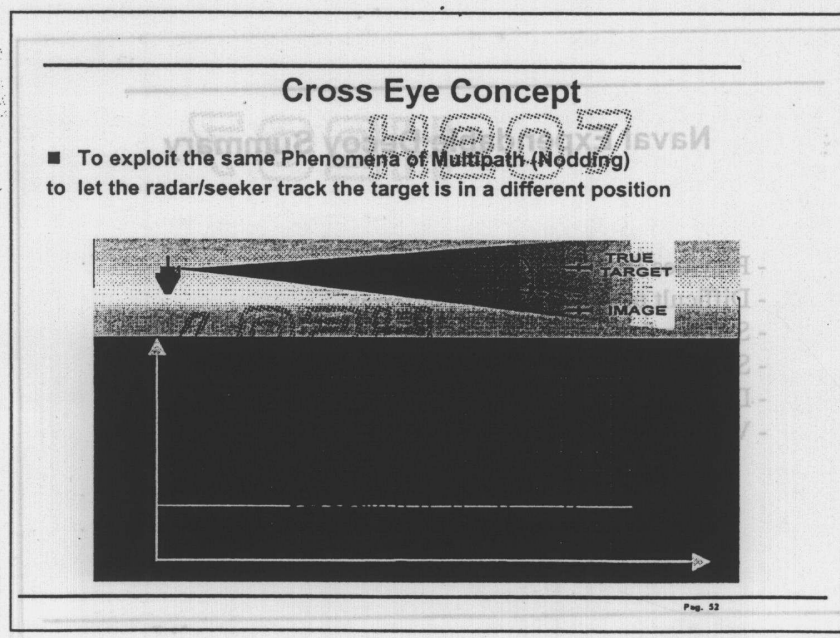
MULTIPATH EFFECT ON SEARCH RADAR: " LOBING"

FREE-SPACE COVERAGE
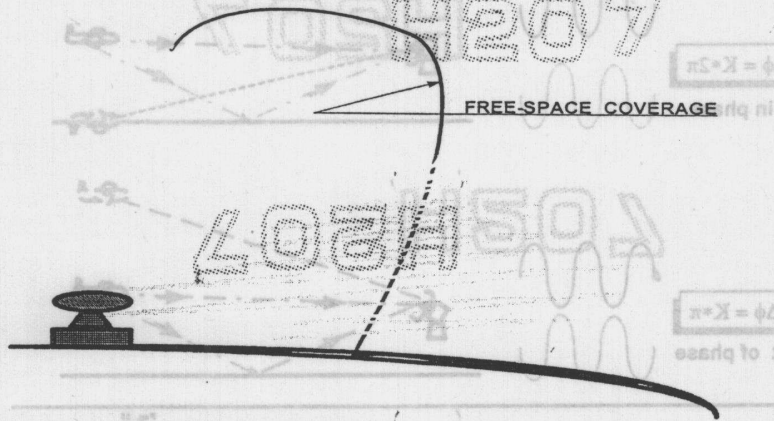
Pag. 53

SPECULAR REFLECTION OF RADAR SIGNALS

RADAR
ANTENNA

TARGET

$$\Delta R = 2*Ha*Ht / R$$

$$\Delta\phi = 2\pi*\Delta R/ \lambda$$
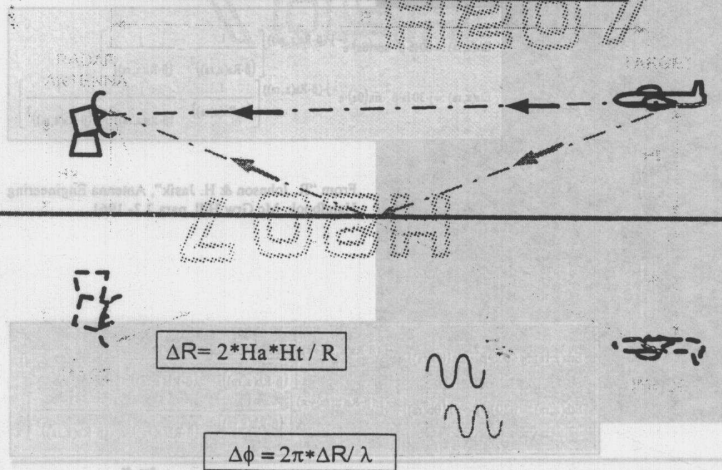
Pag. 54

TARGET APPARENT ELEVATION VERSUS SIGNALS RELATIVE PHASE

$\Delta\phi = K*2\pi$

in phase

$\Delta\phi = K*\pi$

out of phase

Pag. 55

Cross Eye Theory

$$Erx(z,n) := 60 \, Ia \cdot \beta^2 \cdot \cos(\theta_a) \cdot e^{-j(\beta \cdot Ra(z,n))} \left[\frac{1}{(\beta \cdot Ra(z,n))^2} - \frac{j}{(\beta \cdot Ra(z,n))^3} \right]$$

$$Eta(z,n) := j \, 30 \, Ia \cdot \beta^2 \cdot \sin(\theta_a) \cdot e^{-j(\beta \cdot Ra(z,n))} \left[\frac{1}{(\beta \cdot Ra(z,n))} + \frac{j}{(\beta \cdot Ra(z,n))^2} - \frac{1}{(\beta \cdot Ra(z,n))^3} \right]$$

From "R. Johnson & H. Jasik", Antenna Engineering
Handbook, Mc Grw Hill, para 2.2- 1961
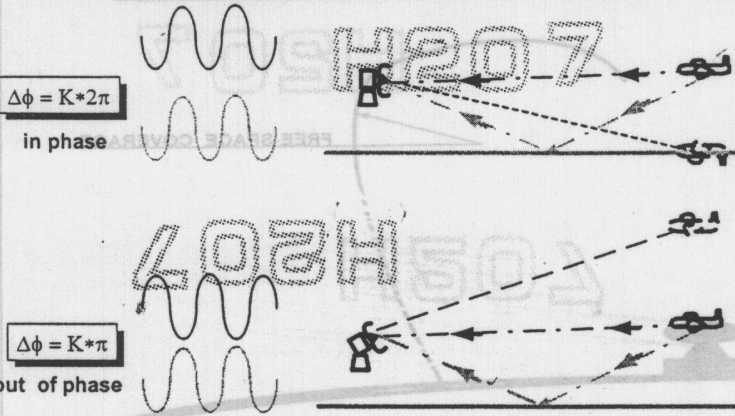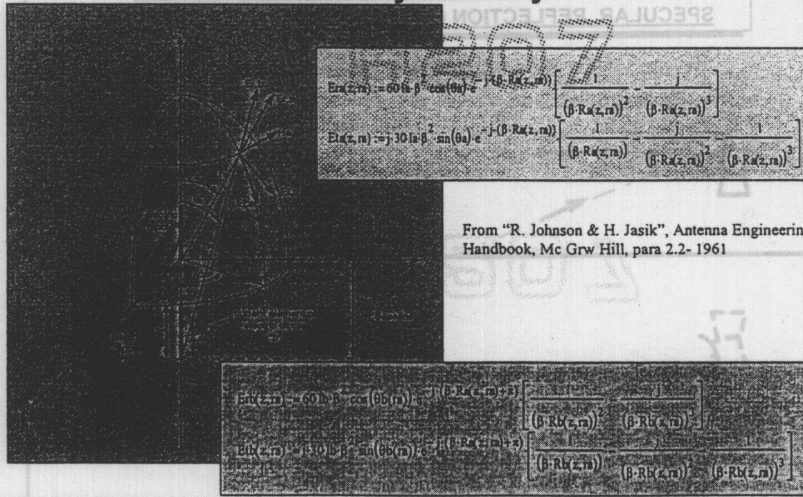
Pag. 56

Cross eye theory

The radial component of electrical field, at long distance, becomes negligible and it is well known that the vector of Pointing (vector product of E and H) is:

$$\vec{P} = \vec{E} \times \vec{H}$$
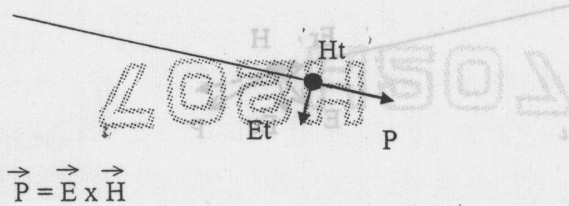
Cross Eye Theory

When two radiating sources are present, the total e.m. field has been computed by D. Howard (see appendix), and in a point Q where their signal are received out of phase, the deviation of vector of Pointing from radial direction is given by:

$$e = \frac{L}{2R}\cos\theta \frac{1-a^2}{1+a^2+2\cos\varphi}$$

That, for $\theta = 0$ and for signals out of phase ($\varphi = 180$), reduces to:

end the displacement error is:

$$e = \frac{L}{2}\left(\frac{1+a}{1-a}\right)$$

$$G = \varepsilon \cdot \frac{2R}{L}$$

29

Cross Eye Theory

If Er is not negligible, the total electric field E will rotate and, since H is always orthogonal E, the resulting vector P will be rotated by the same angle.
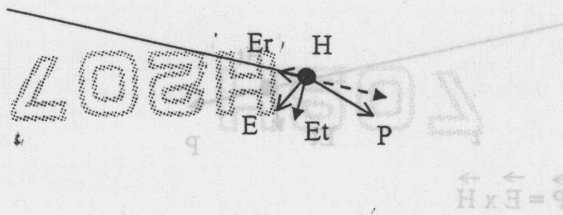
POYNTING VECTOR COMPONENTS FOR A DISTRIBUTE SOURCE OF ENERGY : "ANGULAR GLINT"

Target apparent position
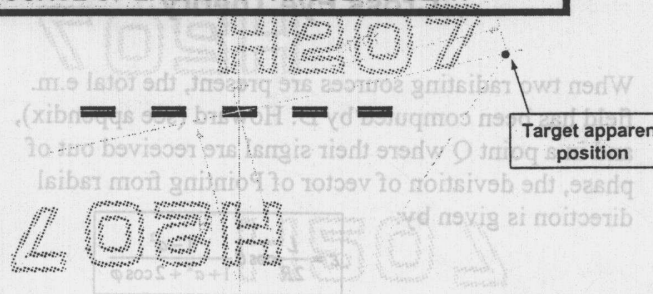
Resultant Poynting vector P

$Pt/Pr=Er/Et=error$

Cross Eye Theory

$$Etsum(ra) := Eta(ra) + Etb(ra) \cos(d\theta(ra)) - Erb(ra) \cdot \sin(d\theta(ra))$$

$$Ersum(ra) := Era(ra) + Etb(ra) \cdot \sin(d\theta(ra)) + Erb(ra) \cdot \cos(d\theta(ra))$$

Dr. V. Rossi (see appendix) underlines that, while for a single source the radial component is negligible, in the case of two sources received out of phase, the energy associated to the transverse component of one source contribute to the build up of the radial component of total electrical field.
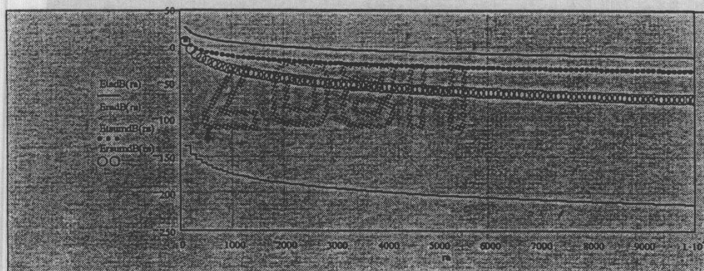
Wavefront Distortion Experiment

31
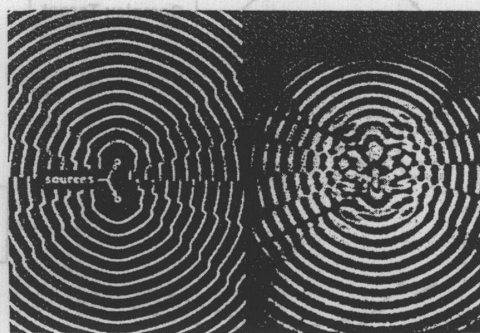
Equivalence of the radar error and the computed Pointing vector direction

$$WFDerror(ra) := \frac{|Ersum(ra)| \cdot ra}{|Etsum(ra)|} + \frac{Baseline}{2}$$

$$XEerror = \left(\frac{1 + Ib}{1 - Ib}\right) \cdot \frac{Baseline}{2}$$
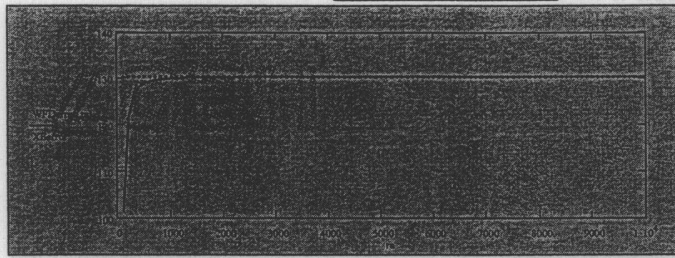
Pag. 63

ASPECT ANGLE OF COMPLEX TARGET : WAVE FRONT DISTORSION

Target apparent position

Complex Target

Phase front of a complex target

Phase front if target was a sphere

Pag. 64

32
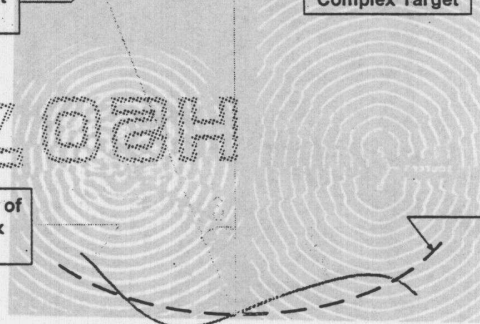
Cross Eye theory Conclusion

The previous equations tell us that

- Cross Eye is not a good ANGULAR jamming technique at long ranges

- Cross Eye is a very good POSITION error (Displacement) generator

- The error is, at practical distances, constant.

CROSS-EYE

- The Cross-Eye jamming technique tries to reproduce the wavefront distortion phenomenon.

- Since Cross-Eye generates a target "Displacement Error" that can be applied to all tracking methods (Monopulse, Conical Scan, etc.), it can be effectively exploited in electronics self-protection equipment.

CROSS EYE AIM

Cross eye aim is that of reproducing the Wavefront Distortion

$G = \dfrac{1+a}{1-a}$

Ref. P.29

$D = G*B/2$

$D = error$
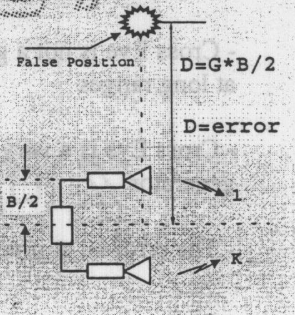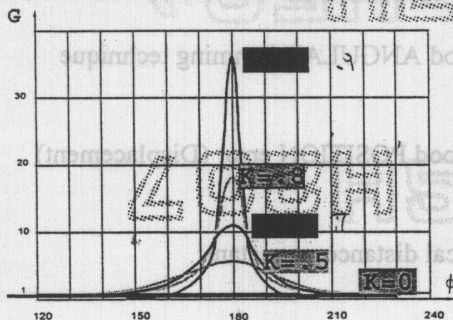
Pag. 67

**CROSS-EYE
WAVEFRONT DISTORTION EFFECT**

False aircraft

$D = L/2$

True aircraft
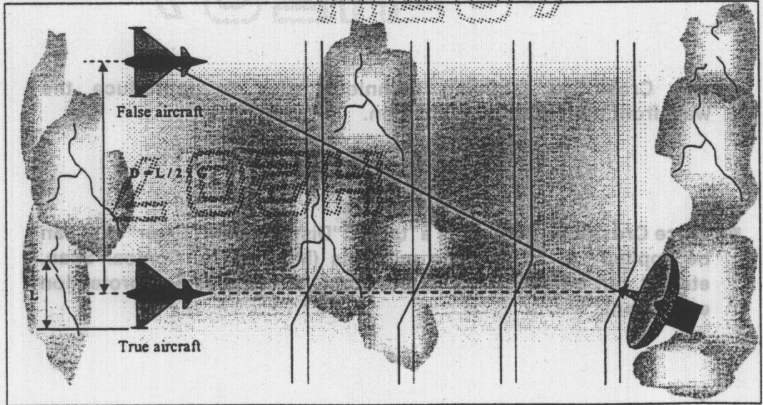
Pag. 68

WHY CROSS-EYE DID NOT EVOLVE?

COMMON OPINIONS ON CROSS EYE JAMMING

- Only suitable for very large platforms
- Only suitable for very small platforms
- Only effective at short distances
- Only effective at long distances
- Requires very high jamming-to-signal power ratio
- Cannot operate against semi-active missiles
- Difficult to tune, affected by manoeuvres and vibrations
- Requires very advanced technologies

And probably it is also a problem of finding the
right "System approach"

Pag. 69

Cross Eye System Approach

First of all, since Cross Eye is mainly a generator of
displacement error, the approach:"I want to generate
one degree of error from a distance of 20 nm" is wrong!
No solution.
By its nature, cross-eye is useful against terminal weapons
(AAA and missile systems).
Questions to be answered are:
- What miss distance do I need?
- What probability of success do I want?

Pag. 70

CROSS-EYE EXPLOITATION OPTIONS

THERE ARE SEVERAL CROSS-EYE EXPLOITATION OPTIONS. FOR INSTANCE:

◆ LONG OR SHORT CROSS-EYE BASE?

◆ LARGE MISS DISTANCES AND LARGE VARIANCE OR MODERATE MISS DISTANCES AND HIGH RELIABILITY?

Pag. 71

LONG OR SHORT BASE CROSS-EYE?

LONG   SHORT
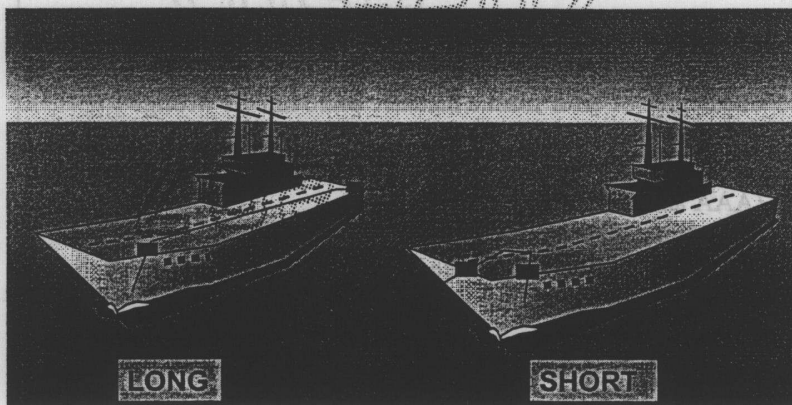
Pag. 72

LONG BASE CONCEPT

ADVANTAGES
- NO SKIN ECHO COMPETITION
- LOWER ERP REQUIRED
- LARGE ANGULAR ERRORS AND POSSIBLE BREAK-LOCK

DISADVANTAGES
- DIFFICULT PRELIMINARY RGPO ACTION REQUIRED
  (E.G. RE-ACQUISITION OF C.E. ECHO)
- PRESENCE OF SEPARATE REAL AND FALSE ECHOES
- BEACONING EFFECT AT SHORT DISTANCES

REAL   FALSE
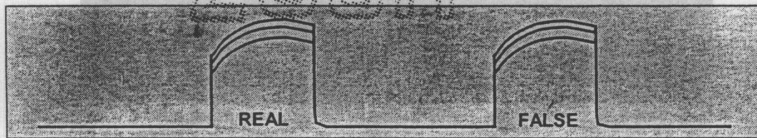
would be out of range gate

Pag. 73

SHORT BASE CONCEPT

ADVANTAGES
- NO RGPO REQUIRED
- NO REAL AND FALSE TARGET SIGNALS, BUT ONLY ONE SIGNAL IS PRESENT
- VERY RELIABLE PERFORMANCES

DISADVANTAGES
- VERY FAST SIGNAL PROCESSING IS REQUIRED
- MODERATE MISS-DISTANCES ARE ACHIEVED

< 10 m

Pag. 74
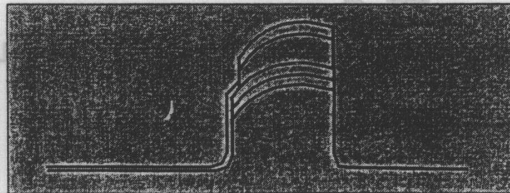
HIGH OR MODERATE AVERAGE MISS-DISTANCE?
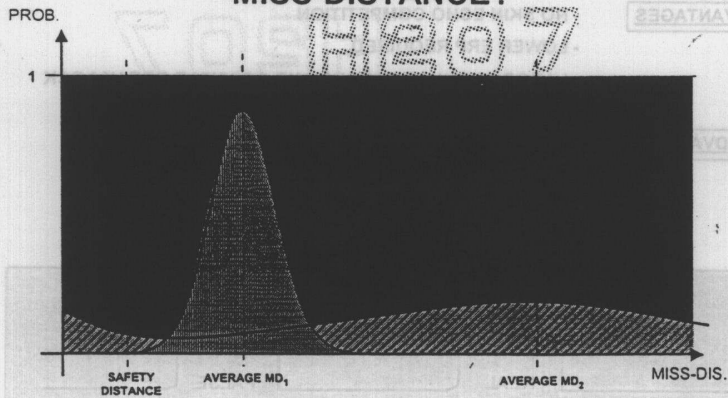
Nothing inside Black region

CROSS-EYE JAMMER "RETROREFLECTIVITY" CONCEPT

$$Rr = R1+R2+R3$$

$$Rr = R1+R2+R3$$

CROSS-EYE JAMMER "RETROREFLECTIVE "
ARCHITECTURES(1)

$s = l \sin \theta$
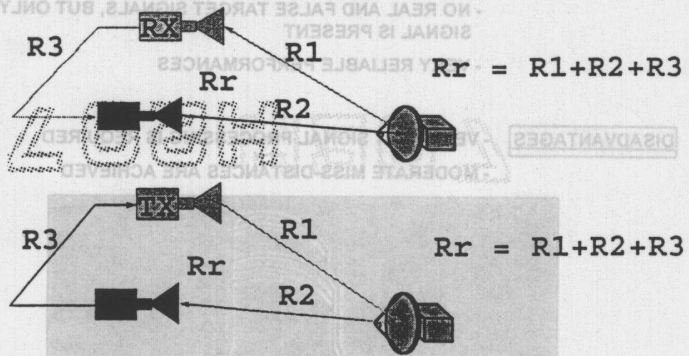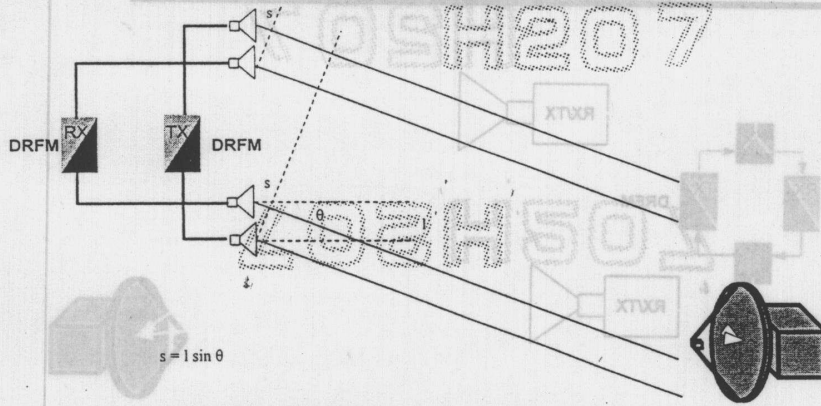
Pag. 77

CROSS-EYE JAMMER "RETROREFLECTIVE "
ARCHITECTURES(1)

e

θ2

θ1

R

Pag. 78

39
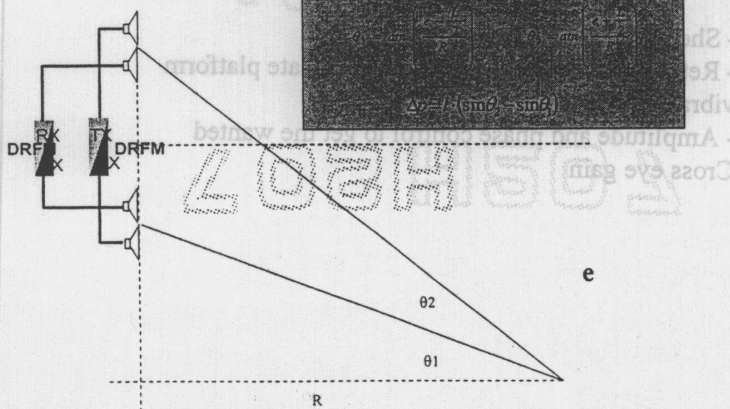
CROSS-EYE JAMMER
"RETROREFLECTIVE " ARCHITECTURE(2)

RX/TX

DRFM DRFM

RX/TX
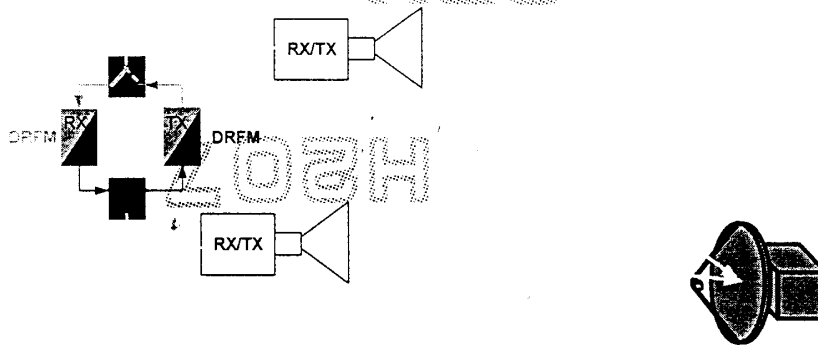
Pag. 79

Preliminary Cross eye requirements

- Short base length to minimise delay
- Retro-reflective structure to compensate platform vibration and manoeuvres
- Amplitude and phase control to get the wanted Cross eye gain

Pag. 80

C.E. EFFECTIVENESS REDUCTION DUE TO SEEKER ANTENNA BEAM SHAPE

(DURING MISSILE APPROACH TO THE JAMMER)
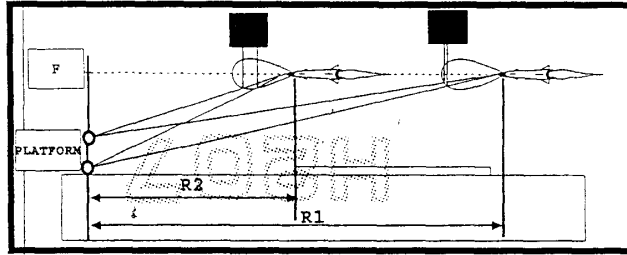
M1,M2:RESULTING AMPLITUDE MISMATCH WEIGHTED BY

ANTENNA BEAM SHAPE

Saturated and Linear Cross Eye
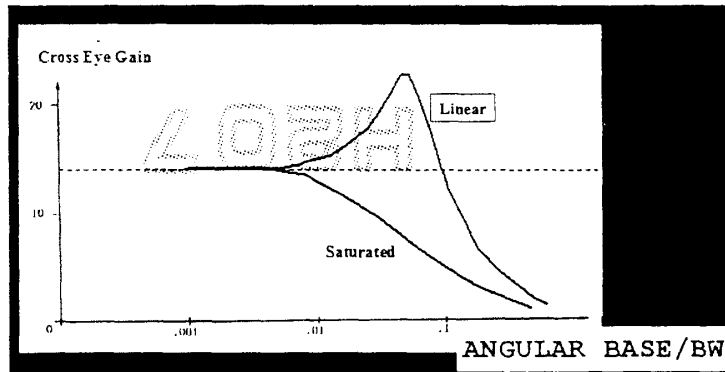
Cross eye error vs J/S
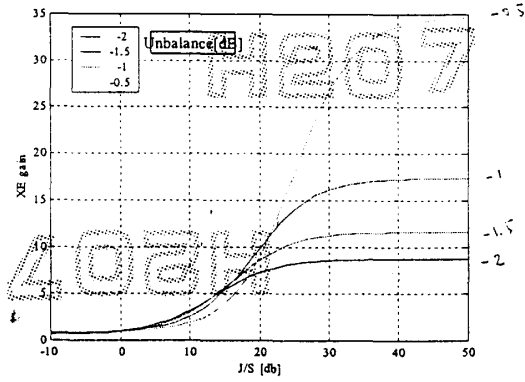
A proper unbalance choice is mandatory

Cross eye error vs angle of arrival

In static condition the cross eye error varies as cos(θ)

$$\varepsilon = \frac{L}{2R}\cos\theta \cdot \frac{1-a^2}{1+a^2+2\cos\varphi}$$

Cross eye System implementation

In order to implement a good retro-reflective Cross Eye
system the following guidelines apply:
- DRFM exploitation for a good and reliable phase control
- Active solid state phased array antenna for:
- amplitude and phase control,
- same antenna phase centre both in receiving and
in transmitting modes
- Calibration system to keep under control the system in
frequency and time.

Cross Eye Implementation: errors budget

Amplitude inaccuracies:
- Path VSWR
- Detector (linearity, dynamic, LSB)
- Amplitude control (linearity, dynamic, LSB)
- Calibration circuit amplitude accuracy
Phase inaccuracies:
- Phase matching
- quantisation errors
- Calibration circuit phase accuracy

$\epsilon = sqr(\epsilon1^2 + \epsilon2^2 + \epsilon3^2 + ...)$

Cross Eye Implementation: Response time

1) Physical Path
    1.a: Transit Time:
        antenna (Rx)
        receiver
        processing
        transmitter
        antenna (Tx)
    1.b: Interconnection
        cable: 4-5 ns/m
        wave guide: 3ns/m

2) Processing
    Detection time
    Signal generation & Logic

Cross eye requirements

- Short base length to minimise delay
- Retro-reflective structure to compensate platform vibration and manoeuvres
- Amplitude and phase control to get the wanted Cross eye gain
- Linear receiving-transmitting path
- ERP such to guarantee a J/S of at least 15 dB at the minimum engagement range

Cross eye feasibility verification

ANTENNA BORE-SIGHT   TARGET POSITION
(VIRTUAL TARGET)   (REAL TARGET)
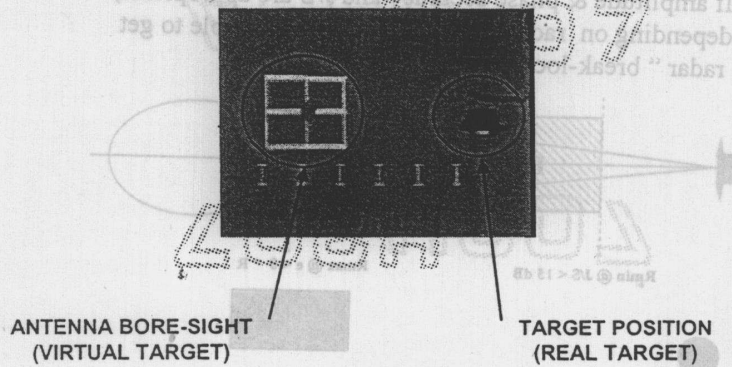
Cross eye operational performances

To predict and evaluate operational Cross eye performances
it has been necessary to use adequate simulators

Cross Eye Break Lock Capability

If amplitude & phase accuracy and J/S are appropriate, depending on radar beam-width θ, it is possible to get radar " break-lock"

Break Lock zone

Rmin @ J/S < 15 dB

Rmax @ e < θ * R
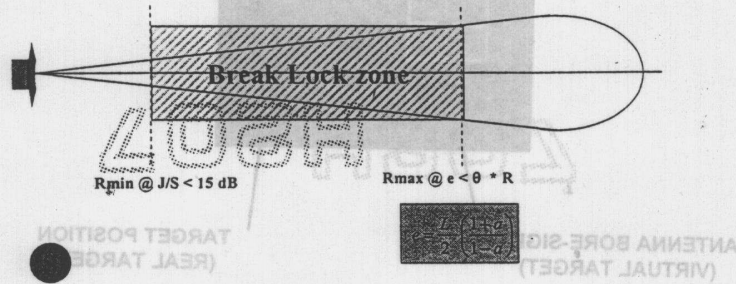
Pag. 91

Airborne Cross Eye Exploitation

Possible installations

Depending on cinematic, it is necessary an adequate "power management" in order to maximise the miss-distance

Pag. 92

Cross eye and aircraft manoeuvres

If horizontal angle of arrival is not adequate, aircraft can exploit the vertical cross eye base created by a roll
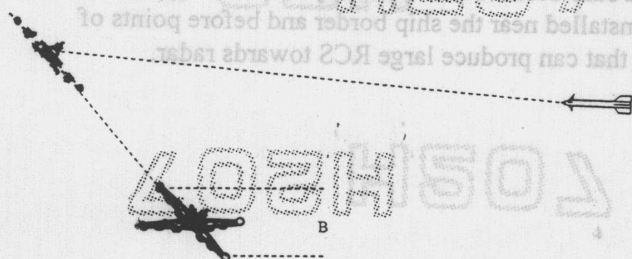
Naval Cross Eye

Cross Eye Jamming can be used by ships to activate a valid "soft kill" defence.
Since a ship is generally a very large platform, several cross eye base (two, three or four) can be necessary depending on the wanted angle sector coverage.

47
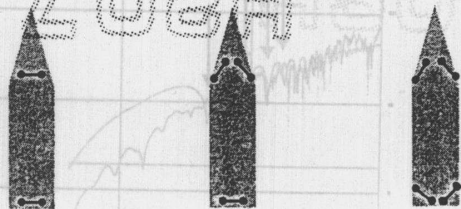
Cross Eye Shipboard Installation

For a sure defence it is necessary that Cross Eye Bases are installed near the ship border and before points of ship that can produce large RCS towards radar.
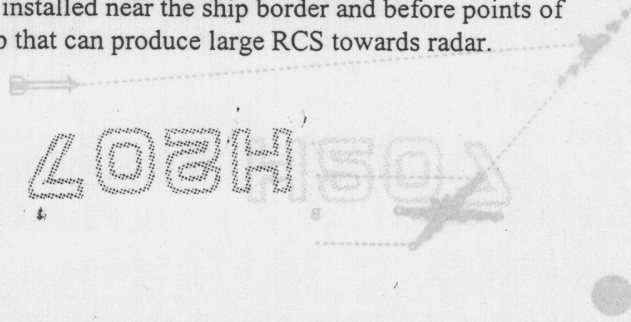
Cross Eye and Naval Environment

As it happens for all jammers (point sources), multipath causes strong jammer signal attenuation at specific ranges, while the ship (extended target) keeps its echo strength. At these ranges the jammer effect decreases.
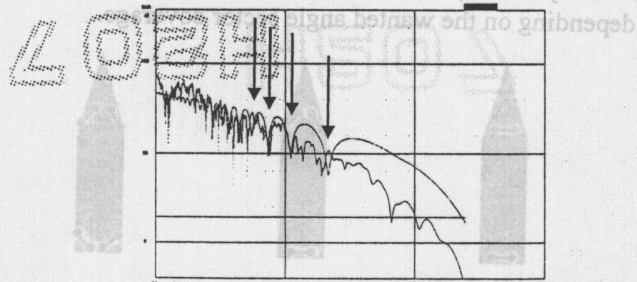
Naval Cross Eye operation

In order to get good Cross Eye defence performances, it is necessary to implement an adequate "power management" to avoid missile "lock" on seeker antenna side lobes.

VIRTUAL COOPERATIVE JAMMING

Cooperative aircrafts

J   J

Crosseye false target

J   J

COOPERATIVE JAMMERS DISCRIMINATION

RESOLVED REAL — COOPERATIVE TARGETS

Antenna beamwidth

J — 100 m — J

UNRESOLVED VIRTUAL — COOPERATIVE TARGETS

J — J

10m

Pag. 99

"REAL" AND "VIRTUAL" REALITY (AIRBORNE)

Pag. 100
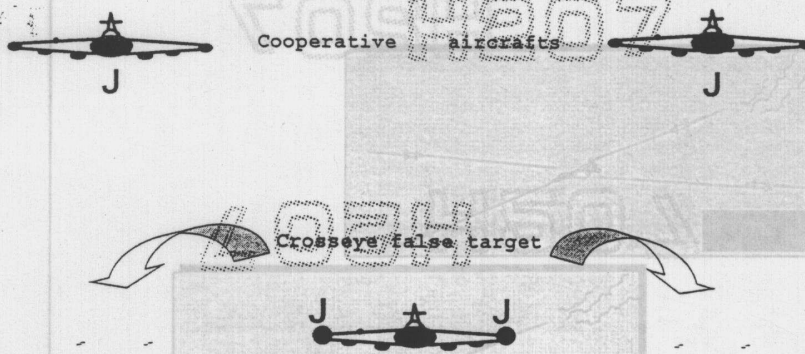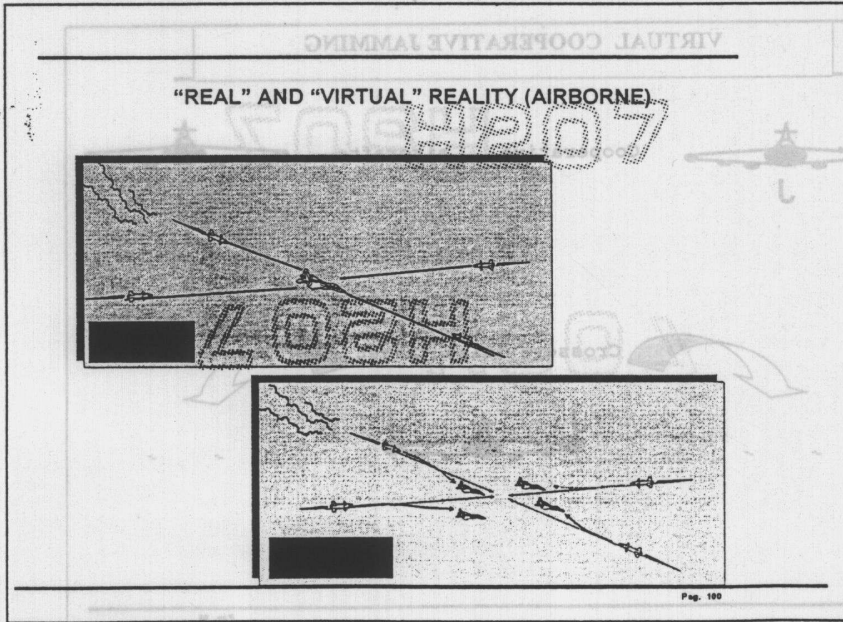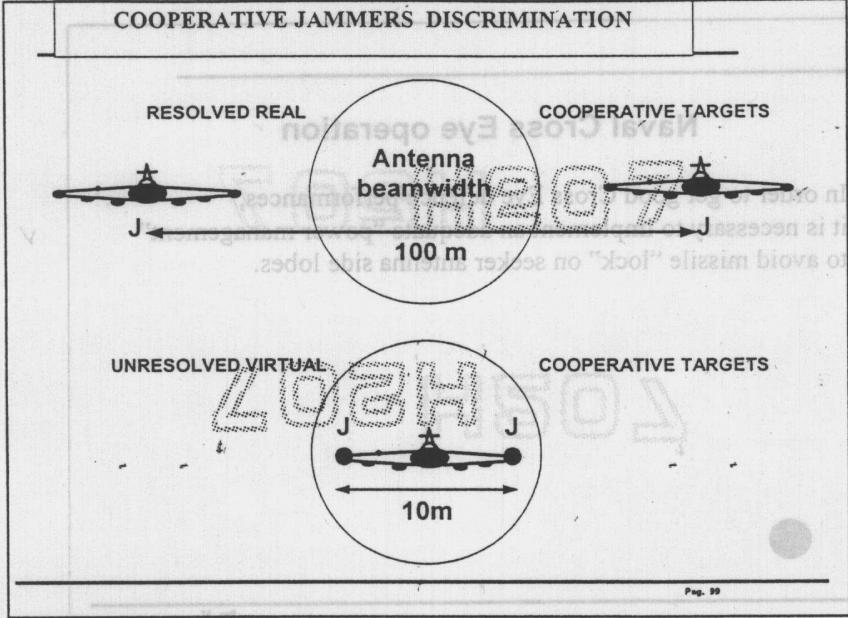
Cross eye against Semi-active missiles

So far it has been shown the sure performances of Cross Eye jamming against active radar guided weapons: AAA, command missiles, active missiles.

The schematic Block diagram of C.E. presented so far, cannot generate sure W.F.D. against passive seeker head
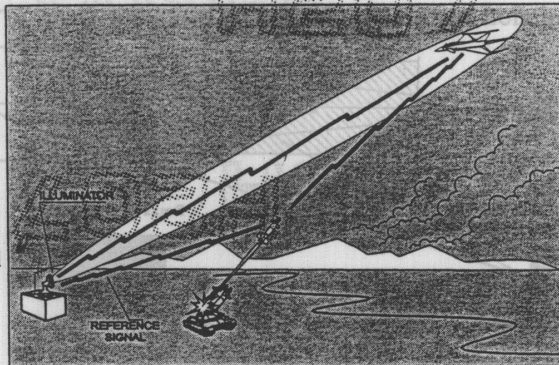
Cross Eye against semi-active missiles(1)

Break Lock of Target Tracking Radar (TTR)

Rmin @ J/S < 15 dB

Rmax @ e < θ * R
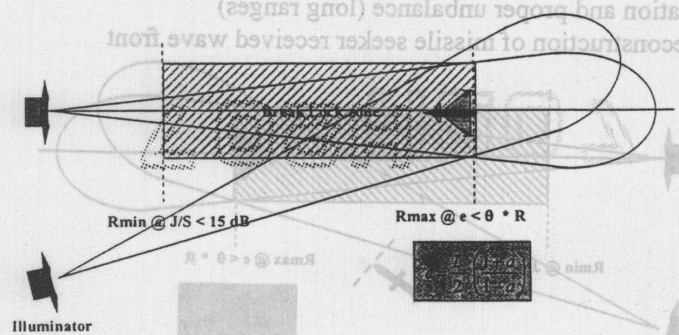
Illuminator

Cross Eye against semi-active missiles(2)

1) - Break Lock of Target Tracking Radar (TTR) (short Ranges)
2) - WF stabilisation through Illuminator + proper Phase modulation and proper unbalance (long ranges)
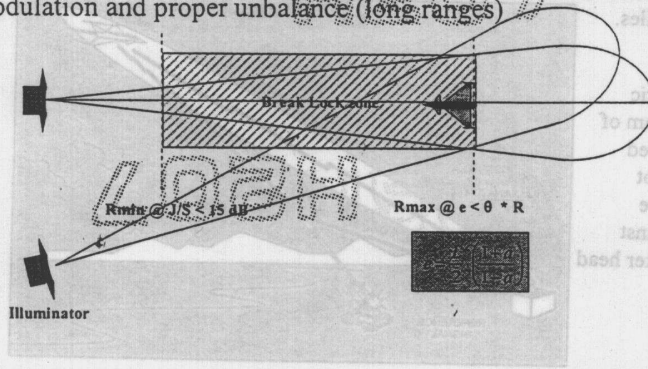
Cross Eye against semi-active missiles(3)

1) - Break Lock of Target Tracking Radar (TTR) (short Ranges)
2) - WF stabilisation through Illuminator + proper Phase modulation and proper unbalance (long ranges)
3) - Reconstruction of missile seeker received wave front
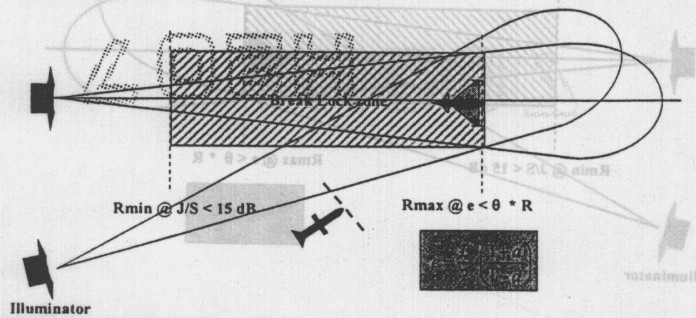
Cross Eye Challenge

One of the most demanding cross eye implementation
is the ERP generation with
adequate amplitude and phase
control. The required ERP
depends on platform RCS.
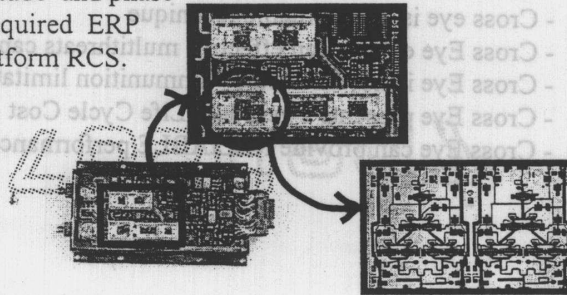
Cross Eye Perspectives

Considering that the RCS of "effective" Stealth platforms can be
small, but not negligible, and considering that Cross Eye
do not requires High Power signals and is a "Repeater" Jammer,
Cross Eye can be successfully used on these platforms.

Therefore, beside INVISIBILITY, cross eye can give
to low RCS platforms (e.g. JSF) also INVULNERABILITY.

Cross Eye Summary

- Cross Eye provides position errors suitable to counter terminal threats
- Cross eye is an affordable technique
- Cross Eye exhibits an effective multithreats capability
- Cross Eye is not affected by ammunition limitation
- Cross Eye presents a very low Life Cycle Cost
- Cross Eye can provide RELIABLE performances

CONCLUSIONS

Cross Eye appears to be a robust answer against tracking radar systems, including Monopulse.

Cross eye can be successfully exploited as "soft kill" weapon to defend platforms, especially if these exhibit low RCS

Cross eye can significantly contribute to build "INVULNERABLE" platforms, the best answer when their "invisibility" is not enough.

CROSS-EYE
EFFECT

Pag. 109
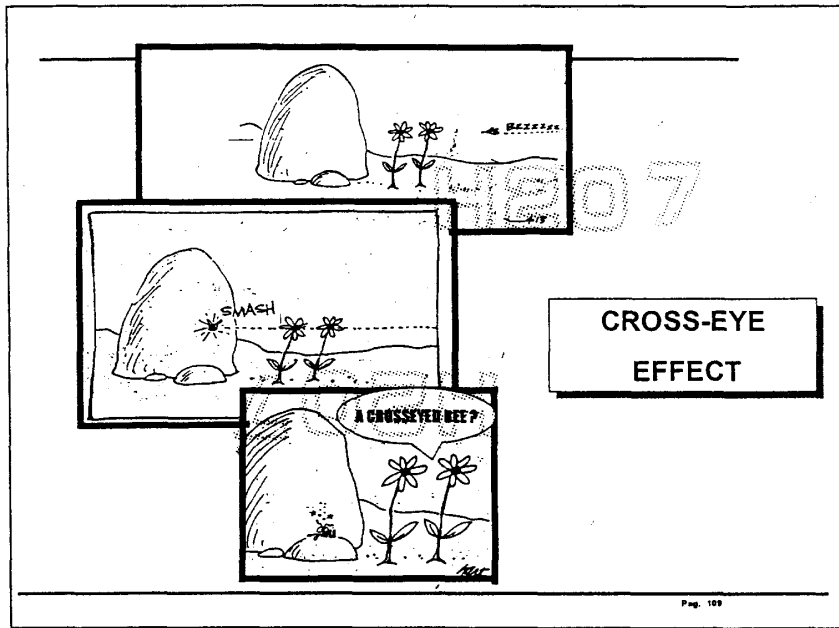
[4] K. G. Schroeder and J. C. Davis, "On the averaging of reflection coefficients in broadband hybrid trees," *IEEE Proc.*, vol. 53, pp. 626–627, June 1965.

[5] K. G. Schroeder, J. C. Davis, and R. C. Fenwick, "Study program leading to the development of a high-gain, broadband, steerable-beam, high-frequency receiving antenna for the USIA," Final Rep. on Study 1A-10146, Collins Engineering Rep. 523-0556652-001B3M, March 26, 1965 (two volumes).

[6] K. G. Schroeder, "Linear broadside arrays of complementary pair element groups," presented at the 1965 Fall URSI Meeting, Hanover, N.H.

[7] ——, "Wideband circular antenna arrays of complementary pair element groups," *IEEE Trans. Aerosp. Electron. Syst.*, vol. AES-3, pp. 309–323, Nov. 1967.

[8] T. S. Cory and L. A. Schriner, "Experimental studies of phased arrays utilizing complementary pair element groups . . .," Collins Radio Company Final Rep. on ARPA Order 160-8, Astia Document AD 842 416, Oct. 1968 (Uncl).

[9] P. E. Mayes, W. T. Warren, and F. M. Wiesenmeyer, "The monopole-slot: A broadband, unidirectional antenna," *IEEE Trans. Antennas Propagat.*, vol. AP-20, pp. 489–493, July 1972.

[10] R. M. Foster, "Directive diagrams of antenna arrays," *Bell Sys. Tech. J.*, vol. 5, pp. 292–306, 1926.

[11] R. N. Ghose, *Microwave Circuit Theory and Analysis.* New York: McGraw-Hill, 1963, pp. 221–223.

[12] G. G. Montgomery, R. H. Dicke, and E. M. Purcell, *Principles of Microwave Circuits.* New York: McGraw-Hill, 1948, p. 148–149.

Co-Polar and Cross-Polar Diffraction Images in the Focal Plane of Paraboloidal Reflectors: A Comparison Between Linear and Circular Polarization

S. I. GHOBRIAL, MEMBER, IEEE

Abstract—Equations for the co-polar and cross-polar fields in the focal plane of paraboloidal reflectors when excited by a plane wave are derived for linear and circular polarization. It is shown that for linear polarization the co-polar diffraction image consists of an elliptically shaped bright region followed by dark and bright zones. On the other hand, the cross-polar image consists essentially of four bright spots separated by a dark cross. These theoretical findings were confirmed by measurements. With circular polarization the co-polar diffraction image comprises a bright central circle followed by dark and bright rings, whereas the cross-polar image consists of a dark central circle followed by bright and dark rings. It is also shown that the field distribution in the image space is affected to a great extent by the angular semi-aperture ψ'. Graphs of the variation of the image characteristics with ψ' are also given.

I. INTRODUCTION

RECENT investigations in the study of reflector antennas utilizing two orthogonal polarizations revealed that high polarization discrimination can be achieved if the fields in the focal plane of the reflector when excited by a plane wave are orthogonal to that of the primary feed when operated in the transmit mode [1], [2]. A knowledge of the polarization nature of the field in the focal plane is therefore useful for the design of primary feeds with high cross-polar discrimination. The polarization characteristics of focal plane fields in the case of paraboloid excited by a linearly polarized wave was studied by a number of authors [3]–[5]. However, the case of circular polarization remains to be investigated. In this work equations for co-polar and cross-polar focal plane fields will be

derived when a circularly polarized wave is exciting reflector. It will be shown that while in the case of linear polarization the co-polar diffraction image consists of almost elliptical bright region followed by dark and bright zones, with circular polarization the co-polar diffraction image consists of a bright circular region followed by dark and bright rings. This distribution is very similar to well-known Airy distribution. On the other hand, the co-polar diffraction image consists of a dark circle followed by bright and dark rings. This is very different from distribution arising from linear polarization where cross-polar image consists of four bright zones separated by a dark cross [6]. It is also shown that the deviation of co-polar image from the Airy distribution decreases monotonically with ψ', the angular semi-aperture (in case of linear polarization). As ψ' approaches zero co-polar field distribution approaches the Airy distribution where as the cross-polar image vanishes completely.

II. ANALYSIS—FOCAL PLANE FIELDS

A. Linear Polarization

Consider a plane wave linearly polarized along the incident on the reflector: $e_i = i|e| + j0 + k0$. On tion the incident vector e_i changes direction and the ponents of the field in the focal plane can be obtained the current distribution method as (Appendix I):

$$E_x(r,\zeta) = A + B \cos 2\zeta$$

$$E_y(r,\zeta) = B \sin 2\zeta$$
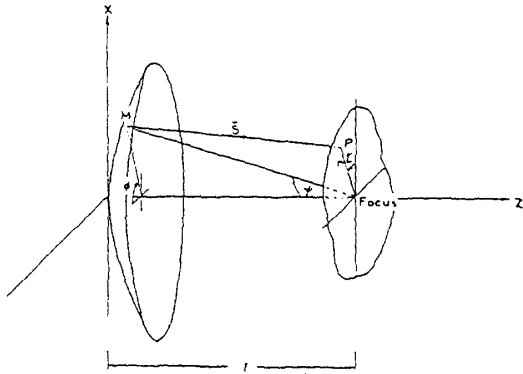
Fig. 1. Coordinate systems.

:re

$$A = K \int_0^{\psi'} J_0(\beta \sin \psi) \sin \psi \, d\psi \tag{3}$$

$$B = K \int_0^{\psi'} \frac{1 - \cos \psi}{1 + \cos \psi} J_2(\beta \sin \psi) \sin \psi \, d\psi \tag{4}$$

l

} $2\pi r/\lambda$;

$I_0(\beta \sin \psi)$ and $J_2(\beta \sin \psi)$ Bessel functions of the first kind;

λ wavelength of the incident wave;

ψ, r, and ζ as defined in Fig. 1.

n the other hand, if the incident wave is polarized along e y-axis, i.e., $e_i = i0 + j|e| + k0$, then the following :pressions are obtained:

$$E_x(r,\zeta) = B \sin 2\zeta \tag{5}$$

$$E_y(r,\zeta) = A - B \cos 2\zeta. \tag{6}$$

l. Circular Polarization

If the polarization of the incident wave is circular, then /e may express this as the sum of two linearly polarized waves in time quadrature. Thus the field incident on the reflector can be expressed symbolically as

$$e_i = |e|(i + je^{j\pi/2}). \tag{7}$$

The x and y field components in the focal plane can now be obtained by using (1), (2), (5), and (6) in conjunction with (7); thus the following results are obtained:

$$E_x = A + B \cos 2\zeta + jB \sin 2\zeta = |E_x| \exp (j\phi_x) \tag{8}$$

$$E_y = B \sin 2\zeta + j(A - B \cos 2\zeta) = |E_y| \exp (j\phi_y) \tag{9}$$

and the field in the focal plane can be written as

$$|E_x| \exp (j\phi_x)i + |E_y| \exp (j\phi_y)j.$$

tion is elliptical, indicating that cross-polarization has taken place as expected. The cross-polar component in this case consists of a circularly polarized wave but with its sense of rotation opposite to that of the incident wave. In order to determine the relative magnitude of the cross-polarized field we need to express the focal plane field as a sum of two circularly polarized waves: one right hand circular and the other left hand circular. Now, rewriting the expression for the field in the focal plane,

$$E = |E_x| \exp (j\phi_x)i + |E_y| \exp (j\phi_y)j$$
$$= |E_x| \exp (j\phi_x)[i + jm \exp (j\phi')] \tag{10}$$

where

$$m = |E_y/E_x| \quad \text{and} \quad \phi' = \phi_y - \phi_x$$

expressing E as the sum of two circularly polarized waves, we have

$$E = c[i + j \exp (j\pi/2)] + d[i - j \exp (j\pi/2)] \tag{11}$$

where c and d are complex quantities whose magnitudes are given by

$$|c| = |E_x/2|(1 + m^2 + 2m \sin \phi')^{1/2} \tag{12a}$$

$$|d| = |E_x/2|(1 + m^2 - 2m \sin \phi')^{1/2}. \tag{12b}$$

In (12) $|c|$ and $|d|$ represent the magnitudes of the co-polar and cross-polar fields, respectively.

From (8) and (9)

$$|E_x| = (A^2 + B^2 + 2AB \cos 2\zeta)^{1/2}$$

$$|E_y| = (A^2 + B^2 - 2AB \cos 2\zeta)^{1/2}$$

Therefore,

$$m = [(A^2 + B^2 - 2AB \cos 2\zeta)/(A^2 + B^2 + 2AB \cos 2\zeta)]^{1/2}$$

and

$$\phi' = \tan^{-1} \frac{A - B \cos 2\zeta}{B \sin 2\zeta} - \tan^{-1} \frac{B \sin 2\zeta}{A + B \cos 2\zeta}$$

from which

$$\sin \phi' = \frac{A^2 - B^2}{[(A^2 + B^2 - 2AB \cos 2\zeta)(A^2 + B^2 + 2AB \cos 2\zeta)]^{1/2}}.$$

Substituting for $|E_x|$, m, and $\sin \phi'$ in (12) we get

$$|E_{co-pol}| = |c| = A = \kappa \int_0^{\psi'} J_0(\beta \sin \psi) \sin \psi \, d\psi \tag{13}$$

which quantity is independent of ζ. This clearly shows that the co-polar field distribution in the focal plane is a function of the distance between the point at which the field is to be calculated and the focus only. Therefore, the co-polar diffraction image in the focal plane is circularly symmetrical. Similarly, the cross-polar field distribution is obtained as

$$|E_{cross-pol}| = |d| = B$$
$$= \kappa \int^{\psi'} \frac{1 - \cos \psi}{1 + \cos \psi} J_2(\beta \sin \psi) \sin \psi \, d\psi. \tag{14}$$
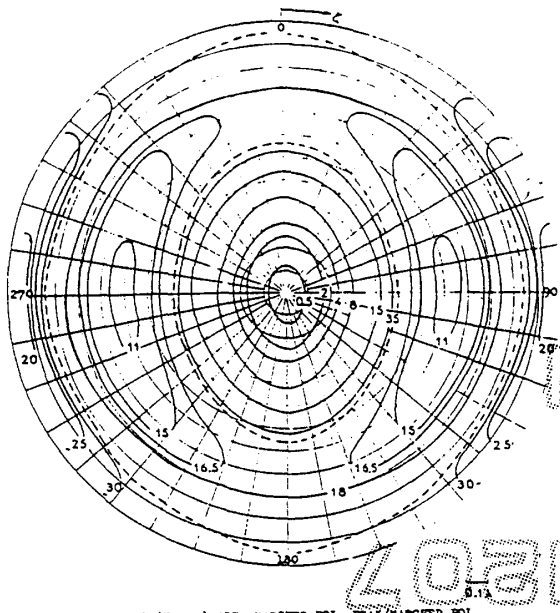
Fig. 2. Co-polar contours in the focal plane of an 80° reflector (linear polarization).
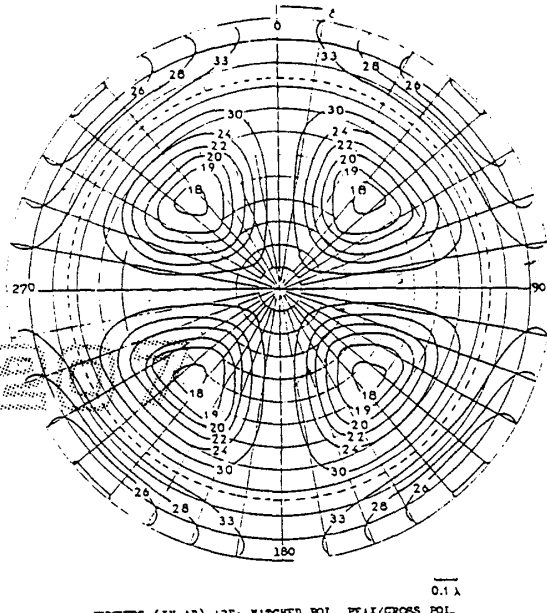
Fig. 3. Cross-polar contours in the focal plane of an 80° reflector (linear polarization).

This is again independent of ζ and therefore the cross-polar diffraction image is also circularly symmetrical about the focus.

Now comparing (1) and (13), which give the co-polar field distribution for linear and circular polarizations, respectively, it is seen that (1) reduces to (13) if $\zeta = \pm 45°$, $\pm 135°$; i.e., in the focal plane the field distribution is the same for linear and circular polarizations along the radial lines defined by $\zeta = (2n + 1)45°$, $n = 0,1,\cdots$. Also the peak value of the co-polar field is the same for both modes of polarization being $K(1 - \cos \psi')$.

III. COMPUTATIONS

Using (1), (2), (13), and (14) contours of constant co-polar and cross-polar focal plane fields were plotted for both linear and circular polarizations. These are shown in Figs. 2–5. An angular semi-aperture of 80° was assumed in these calculations. The following features are to be noted.

1) The linear polarization co-polar diffraction image consists of an almost elliptically shaped region with its major axis along the direction of the co-polar field. For a constant value of r the variation of the co-polar field with ζ is harmonic superimposed on a constant as suggested by the expression $A + B \cos 2\zeta$.

2) The linear polarization cross-polar diffraction image consists of four bright zones separated by a dark cross. Also the field changes sense whenever the principal axes are crossed; i.e., cross-polar fields are in anti-phase in adjacent quadrants. Moreover, the variation of field intensity with ζ is harmonic and is completely determined by $\cos 2\zeta$ as seen from (2).

3) For circular polarization circular symmetry is maintained in both co-polar and cross-polar images. Also the
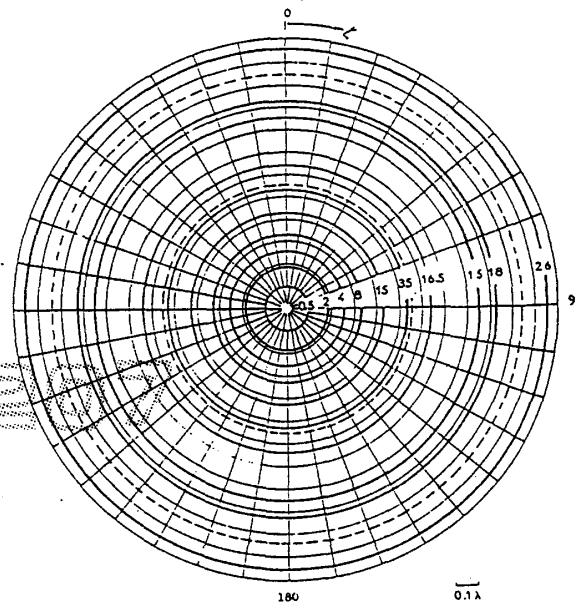
Fig. 4. Co-polar contours in the focal plane of an 80° reflector (circular polarization).

variation of field intensity with r is identical to that of linear polarization along the radius vector defined by $\zeta = (2n + 1)45°$.

Figs. 6 and 7 give the variation of co-polar and cross-polar field intensities with r along the lines $\zeta = 0°$, $45°$ and 90°. The case of $\zeta = 45°$ is of special interest since it gives the variation of field with r for circular polarizatio

A-3

NUMBERS (IN dB) ARE: CO-POLAR PEAK/CROSS-POLAR.
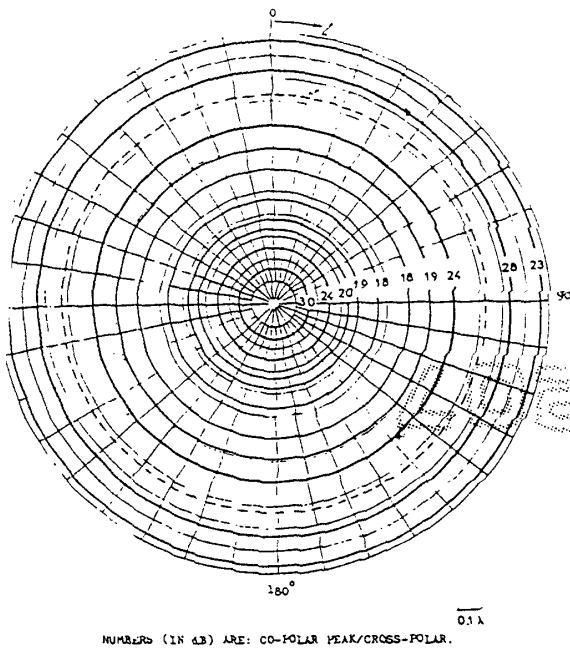
g. 5. Cross-polar contours in the focal plane of an 80° reflector (circular polarization).

DISTANCE FROM FOCUS (WAVELENGTHS)
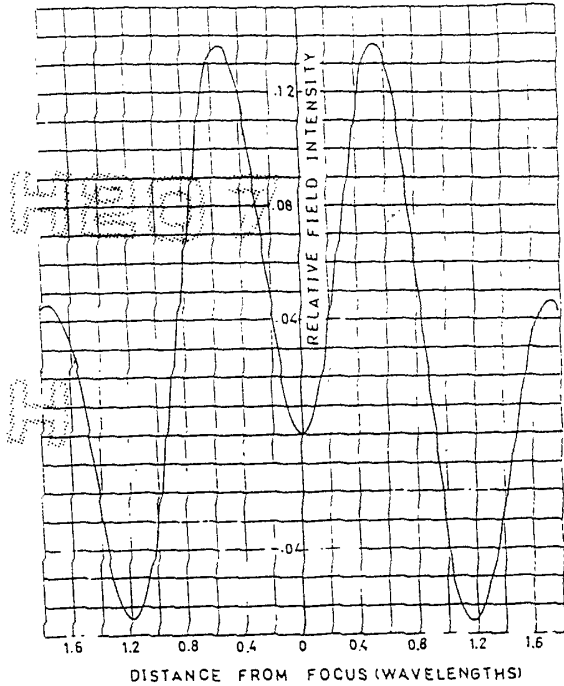
Fig. 7. Cross-polar field intensity variation with r along $\zeta = 45°$

DISTANCE FROM FOCUS (λ)
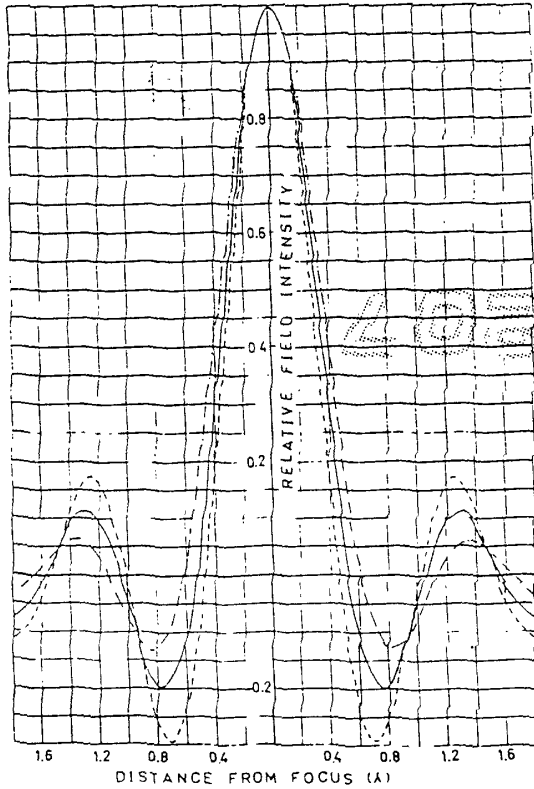
for all ζ. From Fig. 6 it is seen that the three curves intersect at $r = 0.94\lambda$ and $r = 1.48\lambda$. These values of r are the zeros of the function B,

$$B = \kappa \int_0^{\psi'} \frac{1 - \cos \psi}{1 + \cos \psi} J_2(\beta \sin \psi) \sin \psi \, d\psi.$$

Thus for the above mentioned values for r the co-polar image has circular symmetry where as the cross-polar image has nulls.

The cross-polar field variation with r is shown in Fig. 7 for $\zeta = \pm(2n + 1)45°$, $n = 0,1$. Along the radius $\zeta = 0°$ and $\zeta = 90°$ the cross-polar field vanishes as seen from Fig. 3. It is worth noting that Figs. 6 and 7 are true for paraboloids of 80° angular semi-aperture and of any diameter. Changing the diameter affects the absolute value of the field intensity but has no effect on the structure of the diffraction image. However, changing the angular semi-aperture ψ' (this amounts to changing the f/D ratio) affects the diffraction image. This is seen to be true by considering the upper limit of integration of (3) and (4). Figs. (8) and (9) give the variation of some of the characteristics of the co-polar and cross-polar images with ψ'. In Fig. 8 the characteristics of the diffraction image for linear polarization are shown. The solid curves give these characteristics along $\zeta = 45°$. These also represent the characteristics of circular polarization images. It is seen that as ψ' approaches 0°, the curves for $\zeta = 0°$ and $\zeta = 90°$ come closer to those of $\zeta = 45°$. It is also worth noting that as ψ' becomes smaller the position of the first co-polar null moves away from the focus. In fact as ψ' approaches zero the first co-polar null
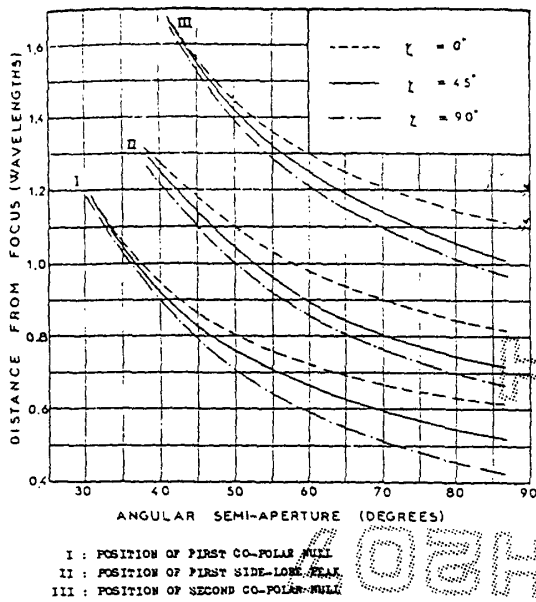
Fig. 8. Co-polar diffraction image characteristics as a function of the angular semi-aperture.

I : POSITION OF FIRST CO-POLAR NULL
II : POSITION OF FIRST SIDE-LOBE PEAK
III : POSITION OF SECOND CO-POLAR NULL
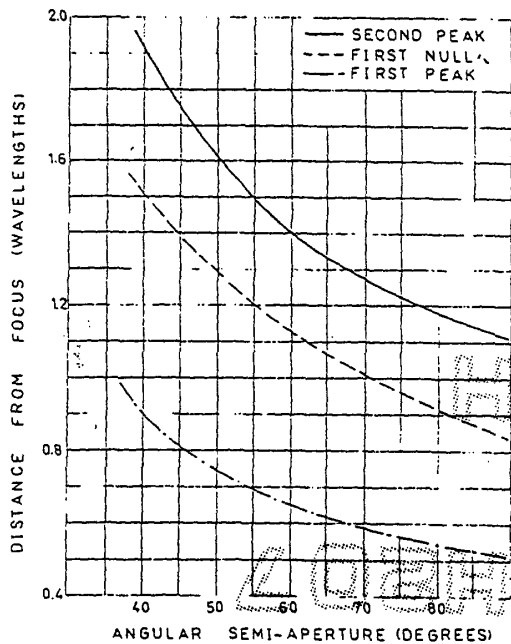
Fig. 9. Cross-polar diffraction image characteristics as a function of the angular semi-aperture.

expected since for $\psi' = 0$ the paraboloid acts no longer as a lens. Also from Fig. 9 it is seen that the position of the first and second cross-polar peaks move away from the focus as ψ' decreases. In the limiting case as ψ' tends to zero, the position of the peaks move indefinitely away from the focus. This is expected since when ψ' is zero the para-

boloidal surface transforms to a plane reflector parallel to the incident wave. Such a surface introduces no depolarization.

IV. MEASUREMENTS

To confirm the above theoretical findings measurements of focal plane fields were conducted using a paraboloid of 31 cm diameter (9.7λ at the frequency used). The transmitting linearly polarized antenna was placed at a far distance from the reflector under test so that a plane wave should be received. The receiving reflector was oriented such that the plane incident wave is normal to the axis of the reflecto. A small dipole was used as the pickup probe. Across this diode was connected and the demodulated voltage was the fed to a meter via thin wires. It was found that this arrang ment introduces but little distortion in the focal plane field The outcome of these measurements are presented in t form of graphs in Figs. 10 and 11. Theoretical curves a also included for comparison. It is seen that the agreeme between theory and measurements is good.

In Fig. 10(a) and (b), the variation of co-polar field w r, the distance from the focus for $\zeta = 0°$ and $\zeta = 90°$ shown. It is clear that the agreement is good, in particu the positions of maxima and nulls are accurately predic by theory. In Fig. 10(c) the variation of cross-polar fi intensity as a function of the distance r is given for 1 values of ζ, namely 20° and 40°. Theoretical curves also given. It is to be observed that the agreement is as good as in the case of co-polar fields. This may attributed to the inevitable misorientation of the pic probe. Needless to mention that unlike co-polar meas ments, small errors in misorientation lead to serious er in measured cross-polar. The deviation between theory measurements is also seen to increase with r. This is to edge diffraction effects which were not taken car in the present theory.

Table I gives relative amplitude of co-polar field function of r for $\zeta = \pm40°$ and $\pm20°$. From this one may conclude that the field is symmetrical abou $\zeta = 0°$ axis. Measurements along $\zeta = \pi\pm40°$ and $\zeta = \pi$ were found to yield similar results to those for $\zeta =$ and $\zeta = \pm20°$, respectively. This demonstrates tha diffraction pattern is symmetrical about the focus as t predicts.

Fig. 11 shows the variation of co-polar and cross fields with ζ (and for $r = 0.4\lambda$). Measured resul represented by crosses. Theoretical graphs of the fur

TABLE I
MEASURED CO-POLAR AMPLITUDE RELATIVE TO THAT AT THE

r (Wavelengths)	Measured Relative Amplitude			
	$\zeta = +40°$	$\zeta = -40°$	$\zeta = +20°$	$\zeta =$
0.00	1.00	1.00	1.00	
0.17	0.85	0.86	0.88	
0.34	0.37	0.42	0.58	
0.68	0.04	0.11	0.10	
0.85	-0.06	-0.06	-0.04	
1.02	-0.15	-0.16	-0.05	
1.36	0.16	0.14	0.15	

(a)

(b)

(c)

Fig. 10. Measured and computed diffraction patterns in the focal plane.

Fig. 11. Measured and computed variation of co-polar and cross-polar fields with ζ.

It is seen that agreement is excellent and one can conclude that measurements to confirm the theoretical findings presented in the previous sections.

To investigate the effect of the pickup probe back lobe on the above presented results measurements were conducted in the absence of the reflector. It was found out that the back lobe had a level of less than -27 dB relative to the co-polar at the focus, the back lobe being measured with the probe oriented to match the polarization of the incident plane wave. With the probe cross-polarized the back lobe had a level better than -50 dB. It was therefore concluded that the effect of back lobe on focal plane measurements was significant only when measuring field near the nulls of the co-polar diffraction image. In the case of cross-polar measurements the effect of the pickup probe back lobe was negligible. The error introduced by the above effect may, however, be isolated by interpolation.

V. CONCLUSIONS

The polarization nature of the field in the focal plane of paraboloidal reflectors was characterized. It was shown that for linear polarization the co-polar field distribution consists of almost elliptically shaped contours with maximum intensity at the focus. The cross-polar field is concentrated at the four quadrants formed by the principal axes. The cross-polar field vanishes at the focus and along the principal axes.

With circular polarization circular symmetry is maintained for co-polar and cross-polar fields. The field intensity variation with r being identical to that of the case of linear polarization along $\zeta = (2n + 1)45°$, $n = 0,1$. The effect of angular semi-aperture on focal plane fields was also studied and the results were given in the form of graphs. Practical measurements confirmed theoretical findings.

APPENDIX

To show that in the focal plane of a reflector excited by a plane wave linearly polarized along the x-axis, the x and y field components are given by

$$E_x(r,\zeta) = A + B \cos 2\zeta$$

$$E_y(r,\zeta) = B \sin 2\zeta$$

$A + B \cos 2\zeta$ and $B \sin 2\zeta$ are given as well. In plotting these theoretical curves the values of A and B were determined from measured results; i.e., A was obtained as the value of the co-polar at $\zeta = 45°$, B was then determined as the difference between the co-polar level at $\zeta = 0°$ and $\zeta = 45°$. This allows comparison of measured field dependence on ζ with theory while eliminating r dependent errors.

where A and B are as defined by (3) and'(4). The incident field is given by

$$e_i = |E|i + j0 + k0. \qquad (A1)$$

The field components after reflection are obtained from the reflecting matrix as

$$e_r = |E|[[\sin^2 \phi(1 - \cos \psi) - 1]i$$
$$+ \sin \phi \cos \phi(1 - \cos \psi)j - k \sin \psi \sin \phi]. \qquad (A2)$$

Using the current distribution method the field at any point in the focal plane can be written as

$$E = C \iint_s [J - (J \cdot S_r)S_r] \exp \left(-j \frac{2\pi}{\lambda} (\rho + d)\right) \frac{1}{\rho} dS \qquad (A3)$$

where

C a constant;
J current distribution density;
S_r unit vector along MP (Fig. 1);
d distance from the point M to a reference plane;
ρ distance MP.

In terms of r, ζ, ϕ, and ψ the distance ρ is approximately[1] given by the relation

$$\rho \approx \frac{2f}{1 + \cos \psi} - \frac{r \sin \psi \sin (\phi + \zeta)}{1 + \cos \psi} \qquad (A4)$$

Substituting for $J = n \times (S_r \times e_r)$ where n is a unit vector normal to the reflecting surface, we get

$$E = C \iint_s e_r(n \cdot S_r) \exp \left(-j \frac{2\pi}{\lambda} (\rho + d)\right) \frac{1}{\rho} dS. \qquad (A5)$$

[1] The validity of this approximation is subject to the constraint $r \ll 2f$.

But

$$dS = \rho^2 \sin \psi \sec (\psi/2) \, d\psi \, d\phi$$

$$n \cdot S_r = \cos (\psi/2)$$

$$d + \rho = 2f - \frac{r \sin \psi \sin (\phi + \zeta)}{1 + \cos \psi}.$$

On substituting the above results in (A5), the following expression is readily obtained,

$$E = C \int_0^{2\pi} \int_0^{\psi'} e_r \frac{\sin \psi}{1 + \cos \psi}$$
$$\exp \left(j \frac{2\pi}{\lambda} r \sin \psi \sin (\phi + \zeta)\right) d\psi \, d\phi. \qquad (A6)$$

Now, using (A2) and (A6) and using the identity

$$\int_0^{2\pi} \begin{Bmatrix} \cos n\phi \\ \sin n\phi \end{Bmatrix} \exp (j\beta \cos (\phi - \phi')) \, d\phi$$

$$= 2\pi(j)^n \begin{Bmatrix} \cos n\phi' \\ \sin n\phi' \end{Bmatrix} J_n(\beta)$$

the required results are easily obtained.

REFERENCES

[1] S. I. Ghobrial, "Some data for the design of low cross-polarization feeds," Electron. Lett., vol. 9, pp. 465–466, 1973.
[2] G. T. Poulton and B. Claydon, "Determination of cross-polarization by use of focal-region fields," Electron. Lett., vol. 9, pp. 568–569, 1973.
[3] B. Richard and E. Wolf, "Electromagnetic diffraction in optical systems. Pt. II—Structure of the image in an aplanatic system," Proc. R. Soc. A., vol. 253, pp. 358–379, 1959.
[4] H. Minnet and B. Thomas, "Fields in the image space of symmetrical focusing reflectors," Proc. Inst. Elec. Eng., vol. 115, pp. 1419–1430, 1968.
[5] S. I. Ghobrial, "A suggested feed for the reduction of cross-polarization in paraboloidal reflector antennas," Postgraduate School of Elec. and Electron. Eng., University of Bradford, Rep. 145, 1973.
[6] ——, "Cross-polarization in reflector antennas," Ph.D. thesis, University of Bradford, 1972.

2-1 RADIATION FROM ELECTRIC
CURRENT ELEMENTS

One of the types of radiators frequently used in antenna practice is some form of thin
wire arranged in a linear configuration. If the current distribution on such a wire is
known or can be assumed with a reasonable degree of accuracy, then the radiation
pattern and the radiated power can be computed. This computation is based on the
integration of the effects due to each differential element of the current along the wire.
It is therefore of interest to set down the complete expressions for the fields at any
distance due to a differential element of current oriented along the z axis as shown in
Fig. 2-1. The rms electric and magnetic field components are given as follows:

$$E_r = 60\beta^2 I \, dz \left[\frac{1}{(\beta r)^2} - \frac{j}{(\beta r)^3} \right] \cos \theta \; e^{-j\beta r}$$

$$E_\theta = j30\beta^2 I \, dz \left[\frac{1}{\beta r} - \frac{j}{(\beta r)^2} - \frac{1}{(\beta r)^3} \right] \sin \theta \; e^{-j\beta r}$$

$$H_\phi = j \frac{\beta^2}{4\pi} I \, dz \left[\frac{1}{\beta r} - \frac{j}{(\beta r)^2} \right] \sin \theta \; e^{-j\beta r}$$

$$E_\phi = H_r = H_\theta = 0$$

where $I \, dz$ = moment of differential current element (I is given in rms amperes and
dz is given in meters.)

r = distance, m, to observation point

$\beta = 2\pi/\lambda$

λ = wavelength, m

$j = \sqrt{-1}$

E is given in volts per meter

H is given in amperes per meter

A time factor of $e^{j\omega t}$ has been omitted, since for all the cases in which we are
interested it is assumed that we have a sinusoidally time-varying current of constant
frequency.
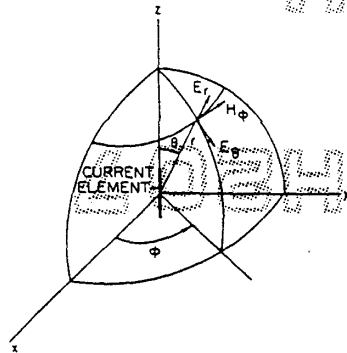
FIG. 2-1 Coordinate system for an electric
dipole.

2-2

For most problems of interest it is only necessary to know the components in the far field, i.e., when r is very much greater than the wavelength. Under these conditions, the field components are simply given by

$$E_\theta = j \frac{30\beta I \, dz}{r} \sin \theta \, e^{-j\beta r}$$

$$= j \frac{60\pi I \, dz}{r\lambda} \sin \theta \, e^{-j\beta r}$$

$$H_\phi = j \frac{\beta I \, dz}{4\pi r} \sin \theta \, e^{-j\beta r}$$

$$= \frac{E_\theta}{120\pi}$$

These expressions apply only for a very short element of current having a constant value along its length. However, they may readily be used to determine the field from any wire having a known current distribution by integrating the field due to each of the differential current elements along the length of the antenna. Taking into account the variation of current and the phase differential due to the varying distance from the observation point to each current element, the general expression for the field of any current distribution becomes

$$E_\theta = j \frac{60\pi \sin \theta}{r\lambda} \int_{-\ell/2}^{\ell/2} I(z) \, dz \, e^{-j\beta r(z)}$$

where both $I(z)$ and $r(z)$ are now functions of z and the integration takes place along the length of the antenna from $-\ell/2$ to $+\ell/2$.

For very short antennas, the above expression can be simplified to

$$E_\theta = j \frac{60\pi \sin \theta}{r\lambda} I_0 L_e e^{-j\beta r}$$

where I_0 = current at center of antenna
$\quad$ L_e = effective length of antenna defined as

$$L_e = \frac{1}{I_0} \int_{-\ell/2}^{\ell/2} I(z) \, dz$$

The effective length is of interest in determining the open-circuit voltage at the terminals of a receiving antenna. It is also used on occasion to indicate the effectiveness of a transmitting antenna.

For a short top-loaded linear antenna which has uniform current distribution as shown in Fig. 2-2a, the effective length is simply equal to the physical length. For a short antenna which is much less than a half wave long, as shown in Fig. 2-2b, the current distribution is essentially triangular and its effective length is one-half of its physical length.

For antennas with an overall length greater than about a quarter wavelength, the variation of the phase term cannot be neglected and the integral must be evaluated by taking this term into account. The method will be very briefly illustrated for the case of a thin half-wave radiator which can be assumed to have a sinusoidal current

(A-10)

Radar Target Amplitude, Angle, and Doppler Scintillation from Analysis of the Echo Signal Propagating in Space

JOHN H. DUNN AND DEAN D. HOWARD, SENIOR MEMBER, IEEE

Abstract—Radar target scintillation is observed in every type of radar system and has generally been analyzed on the basis of the performance of specific types of radar systems. However, the target scintillation phenomenon, including Doppler scintillation, may be expressed as distortions of the radar echo signal propagating in space, independent of radar system parameters. In this form it is convenient for visualizing the overall effects on radar systems and how these effects are altered by the radar system parameters. Past literature has demonstrated the target angle scintillation as a distortion of the radar echo signal phase front. Extension of this approach by a Poynting-vector analysis of the radar echo signal from a complex source shows a corresponding deviation of the direction of power flow consistent with the phase-front distortion theory and target scintillation measurements as well as describing all other target scintillation characteristics. The analysis demonstrates that deviations in the direction of the echo signal power flow from a complex target can be so large that the apparent source falls many target spans away from the actual target location. This is demonstrated by both tracking radar and single-beam search-type radar experiments. Although the theoretical angle deviations approach infinite error in target location, radar parameters, such as the finite size antenna aperture which perform a space integration of the echo signal, impose practical limitations. Typically, when a complex target such as an aircraft subtends an angle approaching a few tenths of a beamwidth, the antenna aperture integration will significantly limit the rms angle scintillation. Furthermore, the ways in which intentional means, such as diversity techniques, may be employed to reduce the effects of target scintillation on a radar are observed in Poynting-vector analysis.

The analysis of the echo signal propagating in space provides a readily visualized basis for derivation of the Doppler scintillation caused by the airframe (rigid body portion) of a complex target which spreads the Doppler over a finite bandwidth when it has random yaw, pitch, and roll motion typical of aircraft in flight. The derivation relates the Doppler scintillation to the angle scintillation and the random motions typical of aircraft targets. A typical aircraft target with Gaussian-distributed angle scintillation and Gaussian-distributed rates of random motion will have a spike-shaped Doppler spectrum described by the modified Hankel function K_0 where the parameters are determined from the values of the rms angle scintillation and the rms angular rates of random motion. These values can be closely approximated without extensive measurements on the target. Experimental results verify the theory. The expressions used to derive the Doppler spectrum may be modified to accommodate non-Gaussian distributed angle scintillation and rates of angle motion.

INTRODUCTION

IN THE PAST, radar target scintillation has generally been considered in terms of specific types of radars and their parameters. This paper describes how target scin-

tillation, including Doppler scintillation, exists in the propagating echo signal. A prior study analyzing the phase front of the echo signal from a complex target [1] showed that angle scintillation is a distortion of the echo signal phase front. This paper provides an analysis of the echo signal by the derivation of the Poynting vector. The results demonstrate that the energy in the radar echo signal from a complex target observed at a point in space can flow in directions deviating from the radial flow from a source. This angular deviation is shown to be identical to the angular errors that have been calculated for a linear radar tracking system [1], [2]. It may not be surprising that some deviation of the Poynting vector occurs with a distributed source; however, these deviations can produce an apparent source at a point far from the actual distributed source. The analysis not only verifies the phase-front distortion concept of angle scintillation but also shows the more fundamental nature of angle scintillation. The deviation of the Poynting vector proves that even a noncoherent energy absorbing aperture, which must be aligned normal to the direction of propagation to absorb maximum energy, is subject to angle scintillation. The practical uses and limitations of diversity techniques in reducing scintillation effects on tracking radars are described here.

This paper also shows how the phase-front distortion concept of angle scintillation provides a readily visualized picture of the source of Doppler scintillation of a complex target. The relation of the spectrum of Doppler scintillation to angle scintillation is derived so that the Doppler scintillation characteristics may be calculated from a knowledge of the rms angle scintillation and the rms rate of random angular motion of the target.

DERIVATION OF THE POYNTING VECTOR FOR A DISTRIBUTED SOURCE

The method for deriving the Poynting vector at a point in space from a distributed source of energy is described by the E- and H-field diagrams in Figs. 1 and 2. Although many possible types of sources could demonstrate the deviations of the Poynting vector, a series of short dipoles with a common axis is used here. This is appropriate because the short dipole is a radiating element that is physically realizable and has electric and magnetic fields that are well known.

The basic approach in determining the Poynting vector is to select a reference point within the distributed source about which the overall E- and H-fields will be determined. Fig. 1 shows the geometric relation of the coordinates and
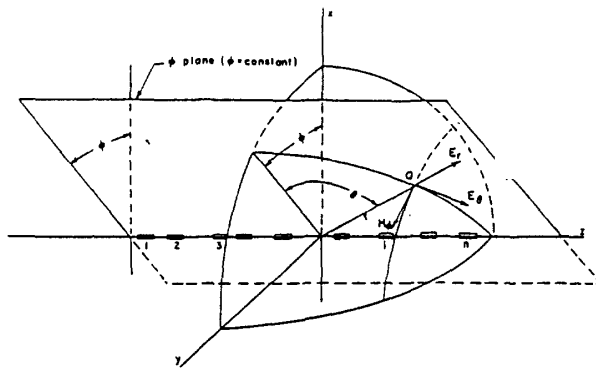
Fig. 1. Coordinate system for the multiple-element radiating source.
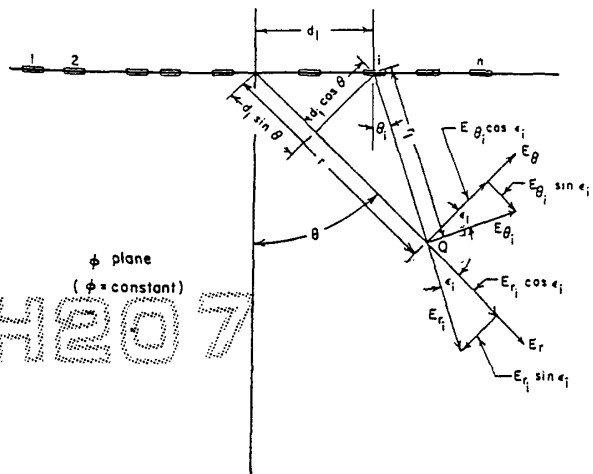
Fig. 2. Diagram of the E vectors in the ϕ plane where the H_ϕ vector is normal to the plane.

the E- and H-fields of interest. The next step is to describe the E- and H-fields of an element with respect to the element's center. The vector E-fields all fall in the ϕ plane; thus a drawing of the ϕ plane, as in Fig. 2, conveniently indicates the relation between the E_r- and E_θ-fields with respect to the origin and the E_{r_i}- and E_{θ_i}-fields of the ith element with respect to the element center. In Fig. 2 the value of d_i is the distance of the ith element from the origin and ϵ_i is the angular separation of the ith element from the origin as observed at point Q.

The fields of the ith element at point Q as shown in Fig. 2 are [3]

$$E_{r_i} = \frac{2m \sin \theta_i}{r_i} I_i \left[\frac{1}{s_i} \cos (\omega t + \alpha_i) \right. \tag{1}$$

$$\left. - \frac{1}{s_i{}^2} \sin (\omega t + \alpha_i) \right],$$

$$E_{\theta_i} = \frac{m \cos \theta_i}{r_i} I_i \left[\left(1 - \frac{1}{s_i{}^2} \right) \sin (\omega t + \alpha_i) \right. \tag{2}$$

$$\left. + \frac{1}{s_i} \cos (\omega t + \alpha_i) \right],$$

$$H_{\phi_i} = \frac{k \cos \theta_i}{r_i} I_i \left[\sin (\omega t + \alpha_i) + \frac{1}{s_i} \cos (\omega t + \alpha_i) \right] \tag{3}$$

where

$m = 30 \beta l$ is a constant determined by the element length in radians,

$k = \beta l / 4\pi$ is a similar constant determined by the element length in radians,

E_{r_i}, E_{θ_i} and H_{ϕ_i} are the electric and magnetic fields of the ith element in volts per meter and amperes per meter, respectively,

l is the length of the element in meters, assumed to be short compared to a wavelength,

r_i is the distance in meters from the ith reflector to point Q,

β is $2\pi/\lambda$ where λ is the wavelength of the source signal in meters,

I_i is the driving current in the ith element in amperes,

t is time,

ω is the RF frequency in radians per second,

γ_i is the relative phase of the driving current in the ith reflector,

θ_i is the angle of point Q with respect to the ith element as described in Fig. 2,

$s_i = \beta r_i$ is the distance of the ith element to point Q in radians, and

$\alpha_i = \beta r_i + \gamma_i$ is the phase of the signal from the ith element observed at Q.

The E_{r_i} and E_{θ_i} fields, as observed in Fig. 2, are not coincident with the corresponding E_r and E_θ, respectively, as defined in Fig. 1. Therefore, E_{r_i} and E_{θ_i} are each separated into components that are coincident with E_r and E_θ and summed. The H_ϕ-fields are coincident with H_ϕ; therefore the magnetic field component of each element adds directly to H_ϕ being affected geometrically only by the range of each element. Summing all the contributions of the elements to E_r, E_θ and H_ϕ gives the total fields:

$$E_r = \sum_{i=1}^{n} E_{r_i} \cos \epsilon_i + \sum_{i=1}^{n} E_{\theta_i} \sin \epsilon_i, \tag{4}$$

$$E_\theta = \sum_{i=1}^{n} E_{\theta_i} \cos \epsilon_i - \sum_{i=1}^{n} E_{r_i} \sin \epsilon_i, \tag{5}$$

and

$$H_\phi = \sum_{i=1}^{n} H_{\phi_i}, \tag{6}$$

where ϵ_i is the angular shift of the E_i-fields of the ith element

:aused by its displacement d_i from the origin. The values of iin ϵ_i and $\cos \epsilon_i$ in terms of the geometry shown in Fig. 2 are

$$\sin \epsilon_i = \frac{d_i \cos \theta}{r_i}, \quad \text{and} \quad \cos \epsilon_i = \frac{r_i - d_i \sin \theta}{r_i}.$$

The Poynting vector is a vector power P such that $P = P_r r + P_\phi \phi + P_\theta \theta$ where the components P_r, P_θ, and P_ϕ are parallel to the E_r, E_θ, and H_ϕ-field vectors (Fig. 1), respectively. The Poynting vector may be calculated from the cross product

$$P = E \times H.$$

Since

$$E_\phi = H_r = H_\theta = 0$$

$$P_r = E_\theta H_\phi, \quad \text{(7)}$$

and

$$P_\theta = - E_r H_\phi. \quad \text{(8)}$$

Thus, there is the expected radial component of power flow P_r plus an orthogonal component P_θ. With r and λ expressed in meters and I in amperes, P is a vector power density in watts per square meter.

P_r and P_θ, including all near-field components, are calculated in Appendix I and integrated to obtain the average power flows $\bar{P}_r$ and $\bar{P}_\theta$. In the radar case the region of major interest is where r is large with respect to the overall span of the source, and in this region $\bar{P}_r$ and $\bar{P}_\theta$ reduce to

$$\bar{P}_r = \frac{km \cos^2 \theta}{2r^2} \sum_{i=1}^{n} \sum_{j=1}^{n} I_i I_j \cos (\alpha_i - \alpha_j) \quad \text{(9)}$$

and

$$\bar{P}_\theta = \frac{km \cos^3 \theta}{2r^3} \sum_{i=1}^{n} \sum_{j=1}^{n} I_i I_j d_i \cos (\alpha_i - \alpha_j). \quad \text{(10)}$$

The significance of $\bar{P}_\theta$ is demonstrated in Fig. 3 from which the apparent source may be determined using the relation

$$\frac{e}{r} = \frac{\bar{P}_\theta}{\bar{P}_r}$$

where e is the displacement of the apparent source from the reference point in the actual source in the same linear units as r.

Solving for e and substituting for $\bar{P}_\theta$ and $\bar{P}_r$, one obtains

$$e = \frac{\sum_{i=1}^{n} \sum_{j=1}^{n} I_i I_j (d_i \cos \theta) \cos (\alpha_i - \alpha_j)}{\sum_{i=1}^{n} \sum_{j=1}^{n} I_i I_j \cos (\alpha_i - \alpha_j)}. \quad \text{(11)}$$

The values calculated from (11) indicate that angle errors will exist which are identical to the errors calculated for a monopulse tracking radar assuming constant angle sensitivity [2] and to the errors calculated when phase front distortion analysis is used [1] The verification of the phase-
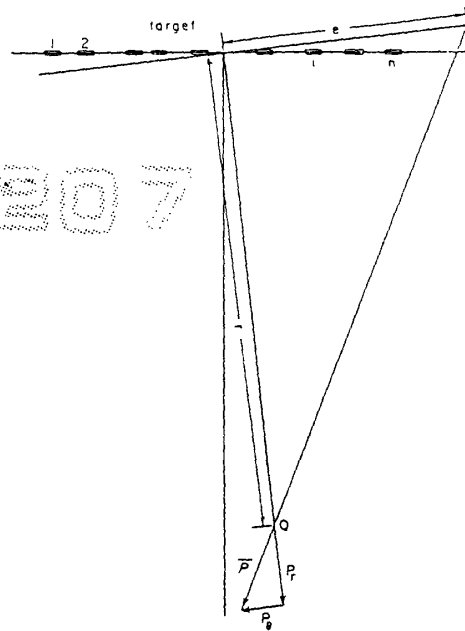
Fig. 3. Geometry relating the tilt of the Poynting vector to the displacement of the apparent source from the target center.

interest because it has frequently been argued that the phase-front distortion cannot take place since it implies a non-radial flow of power. However, this analysis shows that, indeed, the power flow does deviate from the radial direction and is normal to the phase-front contours.

A case of special interest is the two-element target [1], [2], [4] which readily demonstrates the unusual nature of angle scintillation in causing the apparent source to fall outside the physical extent of the target; however, the phenomenon could easily be demonstrated, if desired, with any number of elements. The error function for a two-source target may be obtained in convenient form from (11) by taking:

$$I_1 = 1, \quad I_2 = a, \quad d_1 = d/2, \quad d_2 = - d/2,$$

$$\alpha_1 = k + \phi, \quad \text{and} \quad \alpha_2 = k.$$

This places the radar normal to the dual source whose center is the zero reference. Then (11) reduces to

$$e = \frac{d}{2} \cos \theta \frac{1 + a^2}{1 + a^2 + 2a \cos \phi}, \quad \text{(12)}$$

which agrees with the phase-front concept of errors [1] and the error derived on the basis of a linear tracking radar system [2], [4].

APPLICATION TO ACTIVE TRACKING RADAR

The derivation of the Poynting vector was based on a set of signal sources with a given current I_i and phase γ_i with respect to an arbitrary reference, thus representing the passive tracking of an active source. The active tracking situation may be readily determined by considering the illumina-

illumination determines I_i and γ_i. Generally, the target is at sufficient range such that the elements receive equal illumination amplitude; however, at close range, when the target subtends a significant portion of the illuminating beam, the amplitude of element excitation will be determined by the shape of the one-way transmit antenna beam and the relative element location with respect to this beam.

The relative phase of the illumination will be determined by the distance from the transmitting antenna to each element. For a monostatic radar (same antenna for transmit and receive) the total phase change over the path to the elements and back to the radar will be 2 βr_i rather than the βr_i factor of (1), (2), and (3). The effect on the resultant received signal will be that the rate of change in relative phases as a function of aspect angle ψ will be doubled. This causes broadening of the angle scintillation spectrum by a factor of two, as well as a broadening of the Doppler scintillation spectrum as described later. For a bistatic radar with a transmitter location separate from the receiver there will be a βr_t term for the transmit signal path. This βr_t term must be added to the βr_i term for the receiver.

EXPERIMENTS DEMONSTRATING THE THEORY

An interesting experiment which provides a picture of the phase-front distortion phenomenon using a ripple tank [1] is shown in Fig. 4. Photographed phase fronts of a ripple-tank experiment are compared with a computer plot of the theoretical phase front for two sources separated three wavelengths having equal excitation with 180° relative phase. With equal excitation the amplitude observed for each source is inversely proportional to the distance to the observer causing the upper source to appear larger in the upper half of the plot and the lower source larger in the lower half. The distortion regions of the computer plot correspond closely in location and slope to those of the ripple-tank experiment. This provides a verification of the theory and demonstrates that the phenomenon is not restricted to radar and is equally present in other types of energy propagation. In the high distortion regions it may be seen that an observer looking normal to the phase front would be looking in a direction outside the dual source.

Fig. 5(a) shows the angle errors measured for a two-source target observed by a monopulse tracking radar, and Fig. 5(b) shows the corresponding theoretical plots. Although Fig. 5(a) does not include the effect of letting a exceed unity, thus causing the direction of the error to reverse, radar experiments are consistent with the theory.

The main point of interest is that both theory and measurements demonstrate that the apparent source of a radar signal can fall many target spans away from the target. The limitations to the maximum error are discussed later. This analysis also shows that the direction of power flow is correspondingly altered at the location of the radar. Although it was stated in [1] that this error is effective on any coherent aperture which senses the phase front, the Poynting-vector analysis demonstrates that it would be effective even on a flat black-body absorber, for example, which would be aligned normal to the power flow to absorb maximum energy.
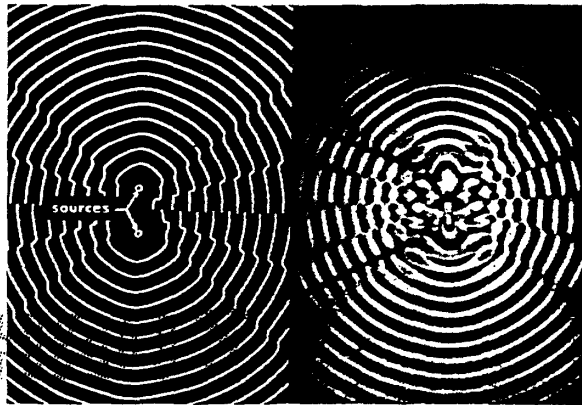
Fig. 4. Phase fronts radiating from a dual source having equal amplitude excitation with 180° relative phase and a separation of three wavelengths. The relative amplitude at each point is inversely proportional to relative range. The phase fronts plotted by a computer are compared to a photograph of experimental phase fronts obtained with a ripple tank having the same source conditions. (The signals from the two sources cancel completely along the horizontal center line between the sources and the phase makes a 180° change as the observer crosses this line.)

An experiment is described in Fig. 6 showing that even a simple antenna simulating the search radar method of target location will have its direction of maximum return shifted by angle scintillation. Although the amplitude drops as the sources are adjusted to the 180° phase relation, the direction of maximum return is shifted as predicted by the above theory demonstrating that even a search radar is affected by angle scintillation. Fig. 6(a) shows the experimental setup of the dual source using two horns illuminating a larger horn. Patterns of the larger horn were plotted by rotating the horn about its phase center for different relative amplitudes and relative phases of the dual source. When the two sources are in phase, a normal H-plane pattern is observed. When the relative phase is adjusted to 180° and the relative amplitude is adjusted to 0.9 with the right horn having the stronger signal, the phase-front tilt predicted by (12) is about ten times the 0.6° separation of the two sources toward the right. This gives approximately a 6° shift of the apparent source from the midpoint of the dual source as verified by the experiment of Fig. 6. Similarly, reversing the relative amplitude so that the left source is larger causes a −6° shift.

The practical limitations to angle scintillation error are readily demonstrated by the phase-front and Poynting-vector concepts of angle scintillation. Some of these limitations are discussed later.

Practical radar targets such as aircraft are composed of many reflecting surfaces distributed over the target extent. For a given instant of time the apparent target angular location could be computed from (11) for known echo amplitude from each reflector I_i and I_j, known location of each reflector d_i, and known relative phase of the reflectors $(\alpha_i - \alpha_j)$ determined by the relative range from their phase centers to the radar. Aircraft in flight, however, have random yaw, pitch, and roll motions which, although small in aspect angle, cause
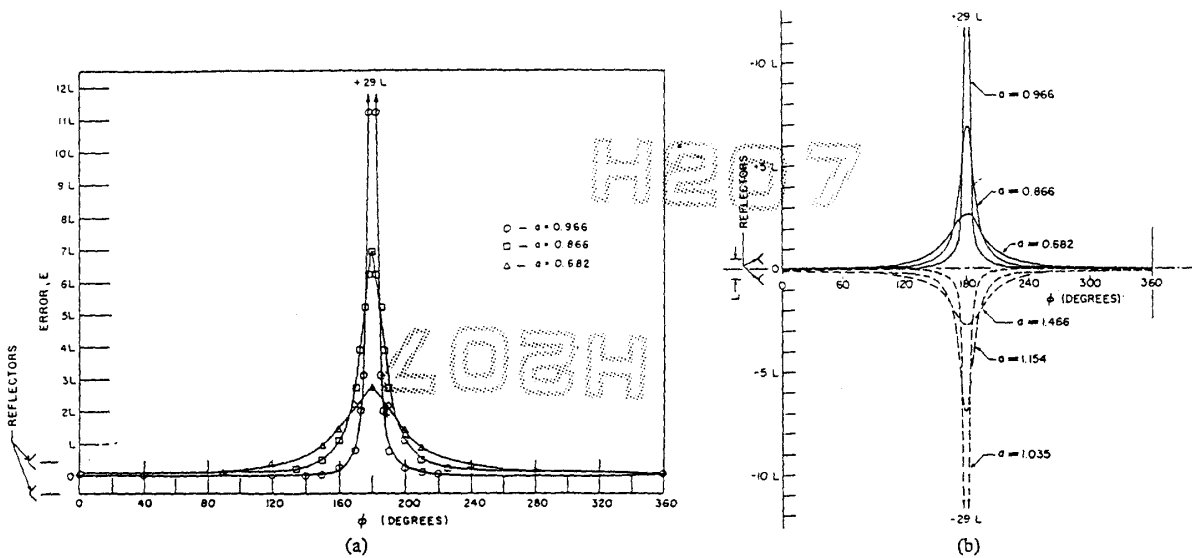
Fig. 5. Apparent location of a dual-source target as a function of relative phase for different values of relative amplitude (a) measured with a tracking radar and (b) calculated. (Fig. 5(a) from [1]).
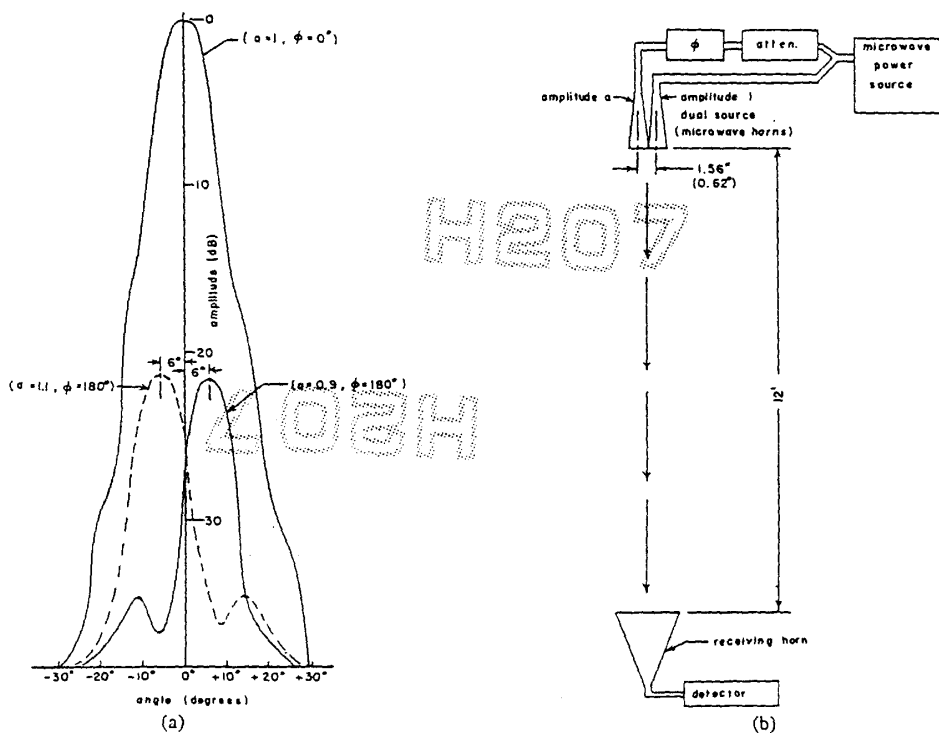
Fig. 6. Demonstration of the distortions of the patterns of a single-beam antenna by a distributed source using (a) a dual horn source illuminating a single horn rotated about its phase center to obtain (b) patterns for the in-phase and out-of-phase dual source excitation with different relative amplitudes.

large changes in relative phase $(\alpha_i - \alpha_j)$. For example, a change in relative range of two reflectors of only 0.6 inch at X-band causes a 360° change in their relative phase as observed by an active tracking radar. With larger aspect changes, the values of I_i and I_j will also change significantly. The random changes in these parameters cause e of (11) to be a random function of time. Fig. 7 shows analyses of typical angle scintillation data measured by a monopulse instrumentation radar tracking an SNB aircraft. Fig. 7(a) shows the typical Gaussian-shaped probability distribution of angle scintillation with significant area extending beyond the extremities of the target. Fig. 7(b) shows typical spectral energy distributions for the aircraft measured at X-band with moderate air turbulence. The total rms value of the angle scintillation is essentially constant for a given target, aspect, and RF frequency [2] giving constant area under the spectrum when plotted as a power density spectrum; however, the spectrum will spread or reduce as a function of increased or decreased atmospheric turbulence, respectively, and will change proportional to RF frequency [2].

PRACTICAL LIMITATIONS ON ANGLE NOISE IMPOSED BY RADAR EQUIPMENT CHARACTERISTICS AND BY DIVERSITY TECHNIQUES

The phase-front and Poynting-vector calculations define the target signal at a point in space. However, radar antennas generally have a finite aperture that will average the effects which occur over the extent of the aperture weighted by various factors, for example, illumination taper and echo amplitude variation. The significant factors in determining the extent of aperture integration are the target span (and distribution of the elements and currents), target range, and antenna size. Fig. 8 shows a span of one full cycle of phase-front distortion for a two-point target to demonstrate the relation between these parameters. If the radar antenna spanned only a very small increment of the phase front, it would see an essentially flat phase front and the direction of the apparent source of energy would closely follow the value predicted by (12). However, if the antenna spans a large portion of the distortion region it will average the phase-front contour.

To demonstrate typical relations between target size, target range, and radar aperture size, Fig. 8 shows a convenient example of a two-element target whose elements are separated by a distance d, where the radar aperture D spans a full cycle of the distorted phase front (a full cycle occurs when the relative phase between the target elements changes by 2π radians as observed from one side of the radar aperture with respect to the other). It is assumed that the radar and the phase center of the transmitter are stationary and that the relative phase of the echo from the two elements is observed at point Q at one extremity of the aperture. The paths from the transmitter to the elements are equal but the return paths to point Q differ by an amount 2δ. From the geometry it is observed that

$$\frac{D/2}{r} = \frac{\delta}{d/2} \qquad (r \gg d),$$

TRACKING ERROR (YARDS)

(a)

TRUE NOISE FREQUENCY In Hz
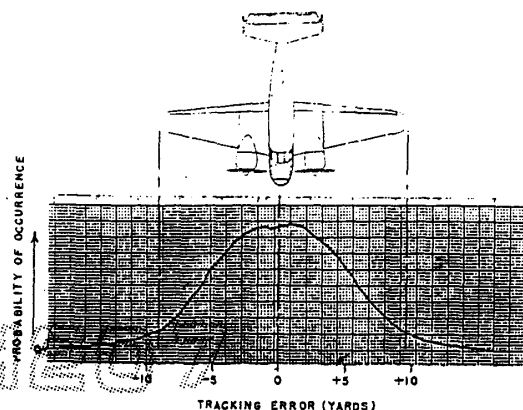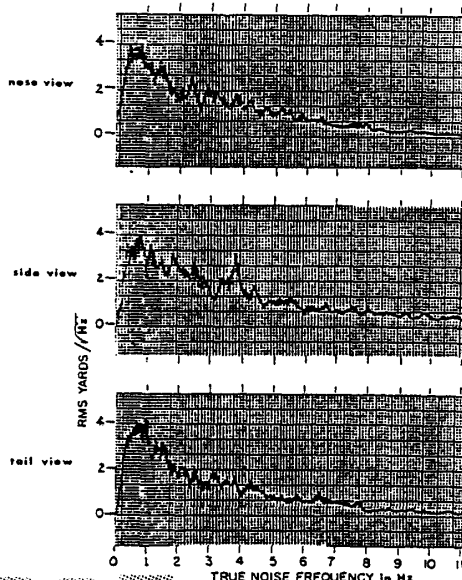
(b)

Fig. 7. (a) Amplitude probability distribution and (b) spectral energy distribution of angle scintillation measured by an X-band monopulse radar tracking an SNB type aircraft.

or

$$D = \frac{4\delta r}{d} \cdot$$

When δ is a quarter-wavelength as observed at point Q, the aperture D will span a full cycle of the distorted phase front, or

$$D_s = \frac{r\lambda}{d}, \qquad (13)$$

where D_S is the condition where $\delta = \lambda/4$. For example, with X-band $(\lambda = 3.53$ cm) illumination of two reflectors separated by 4 m along a normal to the direction of a radar at a 2 nmi range, the span of a full cycle of the phase-front
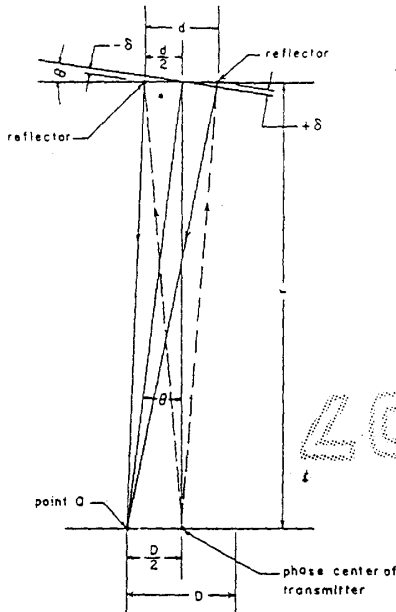
Fig. 8. Diagram relating the relative phase of the echoes from a two-reflector target to linear displacement in the vicinity of the radar antenna.

distortion will be 32.3 m. At a range of $\frac{1}{4}$ nmi the span would be about 4 m, which is typical of an X-band antenna aperture.

This relation may also be expressed in terms of the ratio of target span to radar beamwidth. Typically, the one-way half-power beamwidth is 1.2 λ/d radians and the target span is d/r radians for $r \gg d$. The ratio of target angular span θ_t to the one-way radar beamwidth θ_b is

$$\frac{\theta_t}{\theta_b} = \frac{dD}{1.2\lambda r}.$$

Substituting the condition that the radar aperture spans a full distortion cycle, described by (13), the ratio of the target span to the beamwidth becomes

$$\frac{\theta_t}{\theta_b} = 0.83.$$

For this example with a dual source, the radar aperture will give considerable averaging of the distorted phase front. In practical tracking problems the relation depends on many factors including the antenna illumination taper, the echo-signal amplitude function across the antenna aperture, and the target reflectivity distribution. From experiments, consistent with estimates from this calculation, the aperture integration will become significant for radar tracking of aircraft when the target is sufficiently large and is close enough to span a few tenths of the one-way radar beamwidth. For a given target span (this may include multiple unresolved targets) the aperture integration will be most effective on a

two-element target. Because of this averaging effect, measurements made on three small aircraft in formation show a significant decrease in the rms target angle scintillation when the target exceeded approximately 0.25 beamwidth.

This space averaging by the antenna aperture is called space diversity. Multiple-radar receivers could be spaced to track the target from widely separated locations (wide with respect to the phase-front distortion pattern) so that they will each observe independent samples of the angle noise. Averaging the target angular location would reduce the target noise power. For random Gaussian-distributed angle scintillation, two radar trackers would provide about a 3 dB scintillation reduction.

Frequency diversity is another diversity technique for averaging target scintillation either instantaneously or within a short period of time. This method is to look at the target with different RF frequencies either simultaneously or pulse to pulse with sufficient separation between the frequencies such that the scintillation at one frequency is uncorrelated with that from the next frequency. Equation (11) relates the frequency dependence of target scintillation to the target configuration and aspect. It may be observed in (11) that for $\beta = 2\pi/\lambda$, the phase differences in the terms of the summation for self-excited sources are $2\pi/\lambda(r_i - r_j) + (\gamma_i - \gamma_j)$; for two-way (active tracking) the phase difference is $4\pi/\lambda(r_i - r_j) + (\gamma_i - \gamma_j)$, showing the relation between the relative phase, wavelength, and range separation of the elements of the target. For example, if two reflectors were separated by 10 yards $(r_i - r_j = 10$ yds) and $\lambda = 3.3333$ cm (9000 Hz), the total phase difference of the echoes from the reflectors is 548.74 wavelengths. By decreasing the wavelength to 3.3267 cm the total phase difference is increased one full wavelength to 549.74. The new wavelength corresponds to a frequency of 9.018 GHz. Thus, a frequency change of 18 MHz causes a full 360° change in the relative phase (one full cycle of the phase-front distortion pattern) giving a similar amount of integration to that for the space integration by two radars separated by a full distortion cycle. Even though the example was for X-band, the frequency change required for a given relative phase change between reflectors separated by a given distance is independent of the RF frequency.

It is interesting that space-diversity effectiveness is determined by the angle subtended at the target, while frequency-diversity effectiveness is determined by the range distribution of the target. Therefore, the two diversity techniques may be effectively combined.

Polarization diversity is another means for changing the angle scintillation function. In this case the effectiveness is dependent on the polarization characteristics of each element such that by changing from one polarization to an orthogonal polarization, for example, I_i and γ_i change.

By studying (9) for P_r it may be seen that the diversity techniques also affect amplitude scintillation such that some of the deeper signal fades may be averaged. The Doppler scintillation discussed later may also be reduced by diversity techniques. It should be mentioned that frequency- and space-diversity techniques can also affect the I_i of each element but since the individual elements of a target are us-

ually small, it would require very wide radar spacing or frequency change to make a significant alteration in the values of I_i.

DOPPLER SCINTILLATION DERIVED FROM ANGLE SCINTILLATION AND TARGET MOTION

Doppler scintillation caused by a complex target may be divided into two phenomena [5]: 1) Doppler spectral lines caused by moving parts of the aircraft such as propellers and jet turbine blades and 2) a continuous Doppler spectrum spread, caused by the random motion of the target in flight, which is typically symmetrical with respect to the average Doppler of the target. Time plots of typical aircraft headings, for an aircraft flying a "straight course," are shown in Fig. 9 to demonstrate the typical yaw motion of an aircraft in average low-altitude air turbulence which causes the Doppler scintillation and other scintillations.

The Doppler scintillation caused by the airframe of the target is related to the rate of change of the angle noise previously described. The relation can be readily visualized by considering the phase-front distortion concept of angle noise. Angle noise is the slope of the phase front of the echo of a complex target at any instant with respect to the flat phase front (circular at close range) that would have been radiated if the target were a point source. The slope is a measure of angle error because the angle-tracking system indicates the direction of the target as the direction normal to the phase front. This may be demonstrated under static conditions. The Doppler noise modulation is the time rate of phase change with respect to the phase that would exist if the target were a point source. Fig. 10 demonstrates how the distorted phase front from a complex target (two reflectors for this example) is caused to rotate [1] as the target yaws through a small change in aspect angle. As the distortion region of the phase front rotates past the radar it causes a phase jump, and the rate of this change of phase is frequency. This frequency, at any instant, is referred to as instantaneous frequency. The phase jump also occurs under multipath conditions in FM communications and has been demonstrated and analyzed in detail [6]. If the target aspect angle rotated at a constant rate, the angle-noise time function and the instantaneous Doppler-frequency time function would appear identical [1]. However, where the target has typical random motion, the Doppler modulation may be calculated for a given phase-front distortion pattern and target random motion may be calculated by differentiating the phase deviations (referenced to the phase that would be received if the target were a point source) with respect to time, or

$$f(t) = \frac{d\phi(t)}{dt},$$

where

$f(t)$ is the instantaneous Doppler frequency,
$d\phi(t)/dt$ is the time rate of change of the phase deviation as seen at the radar.
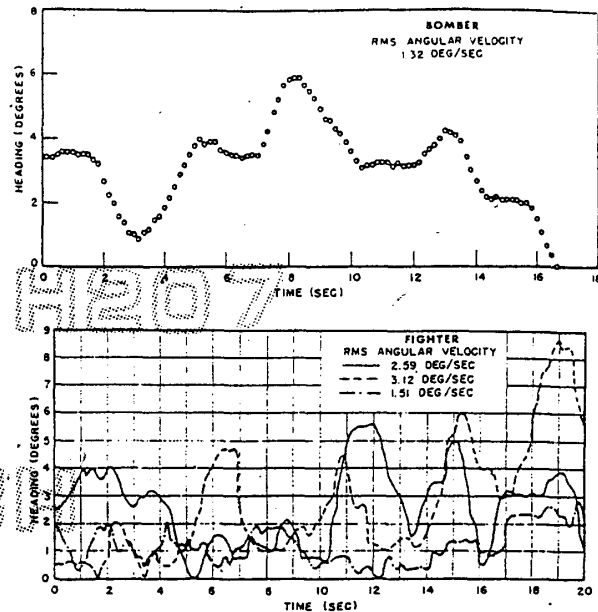
Fig. 9. Typical aircraft yaw gyro data samples measured on a fighter and a bomber attempting to fly a straight course in a clear medium-turbulence atmosphere.
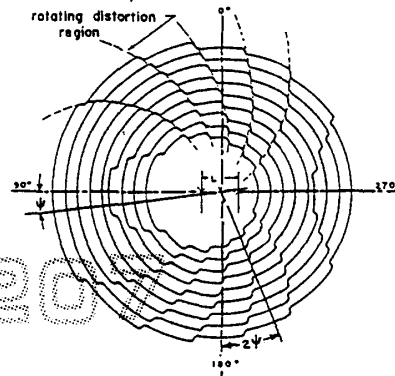
Fig. 10. Rotation of the phase-front distortion pattern through an angle of 2ψ as two reflectors are rotated through an angle of ψ when illuminated by a radar (the rotation rate is exaggerated compared to the propagation velocity of the phase front to aid visualization of the phenomenon).

In considering only the airframe, which may be assumed to be a rigid body, the only time variable in $\phi(t)$ is $\alpha(t)$, the angular rotation rate of the phase front caused by target random motion with respect to the target average flight path, as illustrated in Fig. 10. Thus,

$$f(t) = \frac{d\phi(\psi)}{d\psi} \frac{d\alpha(t)}{dt},$$

where

$\alpha(t)$ is the time function of the angular rotation of the phase-front distortion pattern,

$\phi(\psi)$ is the phase front distortion pattern phase deviation at any instant as a function of the target aspect angle ψ observed by moving in a circular path around the target.

If the target were composed of self-excited elements, the relative phases of the excitation would remain fixed regardless of aspect angle. Therefore, the function $\alpha(t)$ would be identical to the target aspect-angle deviations from the average flight path caused by target random yaw motion. However, in an active radar, where the radar illuminates reflecting elements on the target, the excitation of the elements changes as a function of target aspect. Consequently, the relative phase between the echo signals from the elements, as observed at the radar, changes at twice the rate as in the case of self-excited sources. This causes the phase-front distortion pattern to rotate, as illustrated in Fig. 10 at twice the rate of the target random angle motion shown in Fig. 9. Therefore, $d\alpha(t)/dt$ will be twice the measured rates for target angular motion, or $2d\psi/dt$.

Thus, measurements of target angular motion provide data for the second term of $f(t)$. In addition, angle scintillation measurements provide information that can be used for $d\phi(\psi)/d\psi$, since the angle scintillation error is equal to the phase-front slope.

The information of greatest interest about Doppler scintillation is the spectrum shape rather than the time function of the instantaneous frequency. The Doppler scintillation spectrum is the probability density distribution $f(t)$ which gives the percentage of time the frequency falls within a given increment of bandwidth. The probability density of $f(t)$ may be determined for the known densities of $d\phi(\psi)/d\psi$ and $d\alpha(t)/dt$, as described in Appendixes II and III.

It is assumed that, with a sufficient time sample, the probability density distribution of the measured angle scintillation, which is a time function, is equal to the probability density of $d\phi(\psi)/d\psi$, or the phase-front slope that exists over the same range of aspect angles experienced during the angle scintillation measurements. Appendix II shows how values for angle scintillation, typically in linear units of error measured at the target, may be converted to radians of phase per radian of aspect angle.

A typical example is analyzed for the conditions that the angle scintillation is assumed to be Gaussian with an rms value σ_ψ that may be closely predicted from an aircraft's dimensions [2] and the radar target motion is Gaussian with an rms value estimated from the data of Fig. 9. This rms value will be doubled for the distribution of $d\alpha(t)/dt$, because the phase-front distortion pattern moves at twice the rate of aspect-angle change, as discussed above.

In Appendix III the probability density distribution $p(f)$ of the time function of instantaneous frequency $f(t)$ for the above example is derived. The distribution has the shape of a modified Hankel function, or

$$1 \quad \cdot\cdot \left[\quad f \quad \right]$$

where

K_0 is a modified Hankel function [7],

σ_ψ is the standard deviation of angle scintillation in dimensionless units of radians of phase per radian of aspect angle, and

σ_t is the standard deviation of yaw rate in Hz.

Appendix II shows that σ_ψ may be determined by the relation

$$\sigma_\psi = \frac{2\pi\sigma_{ang}}{\lambda},$$

where

σ_{ang} is the standard deviation of angle scintillation in linear units measured at the target, and

λ is the RF wavelength in the same linear units as σ_{ang}.

The derivation of $p(f)$ assumes a relatively fast AGC circuit giving each value of $f(t)$ equal weight. However, because of the negative correlation between angle noise magnitude and signal amplitude, a slow AGC system will reduce the weight given to the components of the spectrum as a function of displacement from the average Doppler, thus narrowing the spectrum somewhat like the effects of AGC on angle scintillation peaks [2].

The function $p(f)$ was determined with respect to the average Doppler frequency. Its peak is at $f=0$; but, on an absolute basis, the peak will be the average Doppler frequency of the target (after detection). The function $p(f)$ goes to infinity as the argument of K_0 goes to zero; however, it is a density function which, like the probability density function of a sine wave with two infinite peaks, does not imply an infinite probability. The function $p(f)$ behaves properly, having the necessary total probability of unity when it is integrated over all possible values from $-\infty$ to $+\infty$. It will, therefore, have some fractional probability when it is integrated over any finite range of frequencies.

A typical example is calculated for a large aircraft such as a Boeing 707. The wing span is 40 m for the nose view; σ_{ang} is estimated at 6 meters (the method for estimate σ_{ang} is discussed in [2]), and for X-band ($\lambda = 0.032$ m) $\sigma_\psi = 1178$. The typical rms yaw rate[1] of 0.8°/s divided by 360°/cycle gives a σ_t of 0.0022 Hz. This causes a detected Doppler spectrum defined by

$$p(f) = 0.062K_0\left(\frac{f - fd}{5.18}\right),$$

where f_d is the average Doppler frequency of the target airframe. The function $p(f)$ is plotted in Fig. 11 and demonstrates the expected long time average Doppler spectrum for the nose-view straight-line flight of the example aircraft. Measurements on a Boeing 707 at X-band with a high resolution Doppler system are shown in Fig. 12 and agree closely

---

[1] This value was selected lower than that for the bomber data of Fig. 8 because commercial aircraft under medium power have more ... ... relatively high power as in the case
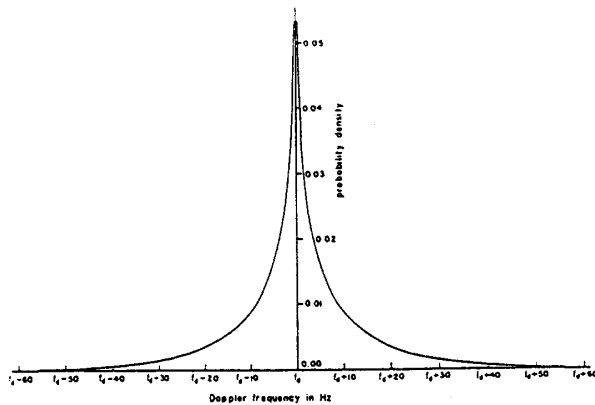
Fig. 11. Probability density distribution of scintillating Doppler frequency of a complex target with random motion.

12.66 12.68 12.70 12.72 kHz.
DOPPLER FREQUENCY
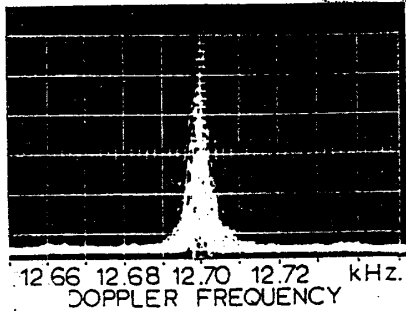
Fig. 12. High resolution measurement of the pulse Doppler spectrum of the airframe of a Boeing 707 jet aircraft at X-band.

2.26 2.28 2.30 2.32 kHz.
DOPPLER FREQUENCY

(a)

0 0.4 0.8 1.2 1.6 kHz
DOPPLER FREQUENCY

(b)

0 2 4 6 8 kHz
DOPPLER FREQUENCY

(c)

Fig. 13. Pulse Doppler spectrum measurements showing (a) amplitude modulation sideband pair caused by the scan of a conical scan radar, (b) FM modulation by the propellers of a DC-7 aircraft causing a single set of sidebands, and (c) sidebands caused by the compressor blades of jet engines displaced from the airframe Doppler by the RPS of the compressor C and multiples of C.

with the theoretical distribution. It should be mentioned that any constant turning rate, velocity change, or aspect change will cause an additional constant value in $d\psi(t)/dt$. This will result in some spreading of the Doppler spectrum and a change toward a less abrupt function near the peak in $p(f)$, in addition to a shift of the entire spectrum resulting from a change in the average radial velocity. The spectrum shift will cause a smearing or spectrum spread which depends on the sample length.

The components of the echo from the target's rotating or moving parts will cause Doppler lines at frequencies displaced from the airframe Doppler spectrum. The periodic amplitude modulation will cause pairs of Doppler lines symmetrical with respect to the airframe Doppler return from the target. Moving parts can also cause some pure frequency modulation which will give a single set of spectral lines on one side of the airframe Doppler spectrum [5]. Examples of Doppler measurements from [5] are shown in Fig. 13.

The major significance of the Doppler modulation is its effect on Doppler measuring radars. A Doppler tracking system which automatically tracks the frequency of a spec-

tral line of the echo is subjected to two problems: 1) the possibility of locking on a false line caused by moving parts of the target, and 2) a noisy Doppler reading, as defined by the random fluctuations in the instantaneous frequency, when the system is properly locked on to the airframe Doppler spectrum. The rms Doppler error for $p(f)$ in (14) will be $2.72 \sigma_\psi \sigma_t$.

Appendix III also shows how the Doppler scintillation spectrum may be determined for other than Gaussian angle scintillation and target motion.

SUMMARY

The derivation of the Poynting vector of the echo signal of a complex radar target demonstrates that the deviations of the apparent source of the echo signal caused by target angle scintillation are accompanied by a corresponding deviation of the direction of power flow. Although some deviation is expected from a distributed source, it is demonstrated that the apparent source can fall many target spans away from the target. Experiments verifying the theory are described for both a tracking radar and a single-beam search system. The practical limitations due to the effects of angle scintillation on radar are demonstrated. It is shown how the angle scintillation becomes limited by integration in space by the radar antenna aperture when the target exceeds a few tenths of a beamwidth. Intentional limitation by diversity techniques is discussed and it is shown how these techniques provide averaging of the target scintillation.

The concepts of angle scintillation as a distortion of the echo signal propagating in space provide a readily visualized means for deriving the Doppler scintillation spectrum from the airframe of the target. When the target angle scintillation and the target yaw rates are Gaussian, the Doppler scintillation spectrum is shown to take the shape of the K_0 modified Hankel function verified by measurements of targets in flight with a high resolution Doppler radar system. The spectrum may be calculated from the rms values of target angle scintillation and yaw rate, which may be closely estimated without measurements on the target. It is also shown how the Doppler scintillation spectrum may be determined from the target angle scintillation and yaw rates which are non-Gaussian.

APPENDIX I

CALCULATION OF P_r AND P_θ COMPONENTS OF THE POYNTING VECTOR

The value of P_r is the product $E_\theta H_\phi$ as described in the text. By substituting the values of E_{r_i} and E_{θ_i} from (1) and (2) in (5), and H_{ϕ_i} from (3) in (4) and multiplying,

$$P_r = \left\{ \frac{km \cos^2 \theta}{r^2} \sum_{i=1}^{n} \sum_{j=1}^{n} I_i'' I_j'' \cos \epsilon_i \left[\frac{1}{s_i s_j} \cos (\omega t + \alpha_i) \right. \right.$$

$$\left. \cdot \cos (\omega t + \alpha_j) + \left(\frac{1}{s_j} - \frac{1}{s_i^2 s_j} \right) \sin (\omega t + \alpha_i) \right.$$

$$\left. \cdot \cos (\omega t + \alpha_j) + \frac{1}{s_i} \sin (\omega t + \alpha_j) \cos (\omega t + \alpha_i) \right.$$

$$\left. + \left(1 - \frac{1}{s_i^2} \right) \sin (\omega t + \alpha_i) \sin (\omega t + \alpha_j) \right] \right\}$$

$$- \left\{ \frac{2km \cos \theta \sin \theta}{r^2} \sum_{i=1}^{n} \sum_{j=1}^{n} I_i' I_j'' \sin \epsilon_i \right.$$

$$\left. \cdot \left[\frac{1}{s_i s_j} \cos (\omega t - \alpha_i) \cos (\omega t - \alpha_j) \right. \right.$$

$$- \frac{1}{s_i^2 s_j} \sin (\omega t - \alpha_i) \cos (\omega t - \alpha_j) + \frac{1}{s_i} \sin (\omega t - \alpha_j)$$

$$\left. \cdot \cos (\omega t - \alpha_i) - \frac{1}{s_i^2} \sin (\omega t - \alpha_i) \sin (\omega t - \alpha_j) \right] \right\} ,$$

where

$$I_i' = I_i \frac{r}{r_i} \frac{\sin \theta_i}{\sin \theta} \qquad I_i'' = I_i \frac{r}{r_i} \frac{\cos \theta_i}{\cos \theta} .$$

Similarly, P_θ is the product $-E_r H_\phi$ as described in the text. By substituting the values of E_{r_i} and E_{θ_i} from (1) and (2) into (4) for E_r and multiplying with H_ϕ, one obtains

$$P_\theta = \left\{ -\frac{km \cos^2 \theta}{r^2} \sum_{i=1}^{n} \sum_{j=1}^{n} I_i'' I_j'' \sin \epsilon_i \right.$$

$$\left. \cdot \left[\frac{1}{s_i s_j} \cos (\omega t - \alpha_i) \cos (\omega t - \alpha_j) \right. \right.$$

$$+ \left(\frac{1}{s_j} - \frac{1}{s_i^2 s_j} \right) \sin (\omega t + \alpha_i) \cos (\omega t + \alpha_j)$$

$$+ \frac{1}{s_i} \sin (\omega t + \alpha_j) \cos (\omega t + \alpha_j)$$

$$\left. + \left(1 - \frac{1}{s_i^2} \right) \sin (\omega t + \alpha_i) \sin (\omega t + \alpha_j) \right] \right\}$$

$$- \left\{ \frac{2km \cos \theta \sin \theta}{r^2} \sum_{i=1}^{n} \sum_{j=1}^{n} I_i' I_j'' \cos \epsilon_i \right.$$

$$\left. \cdot \left[\frac{1}{s_i s_j} \cos (\omega t - \alpha_i) \cos (\omega t - \alpha_j) \right. \right.$$

$$+ \frac{1}{s_i^2 s_j} \sin (\omega t - \alpha_i) \cos (\omega t - \alpha_j)$$

$$+ \frac{1}{s_i} \sin (\omega t - \alpha_j) \cos (\omega t - \alpha_i)$$

$$\left. - \frac{1}{s_i^2} \sin (\omega t - \alpha_i) \sin (\omega t - \alpha_j) \right] \right\} .$$

These values of P_r and P_θ are the instantaneous power as a function of products of sine and cosine terms. All products expand to the sine and the cosine of the sum $(2\omega t + \alpha_i + \alpha_j)$ and the difference $(\alpha_i - \alpha_j)$ or $(\alpha_j - \alpha_i)$ of the arguments of the terms of the product. To determine the average power flow, by integrating P_r and P_θ over an RF cycle, all sin $(2\omega t + \alpha_i + \alpha_j)$ and cos $(2\omega t + \alpha_i + \alpha_j)$ terms average to zero, and the following relations may be used:

$$\overline{\cos (\omega t + \alpha_i) \cos (\omega t + \alpha_j)} = \overline{\sin (\omega t + \alpha_i) \sin (\omega t + \alpha_j)}$$

$$= \tfrac{1}{2} \cos (\alpha_i - \alpha_j)$$

or

$$\overline{\sin (\omega t + \alpha_i) \cos (\omega t + \alpha_j)} = -\overline{\sin (\omega t + \alpha_j) \cos (\omega t + \alpha_i)}$$

$$= \tfrac{1}{2} \sin (\alpha_i - \alpha_j).$$

Therefore, the average power flow in the r and θ directions become, respectively,

$$\bar{P}_r = \frac{km \cos^2 \theta}{2r^2} \sum_{i=1}^{n} \sum_{j=1}^{n} I_i'' I_j'' \cos \epsilon_i \left[\left(1 - \frac{1}{s_i^2} + \frac{1}{s_i s_j} \right) \right.$$
$$\left. \cdot \cos (\alpha_i - \alpha_j) + \left(\frac{1}{s_i} - \frac{1}{s_j} - \frac{1}{s_i^2 s_j} \right) \sin (\alpha_i - \alpha_j) \right]$$
$$- \frac{km \cos \theta \sin \theta}{r^2} \sum_{i=1}^{n} \sum_{j=1}^{n} I_i' I_j'' \sin \epsilon_i \left[\left(\frac{1}{s_i} + \frac{1}{s_i^2 s_j} \right) \right. \quad (15)$$
$$\left. \cdot \sin (\alpha_i - \alpha_j) + \left(\frac{1}{s_i s_j} - \frac{1}{s_i^2} \right) \cos (\alpha_i - \alpha_j) \right]$$

and

$$\bar{P}_\theta = - \frac{km \cos^2 \theta}{2r^2} \sum_{i=1}^{n} \sum_{j=1}^{n} I_i'' I_j'' \sin \epsilon_i \left[\left(1 - \frac{1}{s_i^2} + \frac{1}{s_i s_j} \right) \right.$$
$$\left. \cdot \cos (\alpha_i - \alpha_j) + \left(\frac{1}{s_i} - \frac{1}{s_j} - \frac{1}{s_i^2 s_j} \right) \sin (\alpha_i - \alpha_j) \right]$$

$$\quad (16)$$

$$- \frac{km \cos \theta \sin \theta}{r^2} \sum_{i=1}^{n} \sum_{j=1}^{n} I_i' I_j'' \cos \epsilon_i \left[\left(\frac{1}{s_i} + \frac{1}{s_i^2 s_j} \right) \right.$$
$$\left. \cdot \sin (\alpha_i - \alpha_j) + \left(\frac{1}{s_i s_j} - \frac{1}{s_i^2} \right) \cos (\alpha_i - \alpha_j) \right].$$

There are three regions of interest: 1) a very near region within the order of a few target spans from the target, 2) a near region extending from the very near region to the near edge of the far field defined as the distances where the ranges to each element s_i and s_j are essentially equal, and 3) a region in the far field. In the far-field region terms divided by s_i became negligible, and θ_i and θ_j are essentially equal to θ. Equations (15) and (16) must be used in the very near region. In the near region

$$\bar{P}_r(\text{near}) = \frac{km \cos^2 \theta}{2r^2} \sum_{i=1}^{n} \sum_{j=1}^{n} I_i'' I_j'' \cos \epsilon_i \cos (\gamma_i - \gamma_j)$$
$$\quad (17)$$
$$+ \frac{km \cos \theta \sin \theta}{r^2} \sum_{i=1}^{n} \sum_{j=1}^{n} I_i' I_j'' \frac{\sin \epsilon_i}{s_i} \sin (\gamma_i - \gamma_j)$$

and

$$\bar{P}_\theta(\text{near}) = - \frac{km \cos^2 \theta}{2r^2} \sum_{i=1}^{n} \sum_{j=1}^{n} I_i'' I_j'' \sin \epsilon_i \cos (\gamma_i - \gamma_j)$$
$$\quad (18)$$
$$- \frac{km \cos \theta \sin \theta}{r^2} \sum_{i=1}^{n} \sum_{j=1}^{n} I_i' I_j'' \frac{\cos \epsilon_i}{s_i} \sin (\gamma_i - \gamma_j).$$

In the far-field region and the near region the normal to the sources, where $\theta = 90°$ $I_i'' = I_i' = I_i$ and $I_j'' = I_j$, $s_i = \beta r$, $\cos \epsilon_i = 1$, and $\sin \epsilon_i = d_i \cos \theta / 2r$, are

$$\bar{P}_r(\text{far}) = \frac{km \cos^2 \theta}{2r^2} \sum_{i=1}^{n} \sum_{j=1}^{n} I_i I_j \cos (\gamma_i - \gamma_j) \quad (19)$$

and

$$\bar{P}_\theta(\text{far}) = \frac{km \cos^2 \theta}{2r^3} \sum_{i=1}^{n} \sum_{j=1}^{n} I_i I_j d_i \cos (\gamma_i - \gamma_j). \quad (20)$$

APPENDIX II

CONVERSION OF ANGLE SCINTILLATION ERROR IN LINEAR UNITS TO UNITS OF RADIANS OF PHASE SHIFT PER RADIAN OF ASPECT ANGLE

Fig. 14 demonstrates the relations between the parameters of phase-front tilt and angle scintillation error. Reference [1] shows that the tilt of the phase front with respect to the circular phase front that would be present if the target were replaced by a point-source reflector or sphere is a measure of angular error caused by glint. For large r and small $\Delta \psi$, the tilt is an angle δ where

$$\tan \delta = \frac{\lambda \Delta \phi}{2 \pi r \Delta \psi},$$

where

$\Delta \psi$ is an incremental change of aspect angle in radians,
$\Delta \phi$ is the change in phase of the RF signal from the target that occurs when moving at constant range through a small aspect angle $\Delta \psi$,
λ is the wavelength, and
r is the range.

It is also observed in Fig. 14 that

$$\tan \delta = \frac{e}{r},$$

where

e is the angle scintillation error in linear units and
r is the range.

Therefore,

$$\frac{e}{r} = \frac{\lambda}{2 \pi r} \frac{\Delta \phi}{\Delta \psi},$$

or the desired phase-front slope in radians of phase shift per radian aspect change is

$$\frac{\Delta \phi}{\Delta \psi} = \frac{2 \pi}{\lambda} e.$$

As $\Delta \psi$ approaches zero,

$$\frac{d \phi}{d \psi} = \frac{2 \pi}{\lambda} e.$$

Therefore, the error time function and the rms values for the angle scintillation may be converted from the typical linear units to phase-front slope in radians phase shift per radian aspect angle by multiplying by $2\pi/\lambda$.
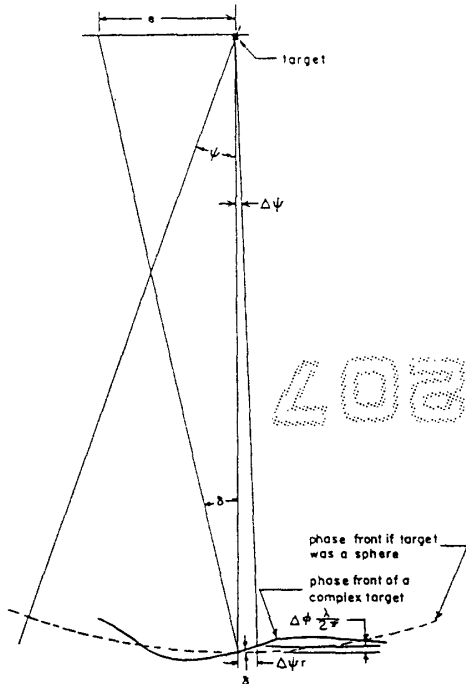
Fig. 14. Diagram relating the linear units of angle scintillation error phase-front slope to units of radians of phase shift per radian change in aspect angle.

APPENDIX III

DERIVATION OF THE DOPPLER SCINTILLATION SPECTRUM

In the text it is shown that the instantaneous frequency from the airframe of the target is the product of two functions

$$f(t) = g(\psi)h(t),$$

where

$f(t)$ is the instantaneous frequency,

$g(\psi)$ is the slope of the distortion of the phase front of the radar echo from a complex target in radians of RF phase per radian of aspect angle ψ, and

$h(t)$ is twice the rate of change of the aspect angle with time, in radians per second.

The functions $g(\psi)$ and $h(t)$ are typically Gaussian for aircraft targets, assuming the target is at sufficiently long range and flying a straight course such that all aspect angle change over the sample time is caused by the random motion of the target.

The object is to obtain the probability distribution of $f(t)$ which will be the spectrum of the Doppler scintillation with respect to the average Doppler of the target airframe. The probability distribution of $f(t)$ is the Fourier transform of the characteristic function of $f(t)$ [8]. The characteristic function of $f(t)$ is

where

$\phi(\epsilon)$ is $\overline{e^{j\epsilon F}}$, the characteristic function of $f(t)$,

$P_A(\psi)$ is the probability density distribution of $d\phi(\psi)/d\psi$, and

$P_T(t)$ is the probability density distribution of $d\alpha(t)/dt$, or $2d\psi(t)/dt$.

Under typical aircraft target conditions $d\phi(\psi)/d\psi$ and $d\alpha(t)/dt$ will be Gaussian distributed so that

$$P_A = \frac{1}{\sqrt{2\pi}\,\sigma_\psi} \exp\left[-\frac{\psi^2}{2\sigma_\psi{}^2} \right]$$

where σ_ψ is $2\pi\sigma_{ang}/\lambda$ and σ_{ang} is rms angle scintillation in linear units of error measured at the target. Also,

$$P_T(t) = \frac{1}{\sqrt{2\pi}\,(2\sigma_t)} \exp\left[-\frac{t^2}{2(2\sigma_t)^2} \right],$$

where σ_t is the rms angular yaw rate in Hz (rms value of $d\psi(t)/dt$). Therefore,

$$\phi(\epsilon) = \int_{-\infty}^{\infty} \int_{-\infty}^{\infty} \frac{e^{j\epsilon\psi t}}{2\pi(2\sigma_t)\sigma_\psi}$$
$$\cdot \exp\left[-\left(\frac{\psi^2}{2\sigma_\psi{}^2} + \frac{t^2}{2(2\sigma_t)^2} \right) \right] d\psi dt,$$

where σ_ψ is the standard deviation of the angle scintillation expressed in radians per radian (Appendix II), and σ_t is the standard deviation of the target random motion in Hz($1/2\pi$ radians per second). Let

$$\mu = \frac{\psi}{\sqrt{2}\,\sigma_\psi} \quad \text{and} \quad \nu = \frac{t}{\sqrt{2}\,(2\sigma_t)}.$$

Then

$$\phi(\epsilon) = \frac{1}{\pi} \int_{-\infty}^{\infty} \int_{-\infty}^{\infty} e^{4j\epsilon\sigma_\psi\sigma_t\mu\nu} e^{-(\mu^2+\nu^2)} d\mu d\nu,$$

$$\phi(\epsilon) = \frac{1}{\sqrt{\pi}} \int_{-\infty}^{\infty} e^{-\nu^2[1+4\epsilon^2\sigma_\psi{}^2\sigma_t{}^2]} d\nu,$$

and

$$\phi(\epsilon) = \frac{1}{\sqrt{1 + 4\epsilon^2\sigma_\psi{}^2\sigma^2}}.$$

The probability density of $f(t)$ is the Fourier transform of ($\phi\epsilon$), or

$$P(f) = \frac{1}{2\pi} \int_{-\infty}^{\infty} \frac{e^{-j\epsilon f}}{\sqrt{1 + 4\epsilon^2\sigma_\psi{}^2\sigma_t{}^2}} d\epsilon.$$

Let

$$2\epsilon\sigma_\psi\sigma_t = \mu.$$

Then

$$1 \quad \int_{-\infty}^{\infty} e^{(-j\mu f)/(2\sigma_\psi\sigma_t)}$$

and

$$P(f) = \frac{1}{2\pi\sigma_\psi\sigma_t} K_0\left(\frac{f}{2\sigma_\psi\sigma_t}\right)$$

where K_0 is a modified Hankel function.

ACKNOWLEDGMENT

The authors express their appreciation to Dr. J. J. Freeman, S. F. George, and Dr. G. V. Trunk of the Naval Research Laboratory for their assistance in deriving the mathematical relations of Appendix III and their review and helpful criticism of this paper. The authors also acknowledge the assistance of R. Hynes and R. Gardener in providing the Doppler scintillation masurements data from [5].

REFERENCES

[1] D. D. Howard, "Radar Target Angular Scintillation in Tracl and Guidance Systems Based on Echo Signal Phase Front Dis tion," *Proc. Nat'l Electronics Conf.*, vol. 15, pp. 840–849, Oct 1959.

[2] J. H. Dunn, D. D. Howard, and A. M. King, "Phenomena of S tillation Noise in Radar Tracking Systems," *Proc. IRE*, vol. 47, 855–863, May 1959.

[3] H. Jasik, *Antenna Engineering Handbook*. New York: McGr Hill, 1961, p. 2-2.

[4] A. S. Locke, *Principles of Guided Missile Design*. Princet N. J.: Van Nostrand, 1955, pp. 440–442.

[5] R. Hynes and R. E. Gardner, "Doppler Spectra of S-Band X-Band Signals," *IEEE EASTCON Conv. Rec.*, pp. 356–365, O ber 1967.

[6] M. S. Corrington, "Frequency-Modulation Distortion Causec Multipath Transmission," *Proc. IRE*, vol. 33, pp. 878–891, Dec ber 1945.

[7] G. A. Korn and J. M. Korn, *Mathematical Handbook for Scien and Engineers*. New York: McGraw-Hill, 1961, pp. 733f.

[8] J. J. Freeman, *Principles of Noise*. New York: Wiley, 1958, 46–49.

Noise in the Presence of Strong Signals

BENJAMIN SENITZKY

Abstract—The electrical noise at millimeter wavelengths generated by an absorbing gas in a cavity is computed as a function of the intensity of an applied coherent signal. The phase of the noise components is strongly correlated with the phase of the coherent signal and the absorption and emission spectrum are similar in the neighborhood of the coherent signal frequency. As the intensity of the coherent field is reduced, the noise emitted by the gas-filled cavity becomes random and can be described by Nyquist's equation.

INTRODUCTION

THE FACT that a material body emits electromagnetic radiation that is a function of its temperature has been known for a long time. Nyquist [1] computed the power per frequency interval emitted by a resistor into a transmission line in the limit $\hbar\omega \ll kT$ as

$$\mathcal{P}(\omega) = (1 - |\Gamma(\omega)|^2)kT/2\pi \tag{1}$$

where $\Gamma(\omega)$ is the reflection coefficient of the resistor in the line. More generally, this formula is valid for any complex load terminating a waveguide when the combined system is in thermal equilibrium at a temperature T. When an electromagnetic field from an external source is applied to the load (1) is in general no longer valid. Nevertheless, it can be used

if the external field does not appreciably perturb the physi properties of the load. To determine, a priori, whether t assumption is valid, one must compute the emitted no power directly without recourse to thermodynamics a then compare the results to (1). Admittedly, this is a diffic task for a solid resistor, but under certain conditions, to described below, the noise power of a gas load perturbed a strong coherent field can be directly computed.

We will consider a specific problem that arose during study of a 1.2-mm wavelength amplifier [2] whose operati is shown in Fig. 1. The active medium of the amplifier i: dipolar gas (HC^{12}N^{15} at 10^{-4} atmospheres pressure) tt exhibits a nonlinear absorption characteristic. A mor chromatic signal (pump) at the resonance frequency of t cavity and gas, ω_0, produces a field that saturates [3] t collision-broadened $J=3 \leftarrow J=2$ rotational transition of t vibrational ground state of the molecule. The response of t gas to a weak information signal at frequency $\omega_0 + \delta$ can analyzed [2] in terms of electric polarizations or curren that are induced at the frequencies $\omega_0 + \delta$, and $\omega_0 - \delta$. T latter component is generated because the degree of satui tion of the medium is modulated at the frequency δ and t resulting time-varying absorption produces the compone at $\omega_0 - \delta$. Analysis of this interaction indicates that inform tion signal components that amplitude modulate the pur have a different susceptibility $\chi_a(\delta)$ than componer that frequency modulate the pump $\chi_f(\delta)$. From the imagina components of these susceptibilities, we find that the F

A simulative approach to the verification of the wave front distortion concept

By Vittorio Rossi (Elettronica spa)
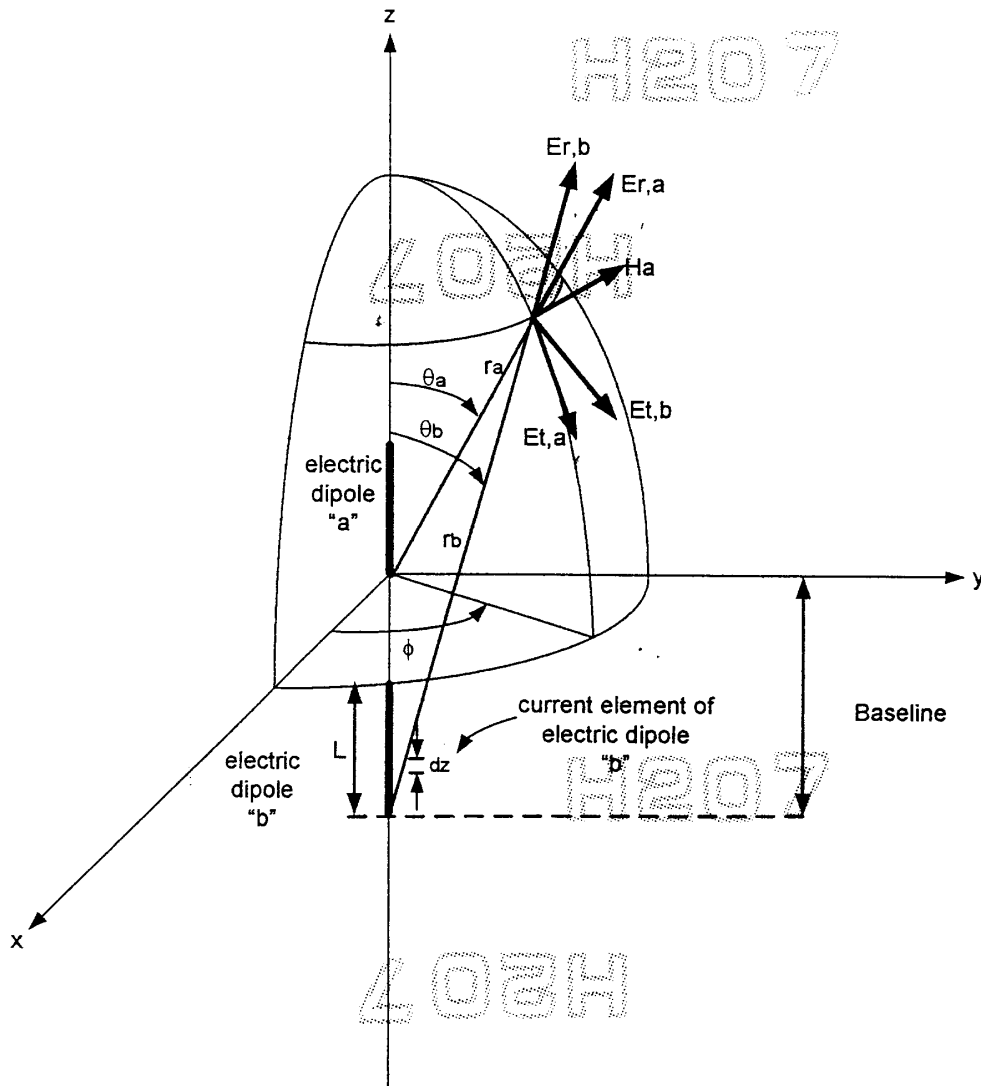
Electrical field generated by dipoles geometry

Input parameters and variables:

- ra , range (meters) from the origin of dipole "a" to the observation point:

- $Ra(z,ra)$, range (meters) from the differential current element of "a" to the observation point

- λ , wavelength (meters) :

- Ia, Ib dipole current intensity (amperes):

- L, dipole length (meters):

- Baseline , distance between dipoles (meters) on z axis :

- Er , electric field radial component (Volts per meter) of each dipole :

- Et , electric field orthogonal component (Volts per meter) of each dipole :

-Ersum radial component (Volts per meter) of the electric field resultant from the two dipoles

-Etsum orthogonal component (Volts per meter) of the electric field resultant from the two dipoles

-θa , observation point angle of view (radians) from dipole "a":

$ra := 100, 200 .. 10000$

$\lambda := 0.025$

$\beta := 2\dfrac{\pi}{\lambda}$

$Ia := 1$

$UnbalancedB := -1$

$Ib := 10^{\frac{UnbalancedB}{20}}$

$L := 10\lambda$

$Baseline := 15$

Calculation of the range from the observation point of each current element of the dipole "a" :

$\theta a := \dfrac{90}{57.3}$

$Ra(z,ra) := \sqrt{(ra \cdot \sin(\theta a))^2 + (ra \cdot \cos(\theta a) - z)^2}$

Calculation of the electric field components radiated from each current element of the dipole "a" (a constant value of the angle of view θa is assumed for all the dipole elements along z axis):

$$Era(z, ra) := 60 \cdot Ia \cdot \beta^2 \cdot \cos(\theta a) \cdot e^{-j \cdot (\beta \cdot Ra(z, ra))} \cdot \left[\frac{1}{(\beta \cdot Ra(z, ra))^2} - \frac{j}{(\beta \cdot Ra(z, ra))^3} \right]$$

$$Eta(z, ra) := j \cdot 30 \cdot Ia \cdot \beta^2 \cdot \sin(\theta a) \cdot e^{-j \cdot (\beta \cdot Ra(z, ra))} \cdot \left[\frac{1}{(\beta \cdot Ra(z, ra))} - \frac{j}{(\beta \cdot Ra(z, ra))^2} - \frac{1}{(\beta \cdot Ra(z, ra))^3} \right]$$

Integration of the electric field components radiated from the differential current elements to produce the field due to the dipole "a" (a constant value of the current Ia is assumed for all the elements along z axis):

$$Era(ra) := \left(\int_0^L Era(z, ra) \, dz \right)$$

$$EradB(ra) := 20 \log(|Era(ra)|)$$

$$Eta(ra) := \left(\int_0^L Eta(z, ra) \, dz \right)$$

$$EtadB(ra) := 20 \log(|Eta(ra)|)$$

Calculation of the range from the observation point of the origin of the dipole "b" (as a function of the range ra) :

$$rb(ra) := \sqrt{(ra \cdot \sin(\theta a))^2 + (ra \cdot \cos(\theta a) + Baseline)^2}$$

Calculation of the observation point angle of view (radians) from dipole "b" (as a function of the range ra) :

$$\theta b(ra) := \mathrm{atan}\left(\frac{ra \cdot \sin(\theta a)}{ra \cdot \cos(\theta a) + Baseline} \right)$$

Calculation of the range from the observation point of each current element of the dipole "b" (as a function of the range ra) :

$$Rb(z, ra) := \sqrt{(rb(ra) \cdot \sin(\theta b(ra)))^2 + (rb(ra) \cdot \cos(\theta b(ra)) - z)^2}$$

Calculation of the electric field components radiated from each current element of the dipole "b" (a constant value of the angle of view θb is assumed for all the dipole elements along z axis): **the fundamental hypothesis is that these components are produced by very close current intensity and are "out of phase" with the corresponding electric field components radiated from the dipole "a" at the observation point :**

$$Erb(z,ra) := 60 \cdot Ib \cdot \beta^2 \cdot \cos\left(\theta b(ra)\right) \cdot e^{-j \cdot (\beta \cdot Ra(z,ra)+\pi)} \cdot \left[\frac{1}{\left(\beta \cdot Rb(z,ra)\right)^2} - \frac{j}{\left(\beta \cdot Rb(z,ra)\right)^3}\right]$$

$$Etb(z,ra) := j \cdot 30 \cdot Ib \cdot \beta^2 \cdot \sin\left(\theta b(ra)\right) \cdot e^{-j \cdot (\beta \cdot Ra(z,ra)+\pi)} \cdot \left[\frac{1}{\left(\beta \cdot Rb(z,ra)\right)} - \frac{j}{\left(\beta \cdot Rb(z,ra)\right)^2} - \frac{1}{\left(\beta \cdot Rb(z,ra)\right)^3}\right] ;$$

Integration of the electric field components radiated from the differential current elements to produce the field due to the dipole "b" (a constant value of the current Ib is assumed for all the elements along z axis):

$$Erb(ra) := \left(\int_0^L Erb(z,ra)\, dz\right)$$

$$ErbdB(ra) := 20\log\left(|Erb(ra)|\right)$$

$$Etb(ra) := \left(\int_0^L Etb(z,ra)\, dz\right)$$

$$EtbdB(ra) := 20\log\left(|Etb(ra)|\right)$$

Calculation of the resultant electric field components projecting the radial and orthogonal components of the field radiated from the dipole "b" along the directione of the **corresponding electric field components radiated from the dipole "a" at the observation point** (the resultant components depend on the relative angle $\theta a - \theta b(ra)$):

$$d\theta(ra) := \theta a - \theta b(ra)$$

$$Etsum(ra) := Eta(ra) + Etb(ra)\cos\left(d\theta(ra)\right) - Erb(ra)\cdot\sin\left(d\theta(ra)\right)$$

$$EtsumdB(ra) := 20\log\left(|Etsum(ra)|\right)$$

$$Ersum(ra) := Era(ra) + Etb(ra)\cdot\sin\left(d\theta(ra)\right) + Erb(ra)\cdot\cos\left(d\theta(ra)\right)$$

$$ErsumdB(ra) := 20\log\left(|Ersum(ra)|\right)$$

From the above calculation the origin of the wave front distortion arises : **the radial component of the resultant electric field depends on the orthogonal components of the field produced by one dipole . A large contribute of energy is transferred to the radial component (** $Ersum$ **) which cannot be neglected as in the case of the field radiated by a single dipole(** E_1 **):**

EtadB(ra)
————
EradB(ra)
—
EtsumdB(ra)
● ● ●
ErsumdB(ra)
○○
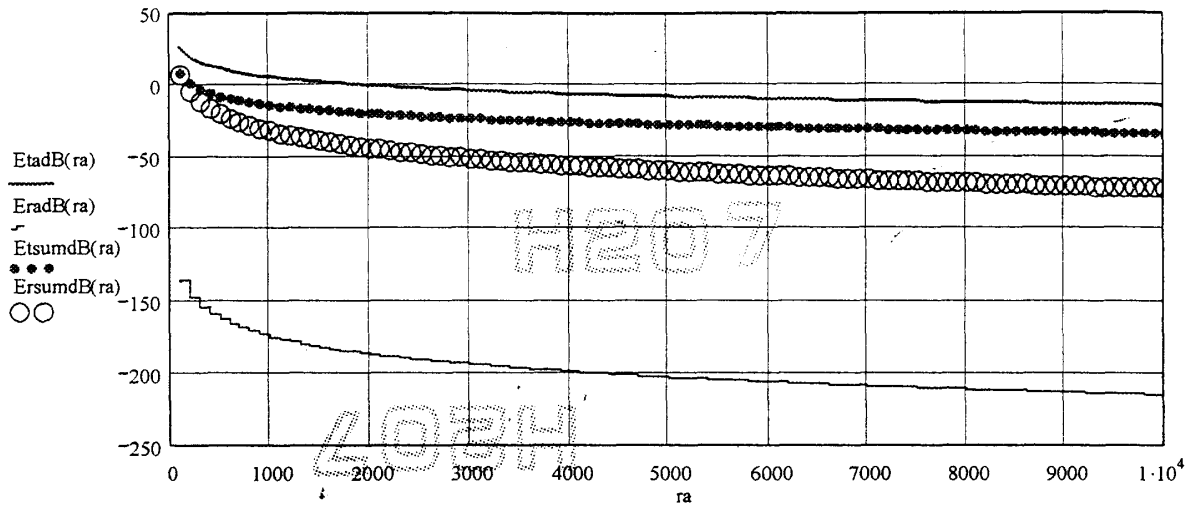
The presence of both radial (Ersum) and orthogonal (Etsum) components of electric field implies the presence of orthogonal (from Ersum) and radial (from the Etsum) components of the Poyntig vector. The ratio of the electric fiefd components is the same as the ratio of the Poynting vector components: the apparent direction of the power flow can be directly calculated from the angle between the vector Ersum and Etsum . From this calculation the linear displacement due to the wave front distorsion is then derived (the reference point is the center of the baseline):

$$\text{WFDerror(ra)} := \frac{|\text{Ersum(ra)}| \cdot \text{ra}}{|\text{Etsum(ra)}|} + \frac{\text{Baseline}}{2}$$

The resultant linear displacement WFDerror is finally compared with the classic and well known expression of the CrossEye error (far range) :

$$\text{XEerror} := \left(\frac{1 + \text{Ib}}{1 - \text{Ib}}\right) \cdot \frac{\text{Baseline}}{2}$$
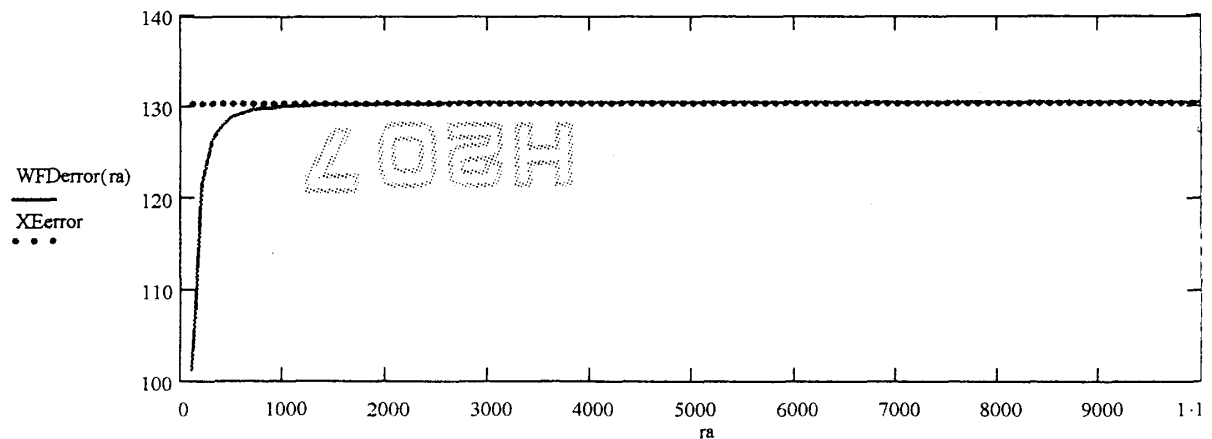
WFDerror(ra)
————
XEerror
● ● ●

A Compact, Long Range, High Resolution, W-Band FMCW Radar for Remote Sensing System Applications

Dr. Lyle Johnson, William Friedrich, Dr. Daniel Wiersma, Curt Hedman, John Lamberg, Dr. John Geddes, and Michael Gawronski.

Alliant Techsystems, Inc
Integrated Defense Company
600 Second St. NE
Hopkins, MN 55343

Abstract - A compact 94 GHz FMCW radar has been developed for remote sensing and guided system applications. A detailed model of the radar has been developed for system trade studies. Extensive testing of the radar has been done to evaluate performance.

INTRODUCTION

A compact, long range, high resolution sensor system has been developed for remote sensing and guided system applications. An integral part of the system development was a detailed simulation model of the sensor. By developing the simulation concurrently with the sensor hardware and software, the critical design decisions were made prior to building the hardware. This process optimizes the design while reducing the development costs.

Based on the simulation output, the hardware and software requirements were determined. From these requirements the form, fit, function hardware was designed. The requirements drove the hardware to use MMIC and microcircuits to achieve the desired packaging and performance. A breadboard processor consisting of multiple digital signal processor (DSP) chips was developed for the testing. Field testing validated the simulation and provided a data base of signatures for performance evaluation.

Simulation and Modeling.

The sensor requirements dictated a small diameter (< 6 inches) with rugged components. To make the system affordable the cost must be kept as low as possible. The sensor was required to detect objects such as vehicles at a long range (> 1 km) and to measure each object's location. In order to achieve this performance the sensor must have sufficient power, sufficient resolution, and very low noise.

A detailed, high-fidelity simulation tool was developed for the sensor system design [1]. The simulation was used for hardware development by generating specifications, performing trade studies, cross-checking laboratory measurements, and evaluating sensor system performance. The detailed simulation is a mathematical model derived from fundamental physical principles. A functional block diagram of this software model is shown in Figure 1. The MMW radar target models were provided by the government as a set of point scatterers with their magnitude and corresponding locations in space. Different sets of scatterers are used for different targets and for different target orientations. The clutter background models consist of a square kilometer of samples representing terrain data from several sites.

The MMW radar sensor model converts the point scatterer target and background models into an amplitude versus range profile as shown in the figure. The signal at the output of the mixer is the summation of the responses to the individual scatterers. The IF filter frequency response and the noise power spectral density are applied in the frequency domain. The range gating process then produces the amplitude versus range output. This data is collected as the radar is scanned in azimuth to provide a range-azimuth map or image. A model of the gimbals provides proper positioning of the sensor to point at the scene and to scan at specified rates.

The detection and object location measurement algorithms are modeled using the same source code as that compiled in the embedded processor. By coding the seeker algorithm functions as single function calls the integration process is simplified, and the transfer of the algorithms to the seeker processor software is facilitated.

The integration of the simulation into a single executable brings together all of the models. This requires careful definition of coordinate systems and system timing to ensure that models are properly registered. It also requires careful management of memory and throughput resources. The signature generation process is very computationally intensive. Hence, we have designed the simulation to write the data to files as well as passing it through the algorithms. The same data format is used for simulation output as for field-test data output.
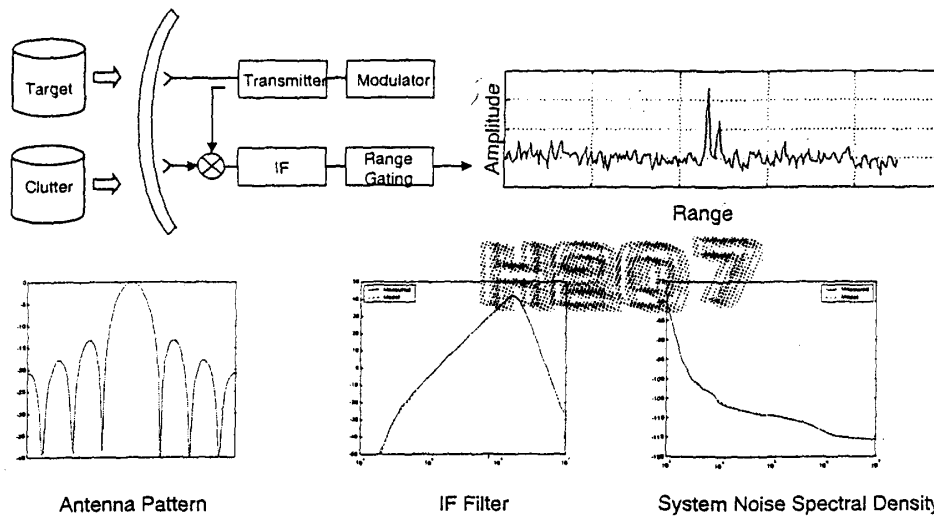
Antenna Pattern   IF Filter   System Noise Spectral Density

Figure 1. Detailed simulation functional block diagram. Models for the antenna, IF filter, and system noise are also shown.

MMW RADAR HARDWARE

Based on the simulation the MMW radar system was designed. It consists of an RF front-end, a preprocessor, and a data processor. The RF front-end shown in Figure 2 is form, fit, function packaged to fit the requirements. The preprocessor is not form, fit, but it performs its functions in real-time. The data processor also operates in real time but is not form, fit. Because the integration of the sensor into the larger system in which functions from the larger system and the sensor are merged into a common processor, the processors were not packaged in their final form.
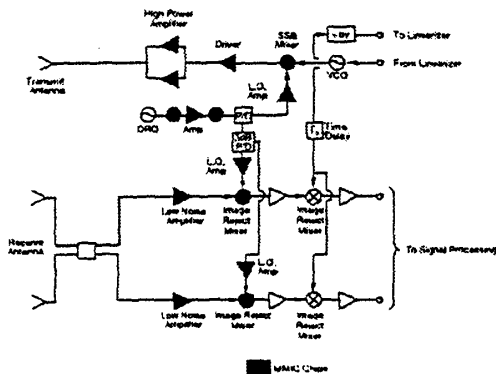

Figure 2. Block diagram of RF front-end .

FMCW radar systems provide a low cost system architecture that is useful in many applications including remote sensing, guided systems, and aircraft all-weather vision systems. W-band operating frequencies are preferred in these applications for small antenna size and high resolution, but in the past, size, and cost have been prohibitive. Recent advances in W-band MMIC devices and planar micro-strip antennas have made it possible to develop the inexpensive, compact, low noise, FMCW radar system described in this paper.

The MMW radar RF front-end consists of the antenna, the transmitter, and the receiver. Key features of the front-end are:

1. Low transmitter phase noise.
2. High power output using MMIC power amplifiers.
3. Use of PHEMT MMIC LNA's for low system noise figure.
4. Dual downconversion design to reduce effects of phase noise.
5. High Transmit/Receive isolation
6. Excellent sweep linearity using a bulk acoustic wave (BAW) based linearizer.
7. Planar microstrip transmit and receive antennas.

The RF portion of the system is assembled in a small ring-like enclosure, shown in Figure 3. The T/R module is constructed from nine separate subassemblies: high power transmitter, upconverter, low phase noise oscillator, frequency multiplier, two LNA receivers, two 2nd downconverters, and a VCO/frequency divider. These subassemblies are fabricated and tested separately before incorporating them into the T/R module.

The transmitter achieves the required power output of 23 dBm by the combination of two TRW power amplifier MMIC's [2]. The power is modeled in the simulation by the range equation which scales the response of each ,
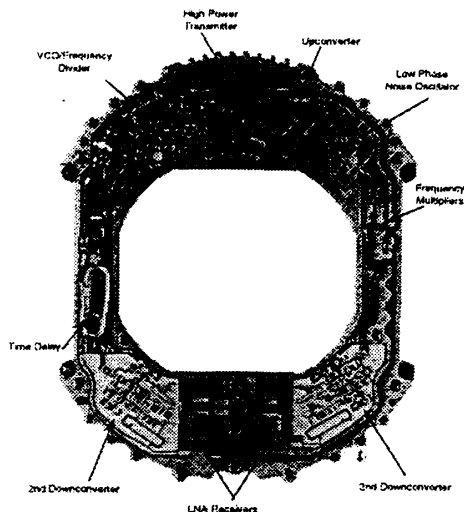

Figure 3. Transmit/Receive ring with cover removed. The antenna is mounted on the other side.

scatterer. The antenna is a standing wave patch array mounted on the front of the RF front-end ring. The transmit and receive beam patterns are measured in the laboratory and compared with the simulation models. The system phase noise is measured at the output of the second image-reject mixer. Leakage signals from several sources can mix with the LO signal resulting in a frequency dependent IF noise level. Low phase noise was achieved by using a low phase noise VCO and DRO by using time delay cancellation, and by transmitter/receiver isolation. Also, low receiver noise is required, which is achieved with PHEMT LNA's. The measured frequency dependent noise is compared to the modeled noise as shown in Figure 1. The overall performance of the RF front-end is summarized in Table 1.

Table 1. System Parameters Values. These values were needed to meet the performance requirements for the sensor.

Transmitter Power Output	23 dBm
Transmitter Phase Noise @1 MHz	<-115 dBc/Hz
Receiver Noise Figure (SSB)	5-6 dB
System Noise Figure (SSB)	8 dB
RF Bandwidth .	> 500 MHz
2-Way Antenna Gain	50.7 dBi

The preprocessor performs digital downconversion on the digitized IF signal. A numerically controlled oscillator is used to select the desired range gates. A Fast Fourier

Transform (FFT) converts the IF signal to range information, thus forming the range gates. The FFT processing was implemented using a commercial DSP.

The data processor itself performs the control of the seeker as well as the detection and track algorithms. Multiple DSP devices are used to implement the data processor in real time.

TESTING

Two captive flight tests were conducted in the winters of 1997 and 1998 at Aberdeen Proving Grounds, MD and Camp Grayling National Guard Facility, MI, respectively. Signature validation data were collected on known targets such as corner reflectors. Signature data were collected on armored vehicles in a variety of backgrounds including heavy snow, scattered snow, grass, and rain soaked backgrounds. Trees and roads were also present. Conditions ranged from clear to rain and snow with temperatures ranging from -15°F to +50°F. Approximately 40, two-hour duration missions were flown with this radar resulting in over 17,000 target encounters. During these tests the sensor functions were demonstrated, detection and track accuracy were evaluated on many targets under a variety of conditions, and sufficient data were collected to validate the simulation models.

The principal validation was done on a known target during the captive flight test. Four corner reflectors of known amplitude were set up in a line with equal spacing between reflectors 1 and 2 and between reflectors 2 and 3. Reflectors 3 and 4 were separated by half that amount. Figure 4 is a plot of the range profiles from the simulation and from the captive flight test. The separation between returns matches very well. The amplitudes match within experimental conditions. Factors such as actual corner reflector calibration accuracy, range gate straddle, and position in the beam make it difficult to obtain exact matches. The system noise was validated by pointing the sensor at the sky and sliding the range gates over the IF bandwidth. This allowed the system noise to be compared to the power spectral density. The match was very close (within a few dB) over all frequencies.

Other validation efforts included estimation of the average clutter background, estimates of target strength, and estimates of detection and track performance. On completion of the testing the seeker demonstrated long range detection performance on a variety of targets in different backgrounds and conditions.

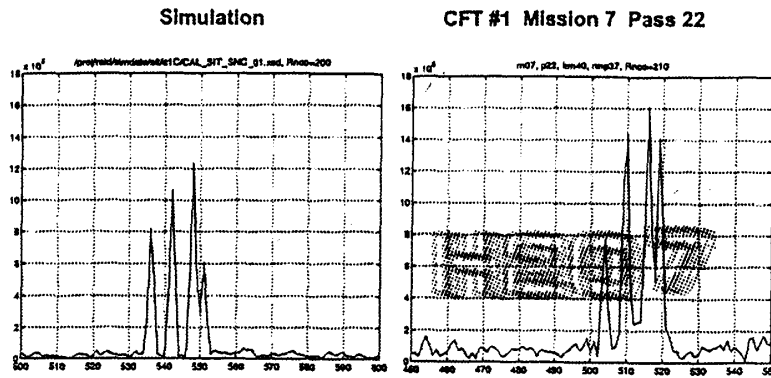**Simulation**   **CFT #1 Mission 7 Pass 22**

Figure 4. Range profile outputs from the simulation and the actual radar. Data was collected at Aberdeen Proving Grounds, MD. The amplitude is the numeric value computed at the output of the preprocessor. Range is in range bin number, which is referenced to the center gate.

CONCLUSIONS

The use of system simulation models and high density microcircuits were instrumental in the design of a compact, FMCW, long-range, radar system. This radar achieves excellent performance at low cost by making use of advanced developments in 94 GHz MMIC technology. The use of simulation techniques during the system design has allowed design decisions to be made before building hardware. The validated simulation was used to predict performance and verify that it met the performance requirements stated at the outset.

REFERENCES

[1] D.J. Wiersma, "Multispectral (IR/MMW) Model for Missile Seeker Design and Performance Evaluation," Proceedings of the Conference on Multispectral Missile Seekers, U.S. Army Missile Command, Redstone Arsenal, AL, Nov. 1995, pp 159-171

[2] J.R. Lamberg, et al., "A Compact High Performance W-Band FMCW Radar Front-End Based on MMIC Technology," 1999 IEEE MTT-S International Microwave Symposium Digest, Anaheim, CA, June 1999, pp 1797-1800.

Contact: Michael Gawronski
Alliant Integrated Defense
Telephone 612-931-5579
Mike Gawronski@ATK.com

ATK_T105031A

James, Shieh,

I enjoyed my visit to Taiwan and Shieh's recent visit to California.

Here are comments re S-1 System Analysis and X-band T/R module spec.

The X-band T/R spec and related S-1 system analysis information provided by PJ, James and Shieh have been reviewed. A Mathcad program was written to analyze the system parameters. The CSIST supplied information was discussed with Long Bui and Yi-Chi Shih of MMCOMM. Below are our comments:

(1) The S-1 system analysis provided by PJ seems about right. We are concerned with the S/I of approx 10 to 20 dB, depending on the effect of the NCI. There does not appear to be much margin considering the recent results that were obtained at CSIST with the RA system. A further area of concern is the possibility that the target may not be as large as you think it is. For example, what happens if the target RCS is 800 sq meters instead of 8,000? Therefore we would recommend building in an extra margin into the design.

(2) Some of this margin can be improved by tightening the transmitted sideband noise spec from -105 dBc to -115 dBc. Such devices are available.
(3) Techniques to reduce leakage sideband noise should be included. The primary technique we recommend is to add a time delay into the reference signal to the receiver LO. The delay is adjusted to match the leakage transit time thus providing additional leakage sideband noise reduction. This technique is discussed in a paper: "A Compact, Long Range, High Resolution, W-Band FMCW Radar for Remote Sensing System Applications", Dr. Lyle Johnson, William Friedrich, Dr. Daniel Wiersma, Curt Hedman, John Lamberg, Dr. John Geddes, and Michael Gawronski, GOMAC 2000 Digest, Paper Session 3: March 21, 2000. (a copy is attached).

(4) When you do build the system we recommend a series of measurements to establish the system performance. We recommend making measurements after the down conversion mixer with a spectrum analyzer. These measurements involve (a) looking at the sky, (b) turning the XMTR off, and (c) putting an absorber over the antenna. Then we recommend pointing the system at a known RCS corner reflector and making measurements. We also recommend making measurements against a dynamic RCS target to simulate different target amplitude and frequency responses.

(5) As a general comment we suggest considering two additional design options to improve the performance of FMCW designs. These are feedthru cancellation and a super het receiver. Both of these have show the capability to provide significant improvement in leakage cancellation and achieving a low receiver noise figure. The Beasley (Pilot radar) paper on feedthru cancellation is also attached.

John

- - - - - - - - - - - - - - -
John C Kirk Jr
Goleta Engineering
P O Box 6208
Santa Barbara, CA 93111
Tel: (805) 967-0600
Fax: (805) 967-0600
Cell: (805) 570-5908

jckirkjr@aol.com
www.goletaengineering.com

SOLVING THE PROBLEMS OF A SINGLE ANTENNA FREQUENCY MODULATED CW RADAR

P.D.L.Beasley*,A.G.Stove*,B.J.Reits*,B-O.As**

*Philips Research Laboratories, Redhill, England
+Hollandse Signaalapparaten, Hengelo, The Netherlands
**Bofors Electronics AB, Järfälla, Sweden

ABSTRACT

This paper describes a Reflected Power Canceller (RPC) using modern PIN diode technology, which enables a Frequency Modulated Continuous Wave (FMCW) radar to operate using a single antenna for transmission and reception. Results are presented which demonstrate that such a canceller solves the problems for many CW-type radars over large r.f. bandwidths (i.e. > 2 GHz at X-band).

The RPC has been successfully installed into the Bofors/Signaal "PILOT", FMCW tactical navigation radar. Results from sea trials are presented.

INTRODUCTION

This paper will describe a Reflected Power Canceller (RPC) using modern PIN diode technology, enabling single antenna operation to be used with Frequency Modulated Continuous Wave (FMCW) radars. It also describes the application of the RPC in the Bofors/Signaal "PILOT", FMCW tactical navigation radar.

The majority of radars in use today are pulse radars, while continuous wave (CW) transmission, has been confined to limited, special applications, e.g. the HAWK and Sea-Sparrow surface-to-air missile systems. Unlike most pulsed radars, these CW radars only give very crude range information and virtually no range resolution.

Recent advances in microwave component technology and signal processing make it possible to design a CW radar with range resolution and range measurement capability at least as good as a conventional, pulsed radar (Ref. 1). The main reason operationally for such a radar is its "indetectability" by ESM equipment. This has led Philips to develop a product called PILOT, Philips Indetectable Low Output Transceiver, based on modulation by linear f.m., FMCW.

CW can be said to be the "ultimate" in high duty cycle, i.e. 100% duty cycle, and therefore also in LPI, Low Probability of Intercept, and "quietness". Furthermore, a CW waveform makes best use of the output power available from solid state devices, peak power becoming average power.

The nominal output power of PILOT, which operates at X band, is 1 W. Together with an antenna with 30 dB gain, typical for an unstabilized navigation type, ranges of 15-20 km are achieved against typical naval targets of 100-1000 m² RCS when taking earth's curvature and multipath into account (Ref. 2). This range is also typical for a conventional, pulsed navigation radar with 10-20 kW peak power; 5-10 W average power.

When it comes to ESM intercept range, there is a dramatic difference between the two radars. A typical, tactical shipboard ESM can be assumed to have a Minimum Detectable Signal (MDS) of the order of -60 dBmi (power received if an isotropic antenna is used). Such an ESM would detect the transmission of the conventional radar at approximately 30 km giving the ESM a substantial "range advantage" over the radar.

PILOT on the other hand would be intercepted by the same ESM at only 2.5 - 3 km range, i.e. much shorter than the detection range of the conventional radar. This difference between the conventional radar and PILOT would be even more pronounced if the ESM were in a helicopter or an aircraft. Intercept range of the pulsed radar would then be >100 km, but remains a few km for PILOT.

THE ANTENNA PROBLEM

One of the greatest problems facing designers of CW type radars is that of achieving sufficient isolation between transmitter and receiver. In a pulse radar this is easily achieved by time gating. In a CW type radar transmission and reception are simultaneous and it is necessary to detect target returns of the order of a picowatt or less in the presence of Watts of transmitted power. This can result in two serious problems;
1. The transmitter noise sidebands can swamp out valid targets.
2. The power leaking into the receiver can desensitize the receiver.

These problems have been appreciated for a long time. The traditional solution has been to use a dual antenna configuration. In a feasibility demonstration model of PILOT this was the solution chosen. However the number of CW radar applications could be increased if a single antenna could be used. This would require that the leakage could be cancelled before it degrades the performance of the receiver.

PREVIOUS SOLUTIONS

The principle of the RPC has been appreciated for a long time and practical implementations have been investigated since the 1960s. Figure 1 shows a typical system.
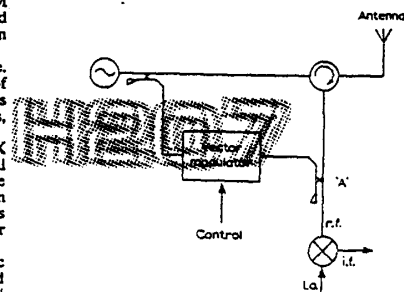

Figure 1 Block diagram of simple canceller

A sample of the signal currently being transmitted is manipulated by a vector modulator so that it is of equal amplitude to, and in antiphase to, the transmitter leakage signal. By adding this signal into the receiver via a directional coupler, 'A', the

391

leakage, including the noise sidebands of the transmitted signal, can be cancelled out. The effectiveness of this method depends upon the accuracy with which the amplitude and phase can be adjusted. In a practical system the RPC must be a closed loop with sufficient gain and bandwidth to track the leakage variations.

The first mention of a practical demonstration of a closed loop RPC was by O'Hara and Moore in September 1963 (Ref. 3). They reported a split milled, 30 lb block, that used ferrite rotators to effect the vector modulation and achieved a power cancellation of 60 dB. They needed the milled block in order to have precise control of the r.f. phase around the cancelling path. The performance was excellent, but the implementation suffered from several serious disadvantages: the ferrite modulators were slow and had limited r.f. bandwidth, and the milled block was very expensive to produce.

REQUIREMENTS OF A REFLECTED POWER CANCELLER

A prototype RPC using a modern implementation of the technique, with PIN diodes, has been investigated and the resulting system has been used in the successful production of the PILOT single antenna FMCW radar. The following sections describe this implementation in more detail. The technique can also be applied, to great advantage, to other types of CW radar.

The RPC which has been produced easily exceeds the requirements for the PILOT radar. The significant parameters of the radar which impinge on the design of the RPC are:

Transmitter power	1 Watt continuous
Sweep rate	1 kHz
Transmit bandwidth	50 MHz maximum
Centre frequency	9.375 GHz +/- 30 MHz
Antenna	1.2:1 VSWR (22 dB return loss)

With these parameters, and by knowing the noise sideband levels of the transmitter, it was calculated that 50 dB of transmitter leakage power cancellation was required. The antenna provides 22 dB of this leaving the RPC to improve this by approximately 30 dB. It is important that the RPC does not inject any excess noise into the receiver. This effectively rules out the use of amplifiers within the cancelling path, which would inject their own thermal noise into the receiver. In addition to this the loop must be able to cancel the reflected power throughout the 50 MHz sweep, i.e. it must track the variations in antenna return (wide loop bandwidth).

The RPC should be easy and cheap to manufacture and simple to install. Once installed the RPC should require no maintenance. It should be able to adapt to ageing of the antenna or to a replacement antenna being fitted. It should also be suitable for its operational environment.

SYSTEM DESCRIPTION

Figure 2 shows a schematic of the canceller as configured for experiments in the laboratory.

The canceller can be considered as two separate channels, I and Q, which operate independently. The residue of the I (or Q) component of the uncancelled signal is detected by the mixer. It is then amplified and filtered to provide the I (or Q) drive for the vector modulator. Each loop, I and Q, is therefore a simple zero order control loop. Lack of othogonality between the two channels will cause one channel to inject a disturbance into the other. Whilst this is not desirable, it is not fatal to the operation of the loops. The orthogonality requirements on the loop components can thus be relatively modest.

The Microwave Circuit

The demonstration canceller (RPC) was built using hybrid microwave components. It was tested with several different antennas and also with a nominally perfect 50 ohm load. The RPC could also be tested with a variety of different microwave sources. This enabled the canceller to be tested using sources with different noise characteristics. The low noise amplifier in the receiver chain puts a very stringent requirement on the maximum level of any noise which may be introduced by the RPC.

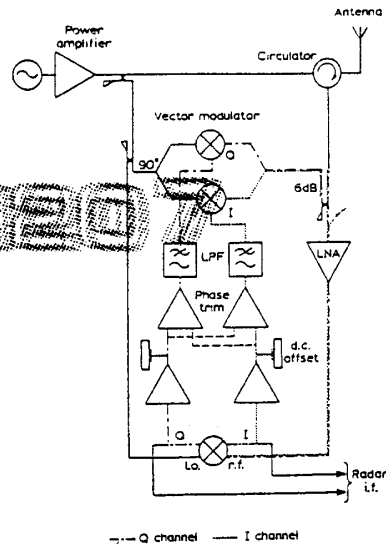
—·— Q channel ——— I channel

Figure 2 The experimental set-up

The power amplifier produced 3 W which is comparable to the power levels of the PILOT radar. Its bandwidth was reasonably flat from 8.5 GHz to 10 GHz but turned out to be the limiting factor to the cancellation bandwidth of the system. The coupler after the amplifier taps off 0.5 W of power for the vector modulator and for the mixer local oscillator. The waveguide circulator had an isolation of better than 30 dB, i.e. 10 dB better than the antenna return loss.

The output of the vector modulator cancels the leakage signal at the 6 dB coupler. This coupler also couples out a small part of the received signal, so a lower coupling factor is used in the production PILOT radar in order to minimise the loss of the received signal. The minimum possible coupling value should of course be used, consistent with the power available from the modulator and the worst case return loss of the antenna.

The key component in the RPC is the vector modulator. A conceptually simple solution to this would be to use a phase shifter and an attenuator. This was ruled out for two reasons:

1. It is very inconvenient to convert the error signal that drives the modulator into polar components.
2. It is practically impossible to control the phase directly and must go back to zero after each complete cycle. This is because the gain of the modulator must approach infinity as the phase flips back from just less than 360 degrees to just more than 0 degrees.

The preferred solution therefore uses bi-phase modulators (BPM) as variable attenuators, operating with quadrature components of the signals. The general requirements on the modulator are;

1. It must not alter the noise characteristics of the input signal i.e. it must not saturate or distort the signal passing through it.
2. It must have quadrature inputs.
3. It must deliver an output power of about 100 mW in order to achieve a satisfactorily low loss in the coupler.
4. The insertion loss should be as low as possible.
5. It must be capable of being driven at the maximum response frequency needed for the loop. For PILOT this meant a flat response up to at least 10 kHz.
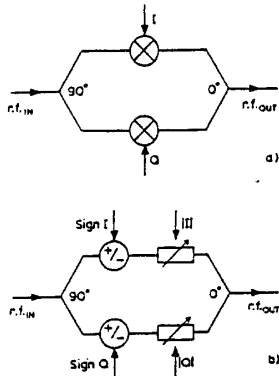
392

Figure 3 Vector modulator configurations
   a) Analogue bi-phase modulator
   b) Conventional approach

Figure 3a shows the circuit of the quadrature modulator. It uses two biphase modulators driven linearly as attenuators. The design of the biphase modulator, using PIN diodes as control elements, is itself quite conventional, but its use as an analogue modulator is believed to be novel. It offers a much simpler solution for the quadrature modulator than the more conventional approach of using digital biphase modulators and variable attenuators, which is shown in figure 3b. Another advantage is that the transfer function is very linear. The cross-channel leakage is almost independent of the attenuation level. These factors greatly simplify the design of the control circuitry, and are in direct contrast to the non-linear behaviour of the more conventional circuit. The analogue biphase modulator also had 2.5 dB less loss than the conventional approach.

The final components in the control loop are the mixer and the low frequency circuits.

The mixer is a double balanced quadrature mixer. The important features required of it are good orthogonality between I and Q channels and a constant, low, d.c. offset across the r.f. bandwidth.

A corollary of the need for good orthogonality in the mixer and the modulator is the need for careful control of the relative path lengths, and hence the relative phases, of the cancelling and local oscillator signals. The loop is stable if the total phase error around the two quadrature channels is less than 90 degrees. In the experimental system the paths were matched for maximum r.f. bandwidth. For a cancellation bandwidth of 2 GHz the l.o. path to the mixer has to be matched to the r.f. path to the mixer (via the modulator) within about 3.5 cm (in air). In practice the path lengths were matched to give a bandwidth much greater than the power amplifier bandwidth.

The requirement on the r.f. path length matching for good operation is much less strict and has no effect on the loop stability.

Low Frequency Circuit

The first l.f. amplifier is a low noise d.c. coupled amplifier with a 200 kHz bandwidth. The d.c. offset potentiometer serves to set the 0.6 V offset needed for the modulator drive voltage.

The phase trimming stage synthesises the correct drive for each channel of the modulator from the two signals available from the mixer and their complements. This is done in order to trim the phase shift around each channel to a minimum.

The l.f. filters remove high frequency noise from the loop and prevent spurious modulation of the cancelling signal by such noise. The unity gain frequency of the loop is set at about 10 kHz. This is high enough to track the variations in return loss in a 1 kHz sweep but not too high as to cancel out close-in targets.

PERFORMANCE OF THE RPC

The theory of operation of the RPC was verified by replacing the circulator by a 20 dB attenuator directly between the transmitter and the receiver. This gave a well-defined 20 dB return loss against which the performance of the RPC could be evaluated. By experimenting with different line lengths in this leakage path the performance of the RPC with different rates of change of leakage phase was evaluated. Figure 4 shows the cancelled and uncancelled outputs for this 20 dB reflection.
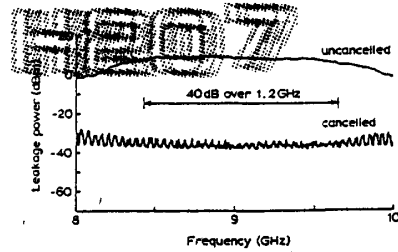

Figure 4 Cancellation of 'perfect antenna'

The sweep rate was 4 MHz/ms corresponding to 35 degrees of phase per millisecond (equivalent to a 2-way path length mismatch of 7 m in air). The power cancellation is 40 dB over 1.2 GHz but this was limited by the bandwidth of the power amplifier. The periodicity of the cancelled signal corresponds to 10 ms, or 360 degrees of phase, and is due to slight variations in the loop gain as the vector modulator loops around.

Having proved that the system successfully cancelled the 20 dB attenuator, experiments were carried out with real antennas. The first antenna to be tested was a 7 foot end fed non-resonant slotted waveguide navigation antenna complete with rotating joint. The return loss was measured on a network analyzer and is shown in figure 5.
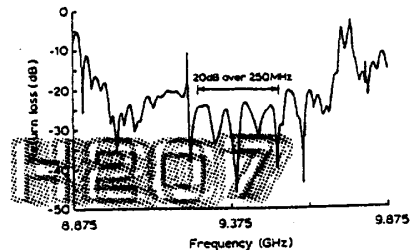

Figure 5 Return loss of 7 foot navigation antenna

The level of the return loss was mainly due to the rotating joint.

The antenna is designed to operate at 9.375 GHz and the return loss is better than 20 dB over about 250 MHz. The RPC was tested over 1 GHz to examine the effects of the poor return loss at the edges of the band. The result is shown in figure 6 for a sweep rate of 50 MHz/ms, i.e. the maximum sweep rate used by the PILOT radar.
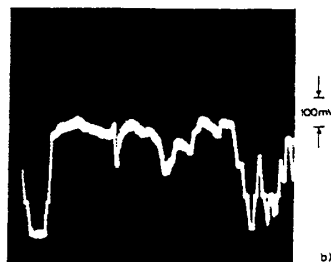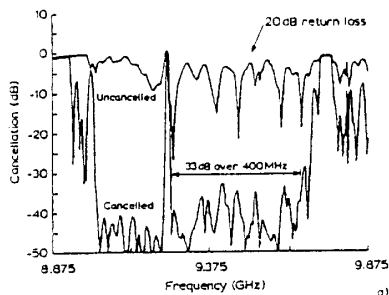
393

Figure 6 Results for 7 foot navigation antenna
     a) Cancellation
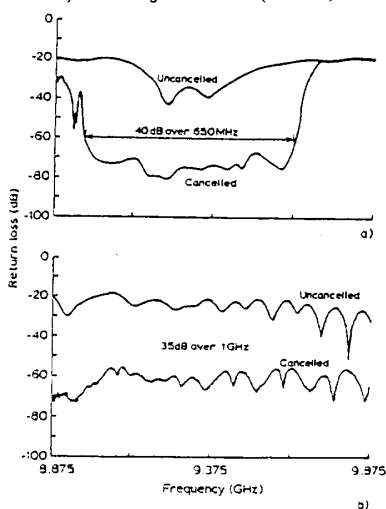   b) Drive voltage at PIN diode (I channel)

Figure 7 Cancellation results
     a) Small navigation antenna
     b) 5 foot navigation antenna

The corresponding drive voltage for the I channel is shown below it. The RPC cancels the power by more than 33 dB over a frequency range of more than 400 MHz, i.e. well within the specified 30 dB over 50 MHz.

The transmitter noise sidebands were also cancelled, and the residue had only a negligible effect on the receiver noise figure.

The results for two other antennas are presented in figure 7.

The first plot shows a power cancellation of 40 dB over 650 MHz (at 50 MHz/ms) for a small navigation antenna. Note that at around 9.375 GHz the RPC had little cancellation to do because the antenna return loss was already 30 dB.

The second plot shows the cancellation of an antenna with 20 dB return loss over 1 GHz. With a sweep rate of 50 MHz/ms the cancellation is 35 dB over the complete sweep!

A prototype unit of the PILOT radar with a single antenna and RPC has been successfully evaluated on board a Royal Swedish Navy Fast Attack Craft.
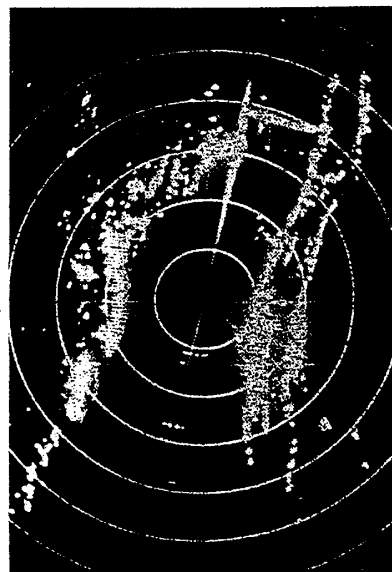

Figure 8 PPI recorded in Sweden with a single antenna PILOT
The illustration shows a PPI recorded of the strait between Sweden's mainland and the island of Öland with a bridge approx. 50 m high at 15 nm. The range scale is 24 nm with range rings every 4 nm.

CONCLUSIONS

The reflected power canceller has far exceeded the specifications for PILOT and it enables CW type radars to be built with single antenna operation over a large r.f. bandwidth (i.e. 2 GHz or more at X band). The design has been proved to be very robust and stable, and is simple to install. An RPC based closely on the laboratory model described above has been successfully incorporated into the PILOT radar.

The work on the RPC began at the start of 1988, and the first prototype PILOT radar equipped with the system was delivered in June 1989. This short timescale indicates both the importance attached to the RPC and the success of the design.

394

REFERENCES

1. Barrett M., Reits B.J. and Stove A.G., "An X Band FMCW Navigation Radar", IEE International Conference Radar-87, London. p448.

2. As, B.-O. and Bergkvist, B., "Radar ranges against ships and low-flying vehicles", Paper presented at the International Naval Technology Conference, Rotterdam, 1980.

3. O'Hara F.J. and Moore G.M., "A High Performance CW Receiver Using Feedthru Nulling", Microwave Journal, Sept. 1963. p63.